CIRCUMVENTING THE SIGN PROBLEM IN ROTATING QUANTUM MATTER

Casey Elizabeth Anderson Berger

A dissertation submitted to the faculty at the University of North Carolina at Chapel Hill in partial fulfillment of the requirements for the degree of Doctor of Philosophy in the Department of Physics and Astronomy in the College of Arts and Sciences.

Chapel Hill
2020

Approved by:

Joaquín E. Drut

Adrienne Erickcek

Charles Evans

Amy Nicholson

Frank Tsui

ABSTRACT

Casey Elizabeth Anderson Berger: Circumventing the Sign Problem in Rotating Superfluids Using Complex Langevin
(Under the direction of Joaquín E. Drut)

Quantum field theories with a complex action suffer from a sign problem in stochastic nonperturbative treatments, making many systems of great interest – such as polarized or mass-imbalanced fermions and QCD at finite baryon density – extremely challenging to treat numerically. Another such system is that of bosons at finite angular momentum; experimentalists have successfully achieved vortex formation in supercooled bosonic atoms, and have measured quantities of interest such as the moment of inertia. However, the rotation results in a complex action, making the usual numerical treatments of the theory unusable.

This thesis treats systems of nonrelativistic bosons with finite angular momentum using two approaches. One approach is to determine the virial coefficients using a semi-classical lattice approximation (SCLA). Through this approach, we are able to compute the thermodynamic equation of state of the bosons for finite trapping frequency, rotation, and inter-particle interaction. The second approach uses the complex Langevin (CL) method – a method which employs an extension of the Langevin equation to complex space and circumvents the sign problem to compute the full quantum behavior of a low energy system of interacting, trapped, and rotating bosons.

We examine the density and angular momentum of the system using all three methods, but the CL method in principal allows us to compute properties unique to rotating superfluids, in particular to show the formation of density singularities (so-called vortex lattices) and compute the circulation of the fluid around those vortices. This work advances our understanding of the quantum effects of rotation on ultracold bosonic gases in two different limits.

ACKNOWLEDGEMENTS

I was fortunate to have a strong support system to see me through my doctoral degree. Foremost, I am grateful for the financial and professional support of two wonderful and unique fellowship programs. The Department of Energy's Computational Science Graduate Fellowship and UNC's Royster Society of Fellows provided not just financial support but two active and vibrant communities of interdisciplinary scholars which became the twin pillars of my doctoral community. I can't thank enough the incredible teams at the Krell Institute and UNC's Graduate School who made sure fellows were able to take full advantage of the opportunities these programs provide. In particular, the two Royster Professors I had the privilege of working with, Professor Marsha Collins and Professor Banu Gökarıksel, both helped me take on leadership roles and become a better teacher, communicator, and colleague.

A few of my colleagues deserve special mention. Jessie: for the weekly lunches and coffee dates, your moral support and encouragement, and your unfailing reminders that we are more than the data we produce. Lukas: for all the enlightening discussions of theory and practical matters in computation, your consistent and infectious enthusiasm, and your thorough feedback on the dissertation which helped me produce a much better final draft. Lauren: for taking me under your wing when I was a confused undergraduate at my first conference, your steady wisdom and outside perspective, and your confidence in my ability to persevere. Jay: for your constant willingness to help, your mentorship in the earliest days of my research career, and your unending thoughtfulness. Emily: for being right there with me through the final push, for giving me snacks and a space to produce my first full draft, and for giving me a much-needed window into the world outside science.

Outreach gave me a window into why this work matters and surrounded me with people who could help me remember those lessons. The SciREN Triangle team worked tirelessly every year to put together an amazing event connecting research to the classroom, and their enthusiasm and energy was infectious. Thanks for making my job easy. And all the members of UNC's Womxn in Physics group and AMWISE who were always pushing for more acceptance and support for underrepresented folks in the sciences. This community was my lifeline: thank you all for being lights in the dark.

I am lucky to have a loving and supportive family, both of the blood relative variety and the kind we choose for ourselves. Katie, Mary Beth, and Larkin, who have been there through my best days and my worst ones. Joe, who keeps me from taking myself too seriously. Liz, who didn't get to see me make it to the end of this journey, but whose memory gives me strength. The Baumanns, who adopted me wholeheartedly and enrich my life in more ways than I can count. The Bergers: Mom, Dad, Michael, and Alannah, who have been on this journey with me, whether they liked it or not, and I'm thankful to have all of their support and love.

And finally, the biggest thank you goes to Justin, who cooked too many dinners alone during my first year of grad school and my last, who celebrated even the smallest of victories with me, who believed in me from the moment we met. For every other thing that I don't have room to enumerate here, thank you.

TABLE OF CONTENTS

LIST OF FIGURES

LIST OF TABLES

LIST OF ABBREVIATIONS

QFT	quantum field theory
QCD	quantum chromodynamics
SCLA	semi-classical lattice approximation
CL	complex Langevin
QED	quantum electrodynamics
QMC	quantum Monte Carlo
GPE	Gross-Pitaevskii Equations
1D	one spatial dimension
2D	two spatial dimensions
3D	three spatial dimensions
FPE	Fokker-Planck Equation
MCMC	Markov chain Monte Carlo

LIST OF SYMBOLS

G	Newton's gravitational constant
e	electron charge
ϵ_0	permittivity of free space
$\hbar$	reduced Planck constant
a_0	Bohr radius
S	action
$\mathcal{Z}$	path integral, grand-canonical partition function
v_c	critical velocity
ϵ_p	energy of excitations of a Bose-Einstein condensate
T_c	critical temperature
$\mathcal{L}$	Lagrangian
λ	contact interaction strength
ϕ	complex scalar field
$\hat{H}$	Hamiltonian operator
$\hat{T}$	kinetic energy operator
$\hat{V}$	potential energy operator
$\hat{L}_z$	angular momentum operator
$\hat{I}_z$	moment of inertia operator
$\hat{n}$	particle density operator
g	bare lattice interaction parameter
β	inverse temperature
μ	chemical potential
ω_{tr}	trapping frequency
ω_z	rotational frequency
b_n	n-th order virial coefficient
z	fugacity
Ω	grand thermodynamic potential
$\hat{N}$	particle number operator

$\mathcal{P}$	probability
s_i	spin value for lattice site i
J	spin interaction coupling
H	magnetic field strength
M	magnetization
α	spin lattice configuration
K	Langevin drift term
η	Weiner noise term
τ	Euclidean time/imaginary time
Q_N	N-body canonical partition function
E	energy
$L_k^{\lvert m\rvert}$	associated Laguerre functions
$P_l^m(x)$	associated Legendre functions
a	spatial lattice spacing
N_x	number of spatial lattice sites
$\mathrm{d}\tau$	temporal lattice spacing
N_τ	number of temporal lattice sites
t_L	Langevin time
ϵ	Langevin stepsize
V	spacetime lattice volume
τ_A	autocorrelation time
σ^2	variance
Δ_A	autocorrelation error
δ_{ab}	kronecker delta
ϵ_{ab}	2 dimensional Levi-Civitas symbol

CHAPTER 1: Introduction

Quantum many-body systems are foundational to a wide range of interesting physical topics, from very small scales (the quark-gluon plasma of the early universe) to very large ones (understanding the structure of neutron stars). Advances in theoretical treatment of these systems can aid in the development of novel materials, provide insights into the stability of nuclei, push forward the boundaries of knowledge about the origin of the universe, and more. However, all but the simplest of these systems can be extremely challenging to understand at a detailed level. Very few are accessible using analytical methods, and those which must be calculated computationally frequently have limitations that prevent us from exploring some of the most interesting physics.

This thesis explores one such system: rotating, interacting bosonic systems. The physics at the heart of these systems is relevant across disciplines, from astrophysics to quantum materials to nuclear structure. We begin with the kind of straightforward problem an undergraduate can solve and show how quickly the complexity grows once we consider interacting quantum systems with many particles.

Section 1.1: From two- to many-body systems

1.1.1: The classical N-body problem

As with all complicated problems, it is best to start with the simplest possible version and build from there. To understand the challenges of the quantum N-body problem, we begin with a problem that all undergraduates learn to solve in the early years of their physics courses: the classical two-body problem[1].

The classical two-body problem is most often introduced when students learn orbital mechanics, in the context of the earth-sun interaction. The earth and the sun are two massive objects which exert equal and opposite force on each other. The motion of the two bodies is determined by the gravitational force between them. Since this force is a Newton's third law pair, we are able to take advantage of the symmetries and conservation laws of this system to greatly reduce the complexity of the problem.

The total momentum of the system is a conserved quantity, so we can perform a change of variables. Instead of measuring our coordinates $\mathbf{r}_1$ and $\mathbf{r}_2$ relative to some external origin, we choose to express the

[1]This is a common example in advanced undergraduate physics courses, and can be found worked out in detail in Refs. [2, 3]

equations above in terms of the center of mass coordinate measured relative to that external origin, **R**, and the relative separation between the two bodies, **r**, and then the principles of conservation of momentum can be applied. Since the total momentum is conserved, the center of mass velocity must be constant, and therefore the center of mass motion, denoted by **R**, becomes a simple linear function of time:

$$\mathbf{R} = \mathbf{v}_{\mathrm{CM}}\, t \tag{1.1}$$

and our two-coordinate problem has now been reduced to a one-coordinate problem. All that remains is to solve for **r** which, while often not trivial, is something that can be done in a straightforward manner.

This classical two-body problem serves as a starting point for the more complicated classical N-body problem, which can't be solved by hand for large N, but can be solved numerically. The equations of motion are given by

$$\ddot{\mathbf{r}}_i = -G \sum_{j=1, j\neq i}^{N} \frac{m_j(\mathbf{r}_i - \mathbf{r}_j)}{|\mathbf{r}_i - \mathbf{r}_j|^3}. \tag{1.2}$$

This is a $6N$-dimensional ordinary differential equation with time being the only degree of freedom and can be solved for some large number of objects, N, with memory requirements scaling linearly with the number of objects.

This is, as mentioned above, a much simpler case than the quantum N-body problem, but it serves to establish the approaches to problems such as these: use symmetries and conservation laws to reduce the problem complexity and then solve computationally. Unfortunately, as we shall soon see, this is a necessary but not sufficient step for studying quantum many-body systems, and quantum many-body problems will require more sophisticated methods to solve, even computationally.

1.1.2: The quantum N-body problem

Quantum mechanics has its own canonical two-body problem: the hydrogen atom. Typically studied in advanced undergraduate quantum courses, this example shows immediately how quantum behavior introduces its own challenges to the approach. Still, it remains a problem with an exactly-solvable three-dimensional wave function, in the absence of external fields or interactions. The approach is fundamentally similar to the classical case, but while in classical mechanics we solve Newton's equations of motion, in quantum

mechanics we solve the Schrödinger equation. The Schrödinger equation for the hydrogen atom is:

$$-\left[\frac{\hbar^2\nabla_p^2}{2m_p}+\frac{\hbar^2\nabla_e^2}{2m_e}+\frac{e^2}{4\pi\epsilon_0 r}\right]\Psi(\mathbf{r}_e,\mathbf{r}_p)=E\Psi(\mathbf{r}_e,\mathbf{r}_p), \tag{1.3}$$

where r is here defined as the magnitude of the separation between the electron and the proton, $r=|\mathbf{r}_e-\mathbf{r}_p|$ [4–6], E is the energy of the system, and we are solving for the quantum wave-function, Ψ.

This equation has two useful features which make it a relatively simple problem. First, the solutions to this equation have no time dependence; and second, since the Coloumb potential $V(r)=-\frac{e^2}{4\pi\epsilon_0 r}$ depends only on the separation $r=|\mathbf{r}_e-\mathbf{r}_p|$, a change of variables can be applied, and the equation can be separated into two independent equations, just as we did in the classical two-body problem, where our central potential was gravitational rather than electrical.

The appropriate change of variables is from $\mathbf{r}_e$ and $\mathbf{r}_p$ to the center of mass coordinate $\mathbf{R}$ and the relative coordinate $\mathbf{r}$, defined below:

$$\mathbf{R}=\frac{m_e\mathbf{r}_e+m_p\mathbf{r}_p}{m_e+m_p}, \text{ and } \mathbf{r}=\mathbf{r}_e-\mathbf{r}_p. \tag{1.4}$$

With the introduction of total ($M=m_e+m_p$) and reduced ($\mu=\frac{m_e m_p}{M}$) masses, the new Schrödinger equation is given by:

$$\left[-\frac{\hbar^2}{2M}\nabla_R^2-\frac{\hbar^2}{2\mu}\nabla_r^2-\frac{e^2}{4\pi\epsilon_0 r}\right]\Psi(\mathbf{R},\mathbf{r})=E\Psi(\mathbf{R},\mathbf{r}), \tag{1.5}$$

which can be solved using separation of variables.

The solution to the center of mass equation is that of a free particle of mass M (just as in the classical case), making it uninteresting to the internal structure of the hydrogen atom. It is the solution to the relative motion equation which is of interest; the relationship between the proton and electron is what gives the hydrogen atom its quantized values of energy and angular momentum.

This is an eigenvalue problem, and the solutions to $\Psi(r,\theta,\phi)=Y_{lm}(\theta,\phi)R(r)$ are the joint eigenstates of the energy ($\hat{H}$) and angular momentum operators ($\hat{L}^2$ and $\hat{L}_z$). For simplicity, we define a dimensionless coordinate, $\rho=\frac{r}{a_0}$, where

$$a_0=\frac{4\pi\epsilon_0\hbar^2}{\mu e^2}, \text{ and } \widetilde{E}=\frac{2\mu a_0}{\hbar^2}E. \tag{1.6}$$

The constant a_0 is the Bohr radius, which is a physical constant corresponding to the average distance of the electron from the nucleus in the ground state. Now the radial equation reads:

$$\frac{-d}{d\rho}\left(\rho^2\frac{dR(\rho)}{d\rho}\right) + \left(\ell(\ell+1) - 2\rho - \widetilde{E}\rho^2\right)R(\rho) = 0 \tag{1.7}$$

The solutions to this equation are related to the associated Laguerre polynomials L_n^k [7]:

$$R_{n\ell}(r) = N\left(\frac{2r}{na_0}\right)^{\ell} e^{-r/(na_0)} L_{n+\ell}^{2\ell+1}\left(\frac{2r}{na_0}\right), \tag{1.8}$$

where ℓ and n are integers and N is obtained by normalizing the radial wave function. Thus, the final hydrogen wave functions are described by

$$\Psi(r) = N\left(\frac{2r}{na_0}\right)^{\ell} e^{\frac{-r}{na_0}} L_{n+\ell}^{2\ell+1}\left(\frac{2r}{na_0}\right) Y_{\ell m}(\theta,\phi) \tag{1.9}$$

with n, ℓ, and m all quantum numbers describing the state. The unperturbed hydrogen energy eigenstates are

Operator	Eigenvalue	State	Range
H_0	$-\frac{e^2}{8\pi\epsilon_0 a_0} = \frac{E_1}{n^2}$	$\|n\rangle$	$n = 1, 2, ..., \infty$
L^2	$\hbar^2\ell(\ell+1)$	$\|\ell\rangle$	$\ell = 0, ..., n-1$
L_z	$\hbar m$	$\|m\rangle$	$m = -\ell, -\|\ell-1\|, ..., \ell-1, \ell$

Table 1.1: The energy H_0, total angular momentum L^2, and z-component of the angular momentum L_z are all operators which are simultaneous eigenstates of the unperturbed hydrogen Hamiltonian.

eigenstates of three operators simultaneously: the Hamiltonian or bare hydrogen atom energy $\hat{H}$ (principal quantum number, n), the total angular momentum squared $\hat{L}^2$ (angular quantum number ℓ), and the z-component of angular momentum $\hat{L}_z$ (magnetic quantum number m). Table 1.1 illustrates these values, the operators they correspond to, their eigenvalues and eigenvectors (states), and the restrictions on their range.

Beyond the hydrogen atom, we quickly depart the realm of exactly-solvable quantum systems. While in principle, the process is straightforward (i.e. solve the N-body Schrödinger equation), in practice, this is only possible for a small number of scenarios, often ones which tell us very little about the complicated physics seen in the universe. The presence of more than two particles with at least a two-body interaction quickly yields intractable equations.

As most of the questions we can pose about the universe – e.g., what is the atomic structure of a particular material? Why are some nuclei stable and others not? What is the internal structure of a neutron

star? – are about large numbers of particles interacting with each other and the environment, this provides a strong motivation for developing new methods to solve for the equations of motion of these systems. Many approaches have been taken to this challenge, and different disciplines prefer different classes of methods. Mean-field theories and related approaches are common in condensed matter and materials science; coupled cluster approaches are often seen both in nuclear theory and quantum chemistry; and lattice gauge theory is employed largely in relativistic systems like quantum chromodynamics (QCD) and quantum electrodynamics (QED). These methods are all united by the need for computational resources to evaluate these numerically-intensive systems.

Section 1.2: Stochastic methods and the sign problem

Computational methods have allowed for great advances in understanding of quantum many-body systems. However, limitations still exist. The computational complexity of many quantum problems scales exponentially with the size of the system due to the size of the underlying Hilbert space, meaning that many systems of great interest are still inaccessible due to lack of fast or powerful enough computers. Nuclear structure is one such example; numerical solutions to the many-nucleon Schrödinger equation can only be achieved for nuclei with atomic mass number of up to four. With well-controlled approximations and innovative methods, calculations can be done for heavier nuclei – up to nickel ($A = O(60)$) [8]. Innovative methods are what drive advancement in many-body quantum mechanics. Exact solutions to the many-body Schrödinger equation simply require more computational resources than exist, and so creative and intelligent alternatives must be developed.

Among these alternatives are quantum Monte Carlo (QMC) methods. These are a well-established set of methods for calculating properties of quantum many-body systems. Their applications cover a massive range of energy scales, from QCD to *ab initio* nuclear structure to neutron stars, and they provide a stable technique for calculating properties of these systems. These methods take advantage of similarities between path integral formulations of quantum mechanics and the statistical mechanics partition function in order to construct a well-behaved probability distribution from which behavior of the system can be sampled using a Markov chain method.

In the path integral formulation of quantum mechanics, the probability amplitude for a quantum process is found by integrating over all possible paths. The contribution of each path is weighted by e^{iS}, where S is

the action. This allows for the calculation of observables, as shown here:

$$\mathcal{Z} = \int \mathcal{D}x e^{iS[x]} \tag{1.10}$$

$$\langle O \rangle = \frac{1}{\mathcal{Z}} \int \mathcal{D}x e^{iS[x]} O(x). \tag{1.11}$$

Assuming a real action, $S[x]$, the complex weight can be made real by performing a Wick rotation $it \rightarrow \tau$, such that now our observable is the integral of that observable over all paths x weighted by a probability measure for that path:

$$\langle O \rangle = \frac{1}{\mathcal{Z}} \int \mathcal{D}x \, \mathcal{P}(x) O(x). \tag{1.12}$$

$$\mathcal{P}(x) = e^{-S[x]}. \tag{1.13}$$

This formulation lends itself to a stochastic treatment of the path integral.

Quantum many-body problems can be written in terms of quantum fields, using quantum field theory (QFT). The fields can then be discretized and placed on a spacetime lattice, a strategy known as lattice field theory. The benefit of lattice methods is that the resulting path integral can often be evaluated stochastically, and the expectation value of an observable can be given by

$$\langle O \rangle \approx \frac{1}{N} \sum_{n=1}^{N} O_n, \tag{1.14}$$

where N is the number of configurations sampled, and O_n is the value of the observable calculated with lattice configuration n. If a good probability measure can be defined for the system, i.e. if $\mathcal{P}(x) = e^{-S[x]}$ is real and positive-definite, then the solution is exact with systematic uncertainties determined entirely by lattice parameters and statistical uncertainties due to the number of samples. Thus, overall uncertainty can be controlled by varying lattice size and spacing and number of samples.

1.2.1: The sign problem in quantum many-body physics

Some quantum many-body systems are inaccessible to QMC methods, for varying reasons. One of the largest sets of these systems are those which suffer from the sign problem, also called the complex phase problem. This is part of a larger group in computer science known as NP-hard problems, for which no general solution is expected to exist (although it remains a topic of ongoing research). The sign problem can arise when a system doesn't have the desired behavior: a real, positive-valued weight in the path integral. In

this case, the crucial step for QMC approaches – i.e. treating the weight like a probability distribution from which we can sample values of the fields and the observables – becomes invalid.

If the action of a quantum many-body system is real and positive, we can use standard Monte Carlo methods to evaluate the path integrals and compute observables. Howevever, there are many very important cases when this condition is not satisfied, for example strongly-interacting QCD systems with non-vanishing chemical potential and superconductors and superfluids under specific conditions. The sign problem confounds our ability to make progress in these areas with the methods that have been so effective in so many quantum many-body systems. In order to move forward in understanding these systems, we must develop new methods to circumvent the sign problem.

Section 1.3: Superfluidity

Superfluids, in the simplest terms, are fluids that flow without friction. In slightly less simple terms, they transport a conserved charge (e.g. mass, particle number, electric charge) without loss of energy due to dissipation for velocities smaller than some critical velocity:

$$v_c = \min_p \frac{\epsilon_p}{p} \tag{1.15}$$

where ϵ_p is the energy of the excitations on the condensate and p is its corresponding momentum.[2]

This behavior was first observed in liquid helium, but can appear in a wide range of substances. Superfluidity is in fact a phase of a system, which occurs below a critical temperature. This temperature can vary wildly across systems, which means superfluidity is a state observed across a dramatic range of energy scales, from helium and other ultracold atomic gases at one end ($T_c \approx 10^{-7} K$) to quark matter at the other end ($T_c \approx 10^{11} K$).

The frictionless flow of a superfluid is not its only remarkable behavior. Superfluid velocity has no curl, and therefore is irrotational. However, nonzero hydrodynamic circulation can exist, and must be quantized in units of $2\pi\hbar/m$, where m is the mass of the particles comprising the superfluid. If we try to rotate superfluid helium – or another cold atomic gas – it develops spontaneous vortices in direct proportion to the amount of angular momentum imposed on the system. This has been predicted as a direct result of the properties of superfluids (see e.g. Refs. [11–13]) and observed in experiments with ultracold atoms (see e.g.

[2]For more information about superfluids, references [9] and [10] provide an excellent framework, on which the discussions in this section were built.

Refs [14–17]).

Superfluids share much with their phenomenological cousin, superconductors. While the two phenomena are not identical, superconductors are also a phase of a system in which a conserved charge is transported without energy loss. Superconductors break a local symmetry, while superfluids break a global symmetry – this is the fundamental difference that separates them on a theoretical level. The strong connections between the two – particularly their dissipationless transport – makes them together a subject of active inquiry.

We can build a theory of superfluids using a complex scalar field. The Lagrangian of the system will be invariant under U(1) symmetry, and a necessary condition for superfluidity is the spontaneous breaking of this U(1) symmetry, i.e. the ground state of the system will not be invariant under this symmetry even though its Lagrangian is. The critical temperature is the point above which the superfluid has “melted," i.e. the point where the ground state *is* symmetric under U(1).

Our system – which can become a superfluid below some critical temperature – is a complex scalar field, representing spin-0 bosons with mass m and interacting via a repulsive contact interaction $\lambda > 0$. The Lagrangian for our system is as follows

$$\mathcal{L} = \partial_\mu \phi^* \partial^\mu \phi - m^2 |\phi|^2 - \lambda |\phi|^4 \tag{1.16}$$

This Lagrangian is invariant under U(1) rotations of the field, that is $\mathcal{L}$ is unchanged for

$$\phi \to e^{-i\alpha} \phi \tag{1.17}$$

which is a global symmetry, as α is a constant and does not depend on spacetime.

There will also be a conserved charge – this is what is transported by the superfluid without loss of energy – and this will arise from Noether's theorem. Generally, the conserved charge of interest with superfluids is a particle number charge.

While superfluidity is in essence a bosonic phenomenon, it does occur under certain circumstances in fermionic substances. Cooper pairing allows fermions to form bosonic states: Fermi surfaces are unstable for attractive interactions between the fermions, no matter how small the attraction strength, and this instability causes a new ground state to manifest, where the fermions form pairs at the Fermi surface. This is best known in the case of electronic superconductors, where the Cooper pairing of electrons leads to a state much

like superfluidity, with a vanishing resistivity below some critical temperature.

Helium 3 is also fermionic, but forms Cooper pairs due to an attractive interaction between the atoms, and can form multiple different superfluid phases. This has been observed in other ultracold atomic gases, most notably by the Ketterle group [18], where vortex formation in lithium 6 demonstrated a superfluid state. In high-energy physics, color superconductors may form in quark matter and inside dense stars.

Section 1.4: Superfluids and rotation

The spontaneous appearance of quantized vortices in a lattice structure is a characteristic feature of superfluids at thermal equilibrium [19–22]. These effects are related to rotation and also external magnetic fields [23], and the vortices can have dynamics that interact with sound waves [24]. Addition of spin-orbit coupling creates further complexity in the system, leading to unique phases depending on the type of coupling [25–28]

In 1949, Lars Onsager first predicted that vortices would form in rotating superfluids [12]. Richard Feynman expanded on Onsager's prediction a few years later, reiterating the expectation that quantized vortices would appear when superfluids were forced to rotate [13]. Another thirty years after these predictions, the first direct observation of quantum vortices was made in rotating superfluid ^{4}He [29]. Experimentally, great progress has been made in studying rotating superfluids since the first direct observation of vortex formation. In 2000, vortex formation was observed in stirred, magnetically-trapped rubidium atoms [17]. The next year, triangular vortex lattices of up to 130 vortices were observed in rotating ultracold sodium atoms [14]. Ultracold atoms provide a highly controlled, tuneable setting for studying vortex formation and other properties of rotating superfluids.

Adding rotation into a complex scalar field introduces new challenges into theoretical treatments of the system. While a nonrelativistic complex scalar field already yields a potential sign problem in stochastic treatments, there are ways to get around this sign problem. The additional complexity of the angular momentum term in the action eliminates those possibilities and yields an irretrievably complex weight for stochastic sampling. As a result, most theoretical work done on rotating superfluids is done using mean-field treatments such as the Gross-Pitaevskii Equations (GPE). These equations have been very successful in describing mean-field behavior of rotation in superfluids, including the spontaneous formation of vortices, but stop short of a fully quantum examination of the system [19].

Rotating bosons exist in important physical systems that cut across disciplines. They are of interest in

condensed matter for understanding the effect of a magnetic field on superconductors, in nuclear physics for describing the behavior of rotating nuclei, and in astrophysics for illuminating the physics of neutron stars and pulsars. In order to continue to progress in these areas of physics, a method to work around the sign problem must be used. Theoretically, treatment of these systems has stalled due to the presence of the sign problem, and the subject of this thesis is to explore alternative methods to understanding rotating bosonic systems.

Section 1.5: Outline

In Chapter 2, we explore an approximate method for describing the behavior of trapped, interacting, non-relativistic many-body bosonic systems under rotation. This approximation is known as the virial expansion and is valid only for certain temperature and density regimes. While useful for elucidating the behavior of these systems at higher temperatures, we desire to use stochastic methods to understand the full quantum effects of rotation. To that end, we introduce a method in Chapter 3 called complex Langevin, which allows us to study systems with a complex action stochastically rather than by using high-temperature or dilute-system approximations. In Chapter 4, we apply this method to a relativistic Bose gas, as a proof of concept and to illustrate the finer points of the method. And finally, in Chapter 5, we apply this method to a nonrelativistic, harmonically-trapped, rotating, and interacting system of bosons, which in the low-temperature regime is a rotating superfluid. We discuss the results of this method and compare them with our virial expansion, in order to shed light on some of the challenges of treating this system.

CHAPTER 2: Semi-classical lattice approximation for trapped, rotating, interacting quantum matter

Section 2.1: Motivation: why use a semi-classical lattice approximation?

One way to avoid the sign problem quantum many-body systems is to use approximate methods. Despite their limitations, approximations are excellent tools that can allow us to examine interesting behavior in particular regimes without having to encounter the sign problem that can arise in a full stochastic calculation. Often, they are our only way to benchmark numerical results.

In this case, we apply the virial expansion to a system of trapped, rotating, interacting bosons in 2D and 3D and implement a semiclassical lattice approximation (SCLA) recently put forward in Refs. [30–32], where it was applied to non-rotating matter.While these systems are not in themselves rotating superfluids, they have the same field theoretical structure and in the right temperature and density regime could support superfluidity. The approximation allows us to bypass the requirement of solving the N-body problem to access the n-th order virial coefficient and describe the thermodynamics of the system using a virial expansion. The virial expansion is valid in a high-temperature, low-density limit, while the semi-classical lattice approximation requires that we use a strongly-interacting or weakly-interacting regime. In this case, we look at the weakly-interacting case, where the interaction potential is significantly smaller than the noninteracting Hamiltonian.

Section 2.2: Hamiltonian and formalism

We use a Hamiltonian formalism to generate our virial coefficients, as it lends itself well to the manipulation of the partition function. Our Hamiltonian is composed of both a non-interacting term H_0 and an interacting term H_{int}:

$$\hat{H} = \hat{H}_0 + \hat{V}_{\text{int}}. \tag{2.1}$$

The noninteracting term can be further broken up into three contributions:

$$\hat{H}_0 = \hat{T} + \hat{V}_{\text{ext}} + \omega_z \hat{L_z}, \tag{2.2}$$

where

$$\hat{T} = \sum_{s=1,2} \int d^d x \, \hat{\psi}_s^\dagger(\mathbf{x}) \left(-\frac{\hbar^2 \nabla^2}{2m} \right) \hat{\psi}_s(\mathbf{x}), \tag{2.3}$$

is the kinetic energy,

$$\hat{V}_{\text{ext}} = \frac{1}{2} m \omega_{\text{tr}}^2 \int d^d x \, \mathbf{x}^2 \, (\hat{n}_1(\mathbf{x}) + \hat{n}_2(\mathbf{x})), \tag{2.4}$$

is the spherically symmetric external trapping potential in d dimensions, and

$$\hat{L}_z = i \sum_{s=1,2} \int d^d x \, \hat{\psi}_s^\dagger(\mathbf{x}) \left(x \partial_y - y \partial_x \right) \hat{\psi}_s(\mathbf{x}), \tag{2.5}$$

is the angular momentum operator in the z direction. The interaction term is given by

$$\hat{V}_{\text{int}} = -g \int d^d x \, \hat{n}_1(\mathbf{x}) \hat{n}_2(\mathbf{x}), \tag{2.6}$$

with g the bare interaction parameter, and where, for the sake of simplicity, we restrict ourselves to two particle species with a contact interaction across species (i.e. no intra-species interaction).

In the above equations, the field operators $\hat{\psi}_s, \hat{\psi}_s^\dagger$ correspond to particles of species $s = 1, 2$, and $\hat{n}_s(\mathbf{x})$ are the coordinate-space densities. In the remainder of this chapter, we will use units such that $\hbar = k_{\text{B}} = m = 1$.

2.2.1: Thermodynamics and the virial expansion

The grand-canonical partition function describes the statistical properties of the the quantum many-body system, as all the thermodynamic quantities of interest can be determined from it. It has the general form

$$\mathcal{Z} = \text{Tr} \left[e^{-\beta(\hat{H} - \mu \hat{N})} \right] = e^{-\beta \Omega}, \tag{2.7}$$

where β is the inverse temperature, $\hat{H}$ is the Hamiltonian given in Eq. (2.1), Ω is the grand thermodynamic potential, $\hat{N}$ is the total particle number operator, and μ is the overall chemical potential.

As the direct calculation of $\mathcal{Z}$ is a challenging problem in the presence of interactions, we will use the virial expansion, which is an expansion around the dilute limit $z << 1$, where $z = e^{\beta \mu}$ is the fugacity. This

is given by

$$-\beta\Omega = \ln \mathcal{Z} = Q_1 \sum_{n=1}^{\infty} b_n z^n. \tag{2.8}$$

The coefficients b_n are known as the virial coefficients, and Q_1 is the one-body partition function, which can be calculated directly without too much trouble, as there is no interaction present (we will show this calculation in Section. 2.2.2). This expansion is valid for small values of the fugacity, which can be affected by both the temperature ($T \propto 1/\beta$) and chemical potential of the system.

We can compare this virial expansion for the partition function with the expression of the grand-canonical partition function in terms of the canonical partition functions Q_N of all possible particle number N:

$$\mathcal{Z} = \sum_{N=0}^{\infty} z^N Q_N, \tag{2.9}$$

and thereby obtain expressions for the virial coefficients

$$b_1 = 1, \tag{2.10}$$

$$b_2 = \frac{Q_2}{Q_1} - \frac{Q_1}{2!}, \tag{2.11}$$

$$b_3 = \frac{Q_3}{Q_1} - b_2 Q_1 - \frac{Q_1^2}{3!}, \tag{2.12}$$

and to higher order. The quantity we are interested in is the change in these virial coefficients due to rotation:

$$\delta b_n = b_n^{(0)}(|\omega_z| > 0) - b_n^{(0)}(\omega_z = 0) \tag{2.13}$$

and due to the presence of interactions:

$$\Delta b_n = b_n - b_n^{(0)} \tag{2.14}$$

where $b_n^{(0)}$ is the virial coefficient of the system when there are no interactions.

The Q_N can themselves be written in terms of the partition functions $Q_{a,b}$ for a particles of type 1 and

b particles of type 2:

$$Q_1 = Q_{1,0} + Q_{0,1} = 2Q_{1,0}, \tag{2.15}$$

$$Q_2 = Q_{2,0} + Q_{0,2} + Q_{1,1} = 2Q_{2,0} + Q_{1,1}, \tag{2.16}$$

$$Q_3 = Q_{3,0} + Q_{0,3} + Q_{2,1} + Q_{1,2} = 2Q_{3,0} + 2Q_{2,1}, \tag{2.17}$$

and so on for higher orders. In the absence of intra-species interactions, only the $Q_{1,1}$ and $Q_{2,1}$ are affected, such that the change in b_2 and b_3 due to interactions is entirely given by

$$\Delta b_2 = \frac{\Delta Q_{1,1}}{Q_1}, \tag{2.18}$$

$$\Delta b_3 = \frac{2\Delta Q_{2,1}}{Q_1} - \Delta b_2 Q_1. \tag{2.19}$$

We will use these expressions to access the high-temperature thermodynamics of the bosons in this system and examine their dependence on the rotation frequency (expressed in dimensionless form as $\beta\omega_z$), the strength of the trapping potential (in dimensionless form, $\beta\omega_{\rm tr}$), and inter-particle interaction (whose dimensionless form, λ, will depend on the bare coupling g and the dimensionality d).

2.2.2: Semiclassical lattice approximation

To calculate the interaction-induced change in the canonical partition functions $\Delta Q_{1,1}$ and $\Delta Q_{2,1}$, we use an approximation. The exponential of the sum of two non-commuting operators can be related to the product of the two exponentiated operators via an infinite series (the Baker-Campbell-Hausdorff formula) [6, 33]:

$$e^{A+B} = \sum_{n=0}^{\infty} \frac{(A+B)^n}{n!} = I + A + B + \frac{1}{2}(A+B)(A+B) + \ldots \tag{2.20}$$

$$e^A e^B = e^{A+B+\frac{1}{2}[A,B]+\ldots} \tag{2.21}$$

Our approximation consists in keeping only the leading term in the Magnus expansion derived from the Baker-Campbell-Hasudorff formula:

$$e^{-\beta(\hat{H}_0+\hat{V}_{\rm int})} = e^{-\beta\hat{H}_0} e^{-\beta\hat{V}_{\rm int}} \times e^{-\frac{\beta^2}{2}[\hat{H}_0,\hat{V}_{\rm int}]} \times \ldots, \tag{2.22}$$

where the higher orders involve exponentials of nested commutators of $\hat{H}_0$ with $\hat{V}_{\rm int}$. Thus, the leading order in this expansion consists in setting $[\hat{H}_0, \hat{V}_{\rm int}] = 0$, which becomes exact in the limit where either $\hat{H}_0$ or $\hat{V}_{\rm int}$

can be ignored (i.e. respectively the strong- and weak-coupling limits).

Single-particle bases in 2D and 3D

In evaluating the results of the semiclassical lattice approximation, we will make use of the eigenstates of $\hat{H}_0$ in 2D polar coordinates and 3D spherical coordinates.

Two spatial dimensions.- The single-particle eigenstates of $\hat{H}_0$ in 2D are given by

$$\langle \mathbf{x}|\mathbf{k}\rangle = \frac{1}{\sqrt{2\pi}} R_{km}(\rho) e^{im\phi}, \tag{2.23}$$

where

$$R_{km}(\rho) = N_{km}^{(2\mathrm{D})} \sqrt{\omega} e^{-\rho^2/2} \rho^{|m|} L_k^{|m|}(\rho^2), \tag{2.24}$$

where $\rho = \sqrt{\omega} r$ and

$$N_{km}^{(2\mathrm{D})} = \sqrt{2} \sqrt{\frac{k!}{(k+|m|)!}}, \tag{2.25}$$

with $L_k^{|m|}$ the associated Laguerre functions. We have used polar coordinates r, ϕ, and a collective quantum number $\mathbf{k} = (k, m)$, with $k = 0, 1, \ldots$ and m any integer value. The corresponding energy is

$$E_{km} = \omega_{\mathrm{tr}}(2k + |m| + 1) + \omega_z m \tag{2.26}$$

These eigenstates are derived in more detail in Appendix A.1.

Three spatial dimensions.- The single-particle eigenstates of $\hat{H}_0$ in 3D are

$$\langle \mathbf{x}|\mathbf{k}\rangle = R_{kl}(\rho) P_l^m(\cos\theta) e^{im\phi}, \tag{2.27}$$

where $P_l^m(x)$ are the associated Legendre functions and

$$R_{kl}(\rho) = N_{kl}^{(3\mathrm{D})} \omega_{\mathrm{tr}}^{3/4} e^{-\rho^2/2} \rho^l L_k^{l+1/2}(\rho^2), \tag{2.28}$$

where

$$N_{kl}^{(3\mathrm{D})} = \sqrt{\frac{1}{\sqrt{4\pi}} \frac{2^{k+2l+3}\, k!}{(2k+2l+1)!!}}. \tag{2.29}$$

Here, we have used spherical coordinates r, θ, ϕ, where θ is the polar angle, and ϕ the azimuthal angle. The collective quantum number $\mathbf{k} = (k, l, m)$ is such that $k \geq 0$, $l \geq 0$, and $-l \leq m \leq l$. The corresponding energy is

$$E_{k\ell m} = \omega_{\mathrm{tr}}(2k + l + 3/2) + \omega_z m. \tag{2.30}$$

The eigenstates in 3D have been derived in great detail in many references, as the single-particle wave function is the same as that of an electron in a hydrogen atom. For detailed derivations, see e.g. Refs [4–7].

Single-particle partition function Q_1

As mentioned above, Q_1 can be computed straightforwardly. The single-particle partition function is described as

$$Q_1 = \sum_{\mathbf{k}} e^{-\beta E_{\mathbf{k}}}. \tag{2.31}$$

Thus, in 2D,

$$Q_1 = 2 \sum_{k,m} e^{-\beta E_{km}} = \frac{2\, e^{-\beta\omega_{\mathrm{tr}}}}{(1 - e^{-\beta\omega_+})(1 - e^{-\beta\omega_-})}, \tag{2.32}$$

where $\omega_\pm = \omega_{\mathrm{tr}} \pm \omega_z$ and the overall factor of 2 reflects the fact that we have two particle species.

Similarly, in 3D,

$$Q_1 = 2e^{-\beta\omega_{\mathrm{tr}}3/2} \frac{1}{(1 - e^{-2\beta\omega_{\mathrm{tr}}})(1 - e^{-\beta\omega_z})} \left[\frac{1}{1 - e^{-\beta\omega_-}} - \frac{e^{-\beta\omega_z}}{1 - e^{-\beta\omega_+}} \right]. \tag{2.33}$$

Two-body contribution $\Delta Q_{1,1}$.

The calculation of the first nontrivial virial coefficient, Δb_2, in our semiclassical approximation requires the above result for Q_1 and $\Delta Q_{1,1}$. At leading order,

$$Q_{1,1} = \mathrm{Tr}_{1,1}\left[e^{-\beta\hat{H}_0}e^{-\beta\hat{V}_{\mathrm{int}}}\right], \tag{2.34}$$

where $\mathrm{Tr}_{1,1}$ represents the trace of the matrix when we have a single particle of each species. This leads to

$$\begin{aligned} Q_{1,1} &= \sum_{\mathbf{k}_1,\mathbf{k}_2,\mathbf{x}_1,\mathbf{x}_2} \langle \mathbf{k}_1\mathbf{k}_2|e^{-\beta\hat{H}_0}|\mathbf{x}_1\mathbf{x}_2\rangle\langle\mathbf{x}_1\mathbf{x}_2|e^{-\beta\hat{V}_{\mathrm{int}}}|\mathbf{k}_1\mathbf{k}_2\rangle \\ &= \sum_{\mathbf{k}_1,\mathbf{k}_2,\mathbf{x}_1,\mathbf{x}_2} e^{-\beta(E_{\mathbf{k}_1}+E_{\mathbf{k}_2})}M_{\mathbf{x}_1,\mathbf{x}_2}|\langle\mathbf{k}_1\mathbf{k}_2|\mathbf{x}_1\mathbf{x}_2\rangle|^2, \end{aligned} \tag{2.35}$$

where we have inserted complete sets of states in coordinate space $\{|\mathbf{x}_1\mathbf{x}_2\rangle\}$ and in the basis $|\mathbf{k}_1\mathbf{k}_2\rangle$ of eigenstates of $\hat{H}_0$, whose single-particle eigenstates $|\mathbf{k}\rangle$ have eigenvalues $E_{\mathbf{k}}$. We have also made use of the fact that $\hat{V}_{\mathrm{int}}$ is diagonal in coordinate space, such that

$$M_{\mathbf{x}_1,\mathbf{x}_2} = 1 + Ba^{-d}\delta_{\mathbf{x}_1,\mathbf{x}_2}, \tag{2.36}$$

where $B = a^d\left(e^{\beta g_{4D}} - 1\right)$ and we have introduced a spatial lattice spacing a as a regulator. This leads to a new expression for $\Delta Q_{1,1}$:

$$\Delta Q_{1,1} = B\sum_{\mathbf{k}_1,\mathbf{k}_2,\mathbf{x}} a^d e^{-\beta(E_{\mathbf{k}_1}+E_{\mathbf{k}_2})}|\langle\mathbf{k}_1\mathbf{k}_2|\mathbf{x}\,\mathbf{x}\rangle|^2, \tag{2.37}$$

which can be computed numerically.

The computationally demanding part of this calculation is the overlap function $|\langle\mathbf{k}_1\mathbf{k}_2|\mathbf{x}\,\mathbf{x}\rangle|^2$. Note that this function can be factorized as $|\langle\mathbf{k}_1|\mathbf{x}\rangle|^2|\langle\mathbf{k}_2|\mathbf{x}\rangle|^2$. Upon summing over $\mathbf{k}_1$, however we obtain a simpler expression

$$\Delta Q_{1,1} = B\sum_{\mathbf{x}} a^d n_\beta^2(\mathbf{x}) \tag{2.38}$$

where

$$n_\beta(\mathbf{x}) = \sum_{\mathbf{k}} e^{-\beta E_{\mathbf{k}}} |\langle \mathbf{k}|\mathbf{x}\rangle|^2. \tag{2.39}$$

The exponential decay with the energy will enable us to cut off the sum over $\mathbf{k}$ in most cases without significantly losing precision. We show a representative example of such cutoff effects in Figure 2.1. We can see in this figure that the relationship between the rotation frequency and trapping potential has an effect on where we can cut off our sum. We see that in 2D when $\omega_z = \omega_{\mathrm{tr}}$, our sum does not converge as we raise the cutoff limit for k and m, but instead grows with that cutoff. This same effect is not visible for values of $\omega_z < \omega_{\mathrm{tr}}$.

This shows that at the specific point where $\omega_z = \omega_{\mathrm{tr}}$, we can no longer calculate virial coefficients efficiently in 2D. Fortunately, we are not concerned with the system at phase transition, but instead we are interested in what happens below the critical rotation frequency.

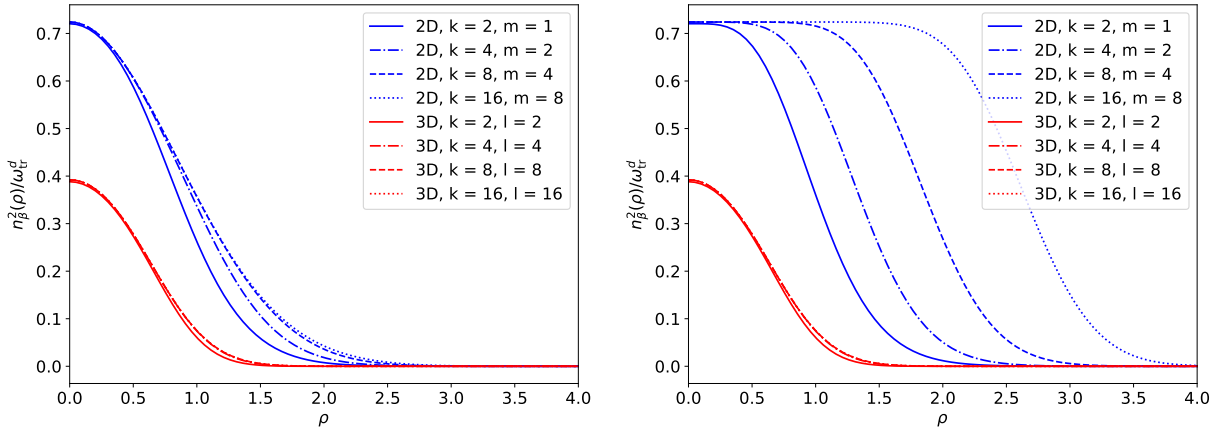

Figure 2.1: The figure shows $n_\beta^2(\mathbf{x})$ as a function of our radial lattice for a few different cutoffs in k and m (2D) or k and l (3D), demonstrating where we can cut off our sums. The left figure is for $\beta\omega_z = \beta\omega_{\mathrm{tr}}/2$, where we see we can cut off our sums at very small values. The right figure is for $\beta\omega_z = \beta\omega_{\mathrm{tr}}$, which represents a phase transition in our system. We can see these effects in the cutoffs, as shown by the figure on the right, where in $2D$, $n_\beta^2(\mathbf{x})$ fails to converge as we raise the cutoff in k and m.

To compute the sum, we refer back to the previously-defined single-particle eigenstates in 2D (Eq. (2.23)), arriving at an expression in 2D for n_β:

$$n_\beta(\mathbf{x}) = \omega_{\mathrm{tr}} \frac{e^{-\rho^2}}{2\pi} \sum_{k,m} e^{-\beta E_{km}} f_{km}^{\mathrm{2D}}(\rho^2), \tag{2.40}$$

whose units come from the prefactor ω_{tr} and, as expected from symmetry considerations, is only a function

of the radial coordinate (concentric with the trapping potential). Here,

$$f_{km}^{\mathrm{2D}}(\rho^2) \equiv \frac{2\,k!}{(k+|m|)!}\rho^{2|m|}\left(L_k^{|m|}(\rho^2)\right)^2, \tag{2.41}$$

Similarly, in 3D,

$$n_\beta(\mathbf{x}) = \omega_{\mathrm{tr}}^{3/2}\frac{e^{-\rho^2}}{\sqrt{4\pi}}\sum_{k,l,m} e^{-\beta E_{klm}} f_{kl}^{\mathrm{3D}}(\rho^2)(P_l^m(\cos\theta))^2 \tag{2.42}$$

where

$$f_{kl}^{\mathrm{3D}}(\rho^2) \equiv \frac{2^{k+2l+3}\,k!}{(2k+2l+1)!!}\rho^{2l}\left(L_k^{l+1/2}(\rho^2)\right)^2 \tag{2.43}$$

Which can be used to calculate $\Delta Q_{1,1}$ using Eq. (2.38).

Calculation of $\Delta Q_{2,1}$

Following the same steps outlined above, it is straightforward to show that

$$\Delta Q_{2,1} = \frac{B}{2}\sum_{\mathbf{k}_1\mathbf{k}_2\mathbf{k}_3} e^{-\beta(E_{\mathbf{k}_1}+E_{\mathbf{k}_2}+E_{\mathbf{k}_3})}\sum_{\mathbf{x}_1\mathbf{x}_2}|\langle\mathbf{x}_1\mathbf{x}_2\mathbf{x}_1|\mathbf{k}_1\mathbf{k}_2\mathbf{k}_3\rangle|^2. \tag{2.44}$$

The overlap can be simplified slightly by factoring across distinguishable species:

$$\langle\mathbf{x}_1\mathbf{x}_2\mathbf{x}_1|\mathbf{k}_1\mathbf{k}_2\mathbf{k}_3\rangle \quad = \quad \langle\mathbf{x}_1\mathbf{x}_2|\mathbf{k}_1\mathbf{k}_2\rangle\langle\mathbf{x}_1|\mathbf{k}_3\rangle, \tag{2.45}$$

where the matrix element $\langle\mathbf{x}_1\mathbf{x}_2|\mathbf{k}_1\mathbf{k}_2\rangle$ is a permanent of single-particle states:

$$\langle\mathbf{x}_1\mathbf{x}_2|\mathbf{k}_1\mathbf{k}_2\rangle = \langle\mathbf{x}_1|\mathbf{k}_1\rangle\langle\mathbf{x}_2|\mathbf{k}_2\rangle + \langle\mathbf{x}_2|\mathbf{k}_1\rangle\langle\mathbf{x}_1|\mathbf{k}_2\rangle. \tag{2.46}$$

As in the case of $\Delta Q_{1,1}$, we will sum over the energy eigenstates first, and then perform the spatial sum. To that end, it is useful to define

$$n_\beta^B(\mathbf{x}_1,\mathbf{x}_2) = \sum_{\mathbf{k}_1\mathbf{k}_2} e^{-\beta(E_{\mathbf{k}_1}+E_{\mathbf{k}_2})}|\langle\mathbf{x}_1\mathbf{x}_2|\mathbf{k}_1\mathbf{k}_2\rangle|^2 n_\beta(\mathbf{x}_1), \tag{2.47}$$

such that,

$$\Delta Q_{2,1} \quad = \quad \frac{B}{2} \sum_{\mathbf{x}_1 \mathbf{x}_2} n_\beta^B(\mathbf{x}_1, \mathbf{x}_2). \tag{2.48}$$

As in the case of $n_\beta(\mathbf{x})$, the exponential decay with the energy allows us to cut off the double sum in $n_\beta^B(\mathbf{x}_1, \mathbf{x}_2)$ without significantly affecting the precision of the whole calculation.

2.2.3: Gauss-Hermite quadrature

As shown above, the single-particle wavefunctions (Eq. (2.23) and Eq. (2.27)) and the associated density functions $n_\beta(\mathbf{x})$ and $n_\beta^B(\mathbf{x}_1, \mathbf{x}_2)$ are governed in the radial variable by a Gaussian decay. For that reason, it is appropriate to calculate the corresponding integrals using Gauss-Hermite quadrature. The corresponding M points x_i and M weights w_i allow us to estimate integrals according to

$$\int_{-\infty}^{\infty} dx\, e^{-x^2} f(x) = \sum_{i=0}^{M-1} w_i f(x_i). \tag{2.49}$$

In this work we use the same quadrature points and weights as in our previous work of Refs [34–36].

Section 2.3: Results

2.3.1: Noninteracting virial coefficients at finite angular momentum

We present here the calculation of the noninteracting (i.e. $g = 0$) virial expansion when $\omega_z \neq 0$. We begin with the partition function of spin-$1/2$ bosons in terms of the single-particle energies E:

$$\ln \mathcal{Z} = 2 \sum_E \ln(1 - z e^{-\beta E}). \tag{2.50}$$

This can be further expanded for small z (the virial expansion) as

$$\ln \mathcal{Z} = -2 \sum_E \sum_{n=1}^{\infty} \frac{z^n}{n} e^{-n\beta E}. \tag{2.51}$$

Two spatial dimensions.- In 2D, $E = E_{km} = \omega_{\rm tr}(2k + |m| + 1) + \omega_z m$, where $k \geq 0$ and m is summed over all integers. Thus, we may write the sum as

$$\ln \mathcal{Z} = -2 \sum_E \sum_{n=1}^{\infty} \frac{z^n e^{-n\beta\omega_{\rm tr}}}{n} \sum_k e^{-\beta\omega_{\rm tr} 2nk} \left[\sum_{m=0}^{\infty} e^{-nm\beta\omega_+} + \sum_{\bar{m}=1}^{\infty} e^{-n\bar{m}\beta\omega_-} \right]. \tag{2.52}$$

where $\omega_\pm = \omega_{\rm tr} \pm \omega_z$. Carrying out the sums over $k, m, \bar{m}$, we obtain

$$\ln \mathcal{Z} = Q_1 \sum_{n=1}^{\infty} b_n z^n, \tag{2.53}$$

where

$$Q_1 b_n = \frac{-2}{n} \frac{e^{-n\beta\omega_{\rm tr}}}{(1-e^{-n\beta\omega_+})(1-e^{-n\beta\omega_-})}. \tag{2.54}$$

Finally, to determine b_n we use Q_1 as derived above in Eq. (2.32)), such that

$$b_n = \frac{-1}{n} e^{-\beta\omega_{\rm tr}(n-1)} \frac{(1-e^{-\beta\omega_+})(1-e^{-\beta\omega_-})}{(1-e^{-n\beta\omega_+})(1-e^{-n\beta\omega_-})}. \tag{2.55}$$

Note that, while the b_n are always finite, Q_1 diverges when $\omega_- \to 0$. This signals an instability due to the fact that, for any $\omega_- < 0$, i.e. $\omega_z > \omega_{\rm tr}$, the system does not have a ground state. In terms of $\ln \mathcal{Z}$, the divergence may be regarded as a phase transition at $\omega_z = \omega_{\rm tr}$. In other words, in that limit the centrifugal motion due to the rotation is strong enough to overcome the trapping potential and the system escapes to infinity.

Three spatial dimensions.- In 3D, $E = E_{klm} = \omega_{\rm tr}(2k + l + 3/2) + \omega_z m$, where $k \geq 0$, $l \geq 0$, and $-l \leq m \leq l$. Therefore, analyzing the problem as in the 2D case, we obtain

$$Q_1 b_n = \frac{-2}{n} \frac{e^{-\frac{3}{2}n\beta\omega_{\rm tr}}}{(1-e^{-n\beta\omega_{\rm tr}})(1-e^{-n\beta\omega_+})(1-e^{-n\beta\omega_-})}, \tag{2.56}$$

and using (Eq. (2.33), we determine

$$b_n = \frac{-1}{n} e^{-\frac{3}{2}\beta\omega_{\rm tr}(n-1)} \frac{(1-e^{-\beta\omega_{\rm tr}})(1-e^{-\beta\omega_+})(1-e^{-\beta\omega_-})}{(1-e^{-n\beta\omega_{\rm tr}})(1-e^{-n\beta\omega_+})(1-e^{-n\beta\omega_-})}. \tag{2.57}$$

As in the 2D case, the b_n are always finite, but Q_1 diverges when $\omega_- \to 0$.

The impact of rotation, i.e. a finite $\beta\omega_z$ on a noninteracting system is displayed in Figure 2.2. In both 2D and 3D, the angular momentum has an approximately linear dependence on the rotation frequency, with the slope of the line decreasing for larger trapping potentials. In 2D, the trap frequency has a much more pronounced effect than in 3D, with the angular momentum collapsing to nearly a flat line for $\beta\omega_{\rm tr} > 2$, while in 3D, the effect is more gradual.

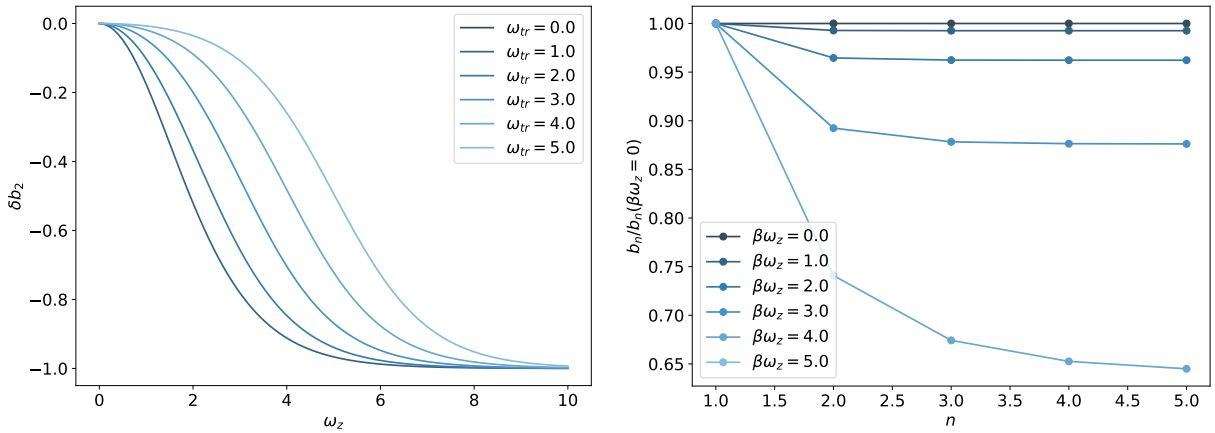

Figure 2.2: The difference in the second virial coefficient, $\delta b_2 = b_2(\omega_z > 0) - b_2(\omega_z = 0)$ (left) as a function of rotation frequency $\beta\omega_z$ in 2D. Noninteracting b_n normalized by their non-rotating, noninteracting values $b_n(\beta\omega_z = 0)$ (right), as functions of n for a few values of $\beta\omega_z$ and fixed $\beta\omega_{\rm tr} = 5$. The ratio $b_n/b_n(\beta\omega_z = 0)$ is the same in 2D and 3D.

2.3.2: Noninteracting thermodynamics at finite angular momentum

We can now derive a virial expansion for the angular momentum L_z and the z component of the moment of inertia I_z:

$$\langle \hat{L}_z \rangle = -\frac{\partial \ln \mathcal{Z}}{\partial(\beta\omega_z)} = Q_1 \sum_{n=1}^{\infty} L_n z^n, \tag{2.58}$$

where

$$L_n = n b_n \frac{e^{-n\beta\omega_+} - e^{-n\beta\omega_-}}{(1 - e^{-n\beta\omega_+})(1 - e^{-n\beta\omega_-})}, \tag{2.59}$$

and

$$\langle \hat{I}_z \rangle = -\frac{\partial^2 \ln \mathcal{Z}}{\partial(\beta\omega_z)^2} = Q_1 \sum_{n=1}^{\infty} I_n z^n, \tag{2.60}$$

where

$$I_n = \frac{1}{Q_1}\frac{\partial(Q_1 L_n)}{\partial(\beta\omega_z)} = -nL_n \left[\frac{e^{-n\beta\omega_+} + e^{-n\beta\omega_-}}{e^{-n\beta\omega_+} - e^{-n\beta\omega_-}} + \frac{2(e^{-n\beta\omega_+} - e^{-n\beta\omega_-})}{(1 - e^{-n\beta\omega_+})(1 - e^{-n\beta\omega_-})} \right]. \tag{2.61}$$

Note that in the limit $\omega_+ = \omega_-$ (i.e. $\omega_z = 0$), $L_n \to 0$ as expected in a system without rotation. In the limit $\omega_- \to 0$ (i.e. $\omega_z = \omega_{\rm tr}$), on the other hand, $L_n \to \infty$ as $\omega_- \to 0$. As discussed in the previous section, in that limit, the rotation overpowers the trapping potential confining the system, resulting in a phase transition

to a system beyond the scope of our study.

Remarkably, because the dependence of $Q_1 b_n$ on ω_+ and ω_- is the same in 2D and 3D, the relationship between L_n and b_n is identical in 2D and 3D. It follows that the relationship between I_n and b_n is identical in 2D and 3D as well. Thus, any differences in the angular momentum and moment of inertia between two and three dimensions arises entirely from the differences between the virial coefficients b_n.

Furthermore, at $\omega_z = 0$, a finite moment of inertia remains, in 2D:

$$I_n \to 2n(-1)^n e^{-(2n-1)\beta\omega_{\rm tr}} \frac{(1-e^{-\beta\omega_{\rm tr}})^2}{(1-e^{-n\beta\omega_{\rm tr}})^4}, \tag{2.62}$$

and in 3D:

$$I_n \to 2n(-1)^n e^{-\frac{1}{2}\beta\omega_{\rm tr}(5n-3)} \frac{(1-e^{-\beta\omega_{\rm tr}})^3}{(1-e^{-n\beta\omega_{\rm tr}})^5}. \tag{2.63}$$

which characterizes the static response to small rotation frequencies within the virial expansion, as a function of $\beta\omega_{\rm tr}$.

The impact of rotation on the angular momentum for a noninteracting system is shown in Figure 2.3, and the impact of rotation on the moment of inertia for a noninteracting system is shown in Figure 2.4

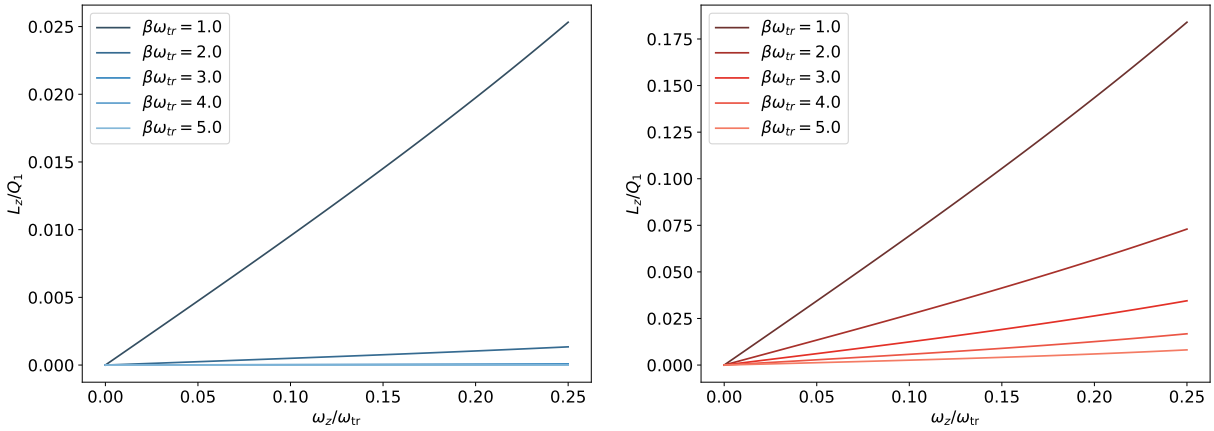

Figure 2.3: Noninteracting L_z/Q_1 to third order in the virial expansion in 2D (left) and 3D (right), as functions of $\beta\omega_z$ for a few values of $\beta\omega_{\rm tr}$.

2.3.3: Interacting virial coefficients at finite angular momentum

Once the inter-particle interaction appears, we can compute the change in the virial coefficients due to this interaction as well as due to the rotation, as in Eq. (2.14). The results for the first two nontrivial virial

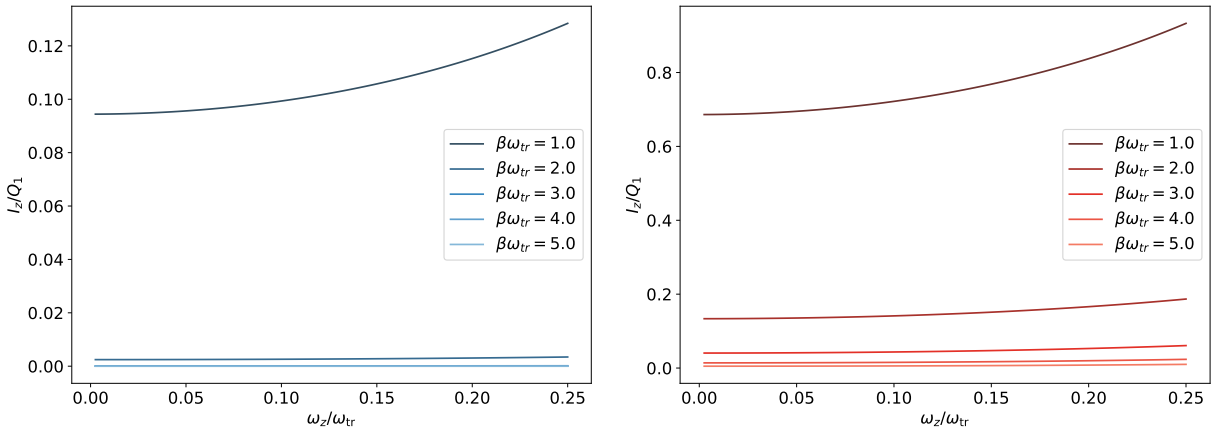

Figure 2.4: Noninteracting I_z/Q_1 to third order in the virial expansion in 2D (left) and 3D (right), as functions of $\beta\omega_z$ for a few values of $\beta\omega_{\rm tr}$.

coefficients, b_2 and b_3 are shown in Figure 2.5 and Figure 2.6 for a range of bare couplings from $g = 0$ to $g = 1$ as a function of $\omega_z/\omega_{\rm tr}$. In all cases, the magnitude of the change in the virial coefficient increases as the interaction strength, g, increases, but the behavior varies with increases in $\omega_z/\omega_{\rm tr}$. (Recall that as $\omega_z/\omega_{\rm tr} \to 1$, the system undergoes a phase transition.)

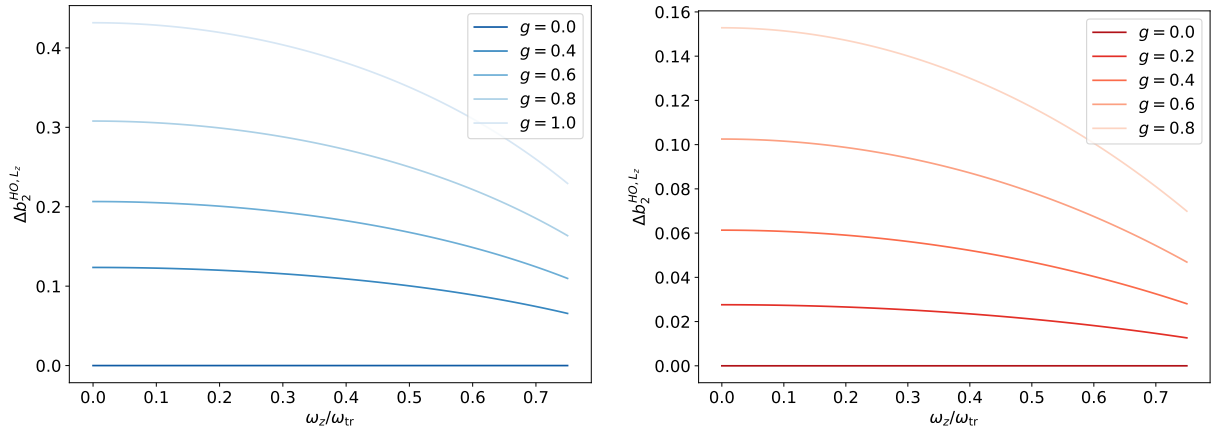

Figure 2.5: Change in the virial coefficient b_2 due to the combination of rotation and interaction, for two (left) and three (right) spatial dimensions.

The change in Δb_2 is similar in 2D and 3D, although the effect is much larger in 2D. The next virial coefficient, Δb_3, behaves very differently in 2D than it does in 3D. We can see that in 2D, Δb_3 looks very similar to Δb_2, while in 3D, Δb_3 is negative rather than positive and its magnitude increases rather than decreases with increasing rotation ω_z.

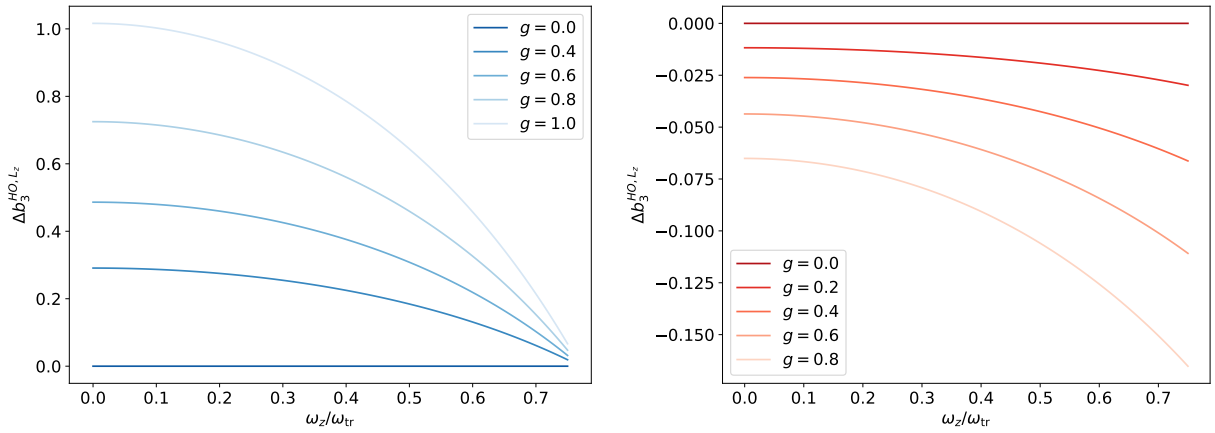

Figure 2.6: Change in the virial coefficient b_3 due to the combination of rotation and interaction, for two (left) and three (right) spatial dimensions.

2.3.4: Interacting thermodynamics at finite angular momentum

We can now use our results for Δb_2 and Δb_3 to calculate the thermodynamics and angular momentum equations of state to third order in the virial expansion, as well as the static response encoded in the moment of inertia. Denoting the noninteracting grand canonical partition function by $\mathcal{Z}_0$, we have

$$\ln\left(\mathcal{Z}/\mathcal{Z}_0\right) = Q_1 \sum_{n=2}^{\infty} \Delta b_n z^n, \tag{2.64}$$

such that the interaction effect on the angular momentum virial coefficient L_n is

$$\Delta L_n = \frac{1}{Q_1}\frac{\partial\left(Q_1 \Delta b_n\right)}{\partial(\beta\omega_z)} = \frac{\partial\left(\Delta b_n\right)}{\partial(\beta\omega_z)} + \Delta b_n \frac{\partial\left(\ln Q_1\right)}{\partial(\beta\omega_z)}, \tag{2.65}$$

and its counterpart for the moment of inertia is

$$\Delta I_n = \frac{1}{Q_1}\frac{\partial\left(Q_1 \Delta L_n\right)}{\partial(\beta\omega_z)} = \frac{\partial\left(\Delta L_n\right)}{\partial(\beta\omega_z)} + \Delta L_n \frac{\partial\left(\ln Q_1\right)}{\partial(\beta\omega_z)}, \tag{2.66}$$

where, using Eq. (2.65) for ΔL_n,

$$\frac{\partial\left(\Delta L_n\right)}{\partial(\beta\omega_z)} = \frac{\partial^2\left(\Delta b_n\right)}{\partial(\beta\omega_z)^2} + \frac{\partial\left(\Delta b_n\right)}{\partial(\beta\omega_z)}\frac{\partial\left(\ln Q_1\right)}{\partial(\beta\omega_z)} + \Delta b_n \frac{\partial^2\left(\ln Q_1\right)}{\partial(\beta\omega_z)^2}. \tag{2.67}$$

Using the above formulas, along with the expressions obtained for Δb_2 and Δb_3 from Eq. (2.18), we are able to obtain expressions for ΔL_2, ΔL_3, ΔI_2, and ΔI_3. Therefore, we can obtain the change due to the

presence of repulsive interactions in the angular momentum and moment of inertia to third order in the virial expansion:

$$\frac{\Delta\langle L_z\rangle}{Q_1} = \Delta L_2 z^2 + \Delta L_3 z^3 + O(z^4) \tag{2.68}$$

$$\frac{\Delta\langle I_z\rangle}{Q_1} = \Delta I_2 z^2 + \Delta I_3 z^3 + O(z^4). \tag{2.69}$$

These results are shown in Figure 2.7 and Figure 2.8.

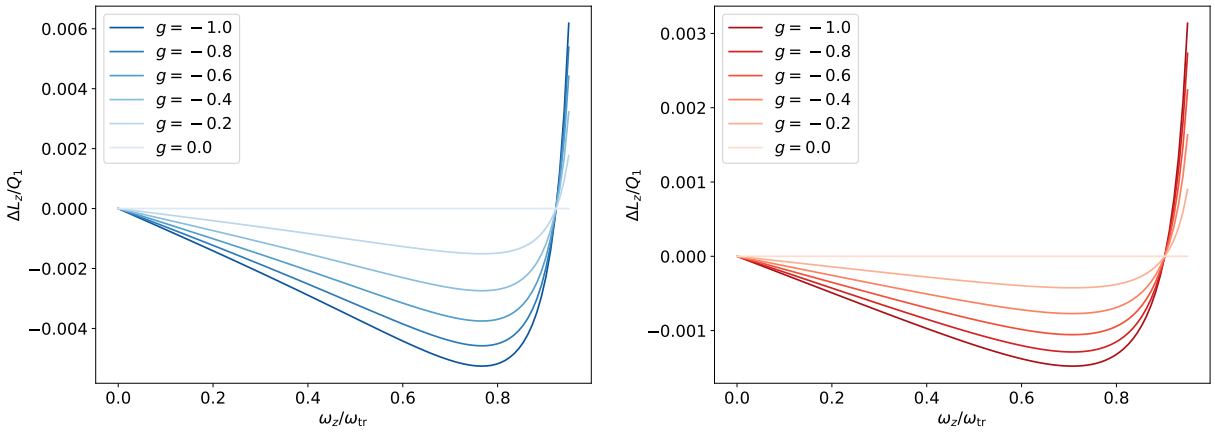

Figure 2.7: Change in the angular momentum $\langle \hat{L}_z \rangle$ due to the combination of rotation and repulsive contact interaction, for two (left) and three (right) spatial dimensions, at $z = e^{-2.0}$.

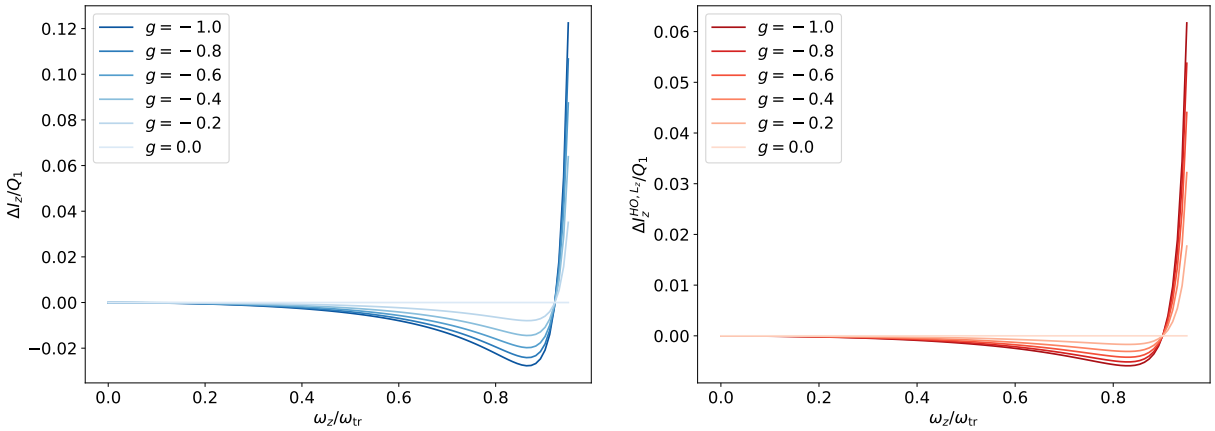

Figure 2.8: Change in the moment of inertia $\langle \hat{I}_z \rangle$ due to the combination of rotation and repulsive contact interaction, for two (left) and three (right) spatial dimensions, at $z = e^{-2.0}$.

The change in angular momentum looks very similar in 2D and in 3D. It is initially roughly linear, but as the rotation frequency begins to approach the trap frequency, the change in angular momentum plateaus and then rapidly crosses zero and increases towards infinity as we approach the phase transition $\omega_z = \omega_{\mathrm{tr}}$.

We can see also that the moment of inertia, while initially changing much more slowly than the angular momentum, starts to grow quickly in magnitude at the same point in rotation frequency where the angular momentum slows its growth, and then also changes direction and increases towards infinity at the phase transition.

Section 2.4: Summary and conclusions

In this chapter we have characterized the thermodynamics of a rotating Bose gase in 2D and 3D using the virial expansion. We implemented the SCLA, which allowed us to bypass solving the n-body problem to calculate the n-th order virial coefficient [37].

In all cases, a finite angular velocity ω_z modifies both the single-particle partition function Q_1 as well as the virial coefficients; the latter are further modified by the interactions. We have presented explicit formulas for the noninteracting case which do not appear elsewhere in the literature, to the best of our knowledge. As can be anticipated, the system becomes unstable at $\omega_z = \omega_{\rm tr}$, as the angular velocity allows particles to escape the trapping potential in that limit. In that case, the virial coefficients remain finite, but Q_1 diverges, leading to divergent thermodynamics.

We have also obtained estimates to third order in the virial expansion for the angular momentum L_z as well as the z component of the moment of inertia I_z, as functions of the angular velocity $0 < \omega_z < \omega_{\rm tr}$ and temperature $\beta\omega_{\rm tr}$.

CHAPTER 3: Stochastic methods: from Markov chain Monte Carlo to Complex Langevin

Section 3.1: Quantum Monte Carlo methods

In order to treat quantum systems fully, we desire to move beyond approximate methods to ones which capture the behavior of the systems more generally, rather than in a limited set of regimes. Among the most popular methods for quantum many-body systems are quantum Monte Carlo (QMC) methods. This section provides an overview of these methods and illustrates them through discussion of the 2D Ising model.

Quantum Monte Carlo methods are a subset of Monte Carlo methods for quantum systems. In these methods, integrals (such as the path integral or the expectation value of the observables) are evaluated stochastically, yielding results that are exact up to some statistical uncertainty which depends on the number of samples used in the stochastic algorithm. This is done by means of a standard approximation scheme, where a generic integral of some function $f(x)$ with weight $p(x)$

$$\mathcal{I} = \int_a^b dx p(x) f(x) \tag{3.1}$$

can be approximated via a sum

$$\mathcal{I}_N = \sum_{i=1}^{N} \Delta x f(x_i) p(x_i) \tag{3.2}$$

where $\Delta x = \frac{b-a}{N}$. The exact integral is reproduced in the limit $N \to \infty$. From this, is can be seen that increasingly accurate approximations can be achieved by increasing the size of N. In QMC, this N corresponds to the number of samples taken in the algorithm. In most cases, evaluating an integral this way is inefficient, as the sort of integrals we wish to evaluate do not have uniform weight across paths. In fact, the weight ($p(x_i)$ in this notation, which corresponds to the e^{iS} of Eq. (1.10) and Eq. (1.11)), is likely to be significant in just a few high-probability regions. Use of an algorithm which focuses the sampling in those high-probability regions, therefore, will result in a much more efficient calculation.

Central to importance sampling is the concept of the Markov chain, in which each sampled value's

probability depends only on the value immediately prior, i.e.

$$\mathcal{P}(\phi_n) = f(\phi_{n-1}). \tag{3.3}$$

This property allows for the generation of a set of random samples from a probability distribution via a sequential sampling process, making it an excellent technique for a computational algorithm. The use of these Markov chains is known as importance sampling, and – as implied by the name – improves the speed of our sampling by allowing us to generate configurations according to the probability distribution of the system, rather than sampling uniformly and weighting the configurations after the fact.

3.1.1: Importance sampling and the Ising model

A classic example from statistical physics of the usefulness of importance sampling algorithms is the Ising model. In 2D, the Ising model can be solved exactly, while in higher dimensions a stochastic solution is necessary. This makes this model a helpful point of comparison between stochastic algorithms and the known solution.

The 2D Ising model is a model for ferromagnetism in which spins are situated on an $N_x \times N_x$ lattice in the presence of an external magnetic field. The Hamiltonian is

$$\mathcal{H} = -J \sum_{\langle i,j \rangle} s_i s_j - H \sum_{i=1}^{N} s_i, \tag{3.4}$$

where J is the strength of the spin coupling and H is the strength of the magnetic field multiplied by the atomic magnetic moment. The partition function is

$$\mathcal{Z} = \sum_i e^{-\beta E_i} \tag{3.5}$$

where $\beta = \frac{1}{k_B T}$ and the energy of a single spin is calculated by summing over the nearest neighbors (n.n.):

$$E_i = -J s_i \left(\sum_{j \in n.n.} s_j + \frac{H}{J} \right). \tag{3.6}$$

The observables of interest in this model are the energy and magnetization. The energy of a single spin

configuration is

$$E(\alpha) = \sum_{i=1}^{N_x^2} E_i \tag{3.7}$$

and the magnetization of that configuration is

$$M(\alpha) = \sum_{i=1}^{N_x^2} M_i \tag{3.8}$$

$$M_i = \mu s_i. \tag{3.9}$$

We can see from this description of the magnetization that it depends on the average direction of the spins. If the spins are largely aligned in the same direction, we find a nonzero magnetization for that configuration, whereas in a randomly-aligned system, we expect the magnetization to be zero.

The average energy and magnetization are computed by summing over all possible spin configurations of the lattice in the following way:

$$\langle E \rangle = \frac{1}{N_\alpha} \sum_\alpha E(\alpha) \tag{3.10}$$

$$\langle M \rangle = \frac{1}{N_\alpha} \sum_\alpha M(\alpha) \tag{3.11}$$

where $E(\alpha)$ and $M(\alpha)$ come from Eq. (3.7) and Eq. (3.8).

Since the total number of possible lattice configurations N_α scales exponentially in lattice size ($N_\alpha \propto 2^{N_x^2}$), for even moderately-sized lattices ($N_x > 4$), we need to use a stochastic algorithm that prioritizes sampling from high-probability configurations. This is where importance sampling comes in.

The importance sampling algorithm most often used with the Ising model is the Metropolis-Hastings algorithm, which uses a random walk in configuration space paired with an accept-reject step to guide the sampling towards higher-probability regions. In this case, what that means is that the algorithm proceeds as follows:

1. Initialize the lattice with some random configuration of spins ($+1$ for up and -1 for down)

2. Calculate the total energy of this spin configuration (using Eq. (3.7))

3. Flip a single spin on the lattice

4. Calculate the energy of this new configuration (again using Eq. (3.7))

5. Determine the ratio of the probability of this new configuration to the old one

$$\mathcal{P}(\alpha) = \frac{1}{\mathcal{Z}} e^{-\beta E(\alpha)} \tag{3.12}$$

$$\frac{\mathcal{P}(\alpha_{\text{new}})}{\mathcal{P}(\alpha_{\text{old}})} = e^{-\beta(E(\alpha_{\text{new}}) - E(\alpha_{\text{old}})} \tag{3.13}$$

6. Accept or reject the new configuration by comparing this ratio to a random number generated uniformly in the range $(0, 1)$.

7. If the new configuration is as probable or more probable than the random number, keep the new lattice configuration. Otherwise, revert to the previous configuration, choose a new spin to flip, and repeat the process outlined above

The algorithm continues until N_α spin configurations have been collected. The energy and magnetization of these configurations are the samples, which we average together according to Eq. (3.10) to get our average values.

3.1.2: Limitations of quantum Monte Carlo algorithms

The previous section relied upon the important assumption that the quantity weighting our observables ($e^{-\beta E}$ in this case and e^{iS} more generally) was positive definite. This allows is to treat the quantity like a probability, and use it to guide our Markov chain. But what happens when we can no longer rely on this assumption? This is an example of the sign problem arising in quantum lattice calculations.

This is where alternative stochastic methods can help. The remainder of this chapter focuses on the stochastic method known as complex Langevin, which can be utilized to circumvent the sign problem.

Section 3.2: Complex Langevin: origins and method

The complex Langevin method first appeared in the 1980s and enjoyed a brief surge of interest following the first successful numerical application for the quantum Hall effect by Klauder [38], which died down as instabilities and mathematical challenges with the method arose. The method reappeared in relativistic physics, particularly QFT, in the mid-2000s to early 2010s, as a viable method for circumventing the sign problem in certain field theoretical studies such as non-equilibrium QFT, which can provide insights into high-energy physics, particularly heavy ion collisions. Due to the non-perturbative nature of these non-

equilibrium systems, standard approximation techniques fail. In 2005, Berges and Stamatescu demonstrated the viability of CL to treat non-equilibrium QFT using first-principles simulations [39]. Later work built on these results to examine how CL could lead to breakthroughs in our understanding of QCD plasmas in heavy-ion collisions, early thermalization, and other open questions in quantum field theory [40, 41].

In 2008, Aarts and Stamatescu demonstrated that CL could be applied to models of finite density QCD that exhibit a sign problem [42]. Shortly after that, Aarts demonstrated that CL could be used to circumvent the sign problem in the relativistic Bose gas with finite chemical potential (see Refs [1, 43], which will be discussed further in Chapter 4). This began a resurgence of interest in this method in the field of finite density lattice QCD (LQCD), in which nonperturbative calculations of strongly interacting matter with finite baryon chemical potential are inhibited by the sign problem. This renewed interest led to work in the next few years on optimization of the method to prevent runaways and improve stability, using stochastic reweighting, gauge fixing, and adaptive step size algorithms [44–46].

The successes of the method, and advances made in treating instabilities and singularities in the fermion determinant, have generated interest in applying CL to non-relativistic systems – particularly many-fermion systems, in which sign problems arise frequently [47–52]. Work with the CL method in the context of non-relativistic systems is just beginning, but is already showing great promise [53]. This dissertation examines the application of CL to bosonic systems, starting with a re-examination of the relativistic Bose gas, and then adapting the method for nonrelativistic bosons, to study the behavior of rotating superfluids. This chapter provides an overview of the CL method, from its derivation to the practical challenges faced in applying the method.

3.2.1: Stochastic quantization: the Langevin method

While QMC techniques are extremely prevalent in quantum many-body physics, there exist other stochastic methods for evaluating properties of interest. One of these alternatives, stochastic quantization, has been used to treat Euclidean field theories since since Parisi and Wu first proposed the connection between the Euclidean field theories and statistical systems coupled to a heat bath [54]. It is now well-established as a successful tool for treating quantum many-body systems with a real Euclidean action [55]. At the center of these methods – just as with Monte Carlo methods – is the use of a Markov process, where a stochastic evolution yields new values whose dependence on the past values extends only to its immediate predecessor,

i.e.

$$x_{n+1} = f(x_n). \tag{3.14}$$

One such Markovian process is Brownian motion, described the the Langevin equation: a stochastic differential equation. Use of the Langevin equation in stochastic quantization has led to an alternative name for the method: the Langevin method. This method, originally developed for the modeling of dynamical variables in molecular systems, evolves the Langevin equation to produce sets of solutions distributed according to some probability.

The Langevin equation is well-established for real-valued fields, ϕ on a real manifold [56]. We can use it to stochastically evaluate path integrals of the form

$$\mathcal{Z} = \int \mathcal{D}\phi \, \mathrm{e}^{-S[\phi]} \tag{3.15}$$

by evolving the fields, ϕ, with respect to a fictitious time. This fictitious time evolution is governed by the Langevin equation:

$$\frac{d\phi}{dt} = -\frac{\delta S[\phi]}{\delta \phi} + \tilde{\eta}. \tag{3.16}$$

The first term on the right hand side is called the drift term, sometimes denoted as K:

$$K[\phi] = -\frac{\delta S[\phi]}{\delta \phi} \tag{3.17}$$

The second term on the right hand encodes the stochastic nature of the equation and is given by white noise. In order to evolve the Langevin equation numerically, we can express the equation in a discrete form:

$$\Delta\phi = K[\phi]\Delta t + \eta, \tag{3.18}$$

where η must fulfill the conditions:

$$\langle \eta(t) \rangle = 0 \tag{3.19}$$

$$\langle \eta(t)\eta(t') \rangle = 2\delta(t - t'), \tag{3.20}$$

and is generally chosen to be a standard Gaussian random variable. This random process will produce time-dependent configurations $\phi_\eta(t)$ distributed according to some probability distribution $\mathcal{P}[\phi, t]$. The expectation value of a given observable $O[\phi]$ is then given by

$$\left\langle O[\phi_\eta(t)] \right\rangle = \int \mathcal{D}\phi \, \mathcal{P}[\phi, t] O[\phi]. \tag{3.21}$$

This illustrates the key ingredient of stochastic quantization, which is that the equilibrium distribution (if it exists) of the $d + 1$ dimensional random process in Eq. (3.18) corresponds to the probability measure in the d-dimensional path integral Eq. (3.15). The extra dimension is simply the fictitious time t, which is integrated out when we compute the observable's expectation value by taking a long-time average.

To establish the validity of such a Langevin average, we need to investigate the temporal behavior of the expectation value and show that the time-dependent probability distribution depends on $S[\phi]$ in the way dictated by Eq. (3.15), at least at large enough t. Such a property will justify the use of temporal averages along the Langevin evolution to estimate the true expectation values of the theory.

An instructive discussion can be found in Ref. [56], which we will follow closely.

As a first step, we take the fictitious-time derivative of the expectation value

$$\frac{d \left\langle O[\phi_\eta(t)] \right\rangle}{dt} = \int \mathcal{D}\phi \, \frac{d\mathcal{P}[\phi, t]}{dt} O[\phi]. \tag{3.22}$$

Note that in the integrand, only the probability distribution carries a fictitious-time dependence. Alternatively, we may perform the same fictitious-time derivative by expanding the observable to second order in its ϕ dependence

$$dO[\phi] = \frac{\delta O[\phi]}{\delta \phi} d\phi + \frac{1}{2} \frac{\delta^2 O[\phi]}{\delta \phi^2} (d\phi)^2. \tag{3.23}$$

According to Eq. (3.18) we may write the incremental $d\phi$ as the result of a stochastic process

$$d\phi = -\frac{\delta S[\phi]}{\delta \phi} dt + dw, \tag{3.24}$$

where dw is the Wiener increment with the properties

$$\langle dw^2 \rangle = \int_t^{t+dt} d\tau \int_t^{t+dt} d\tau' \, \langle \eta(\tau)\eta(\tau') \rangle = 2\, dt \tag{3.25}$$

$$\langle dw \rangle = 0, \tag{3.26}$$

which follows from Eq. (3.19). Substituting this definition for $d\phi$ into Eq. (3.23) and using the properties of dw yields

$$\langle dO[\phi] \rangle = \left\langle -\frac{\delta O[\phi]}{\delta \phi} \frac{\delta S[\phi]}{\delta \phi} + \frac{\delta^2 O[\phi]}{\delta \phi^2} \right\rangle dt \,, \tag{3.27}$$

which allows us to write

$$\frac{d\langle O[\phi_\eta(t)] \rangle}{dt} = \left\langle -\frac{\delta O[\phi]}{\delta \phi} \frac{\delta S[\phi]}{\delta \phi} + \frac{\delta^2 O[\phi]}{\delta \phi^2} \right\rangle \equiv \langle L \rangle \,, \tag{3.28}$$

where we have defined the Langevin operator

$$L_r = \int d\tau d^{\mathrm{d}}x \, \left(\frac{\delta}{\delta \phi} + K[\phi] \right) \frac{\delta}{\delta \phi} \,, \tag{3.29}$$

with the drift $K[\phi] = -\frac{\delta S[\phi]}{\delta \phi}$, according to Eq. (3.18). We may write this expectation value as an integral over configurations and then integrate by parts:

$$\frac{d\langle O[\phi_\eta(t)] \rangle}{dt} = \int \mathcal{D}\phi \left(-\frac{\delta O[\phi]}{\delta \phi} \frac{\delta S[\phi]}{\delta \phi} + \frac{\delta^2 O[\phi]}{\delta \phi^2} \right) \mathcal{P}[\phi, t] \tag{3.30}$$

$$= \int \mathcal{D}\phi \, O[\phi] \left(\frac{\delta}{\delta \phi} \frac{\delta S[\phi]}{\delta \phi} + \frac{\delta^2}{\delta \phi^2} \right) \mathcal{P}[\phi, t]. \tag{3.31}$$

Here we made the important assumption that the probability vanishes at the boundaries (or decays fast enough if the integration region is non-compact). These assumptions are crucial and will be discussed in more detail below.

Comparing the above equation with Eq. (3.22) yields the Fokker-Planck (FP) equation:

$$\frac{d}{dt} \mathcal{P}[\phi, t] = L_r^{\mathrm{T}} \mathcal{P}[\phi, t] \,, \tag{3.32}$$

with the formal adjoint of the above Langevin operator

$$L_r^{\mathrm{T}} \equiv \int d\tau \mathrm{d}^d x \, \frac{\delta}{\delta\phi}\left(\frac{\delta}{\delta\phi} - K[\phi]\right), \tag{3.33}$$

which is also referred to as the FP operator or FP Hamiltonian. To show that the stationary solution of this equation is indeed our desired probability distribution we perform a similarity transformation

$$\widetilde{\mathcal{P}}[\phi, t] = \mathrm{e}^{S[\phi]/2}\mathcal{P}[\phi, t], \tag{3.34}$$

to rewrite the FP equation

$$\frac{d}{dt}\widetilde{\mathcal{P}}[\phi, t] = \widetilde{L}_r^{\mathrm{T}}\widetilde{\mathcal{P}}[\phi, t], \tag{3.35}$$

with

$$\widetilde{L}_r^{\mathrm{T}} = \mathrm{e}^{S[\phi]/2}\, L_r^{\mathrm{T}}\, \mathrm{e}^{-S[\phi]/2} = \int d\tau d^{\mathrm{d}} dx \, \left(-\frac{\delta}{\delta\phi} + \frac{1}{2}K[\phi]\right)\left(\frac{\delta}{\delta\phi} + \frac{1}{2}K[\phi]\right). \tag{3.36}$$

This last equation reveals that, with a real action $S[\phi]$, our modified FP Hamiltonian is a self-adjoint and positive semidefinite operator, with a unique FP ground state $\psi_0 = \mathrm{e}^{-S[\phi]/2}$ and vanishing FP energy $E_0 = 0$.

We can therefore project our probability over the complete set of eigenfunctions and non-negative eigenvalues of $\widetilde{L}_r^{\mathrm{T}}$, and see that our probability collapses to the ground state in the long time limit:

$$\widetilde{\mathcal{P}}[\phi, t] = \sum_{n=0}^{\infty} a_n \psi_n \mathrm{e}^{-E_n t} \xrightarrow{t\to\infty} a_0 \mathrm{e}^{-S[\phi]/2}. \tag{3.37}$$

Upon performing the back-transformation according to Eq. (3.34) we obtain

$$\lim_{t\to\infty} \mathcal{P}[\phi, t] \sim \mathrm{e}^{-S[\phi]}, \tag{3.38}$$

which shows that the Langevin equation produces field configurations distributed according to the Boltzmann weight $\mathrm{e}^{-S[\phi]}$ in the limit of large fictitious time.

The above justifies the use of temporal averages to estimate equilibrium expectation values. In practice,

we obtain these by performing an integration over a time T:

$$\langle O \rangle \approx \frac{1}{T} \int_{t_{\rm th}}^{t_{\rm th}+T} dt\, O[\phi_\eta(t)], \tag{3.39}$$

where $t_{\rm th}$ reflects the equilibration time that is needed to approach the stationary probability distribution. Thus, the Langevin equation produces a fictitious time evolution of a system governed by an action $S[\phi]$, and after some thermalization time, the solutions converge to a set that can be averaged to determine the expectation value of the observable.

3.2.2: Extending the Langevin method to complex variables

The Langevin method has been established as effective in the case of real-valued variables, but we seek an alternative to QMC that will allow us to examine systems with both real and imaginary components, in order to circumvent the sign problem that arises when treating those systems with QMC. In this section, we show that the Langevin equations can be extended to a complex plane, yielding a set of stochastic differential equations for the real and imaginary components of the fields. This generalization of the Langevin method is naturally called the complex Langevin (CL) method, and was first suggested in the early 1980s independently by Parisi [57] and Klauder [58, 59]. One of the benefits of extending the Langevin method to complex variables is that it replaces the importance sampling process in QMC, which eliminates the the restriction to real and positive semidefinite measures.

For a complex measure, $e^{-S[\phi]}d\phi$, with S a holomorphic function $S = u(\phi) + iv(\phi)$ on a real manifold $\mathcal{M}$, we cannot treat $e^{-S[\phi]}$ as a real probability measure. In that case, the probability distribution in Eq. (3.21) becomes a complex distribution

$$\rho[\phi] = \frac{\mathrm{e}^{-S[\phi]}}{\mathcal{Z}}, \tag{3.40}$$

while the field ϕ is still a real quantity. However, if we replace $e^{-S[\phi]}d\phi$ by a real measure $\mathcal{P}(\phi_R + i\phi_I)d\phi_R d\phi_I$ defined on a complex manifold $\mathcal{M}_c$, we can evaluate the equilibrium measure of $\mathcal{P}$ using the complex Langevin process.

Complex Langevin extends the target manifold of the field ϕ to the complex plane by setting

$$\phi \to \phi_R + i\phi_I, \tag{3.41}$$

and analytically extending the domain of the action functional:

$$S[\phi] \to S[\phi_R + i\phi_I]. \tag{3.42}$$

	Real Langevin	Complex Langevin
Fields	ϕ	$\phi_R + i\phi_I$
Action	$S[\phi]$	$S[\phi_R + i\phi_I]$
Langevin step	$\Delta\phi = K\Delta t + \eta(t)$	$\Delta\phi_R = K_R\Delta t + \eta_R(t)$ $\Delta\phi_I = K_I\Delta t + \eta_I(t)$
Drift	$K = -\frac{\delta S}{\delta\phi}$	$K_R = -\mathrm{Re}\left[\frac{\delta S[\phi]}{\delta\phi}\right]$ $K_I = -\mathrm{Im}\left[\frac{\delta S[\phi]}{\delta\phi}\right]$
Noise	$\langle\eta^2\rangle = 2\Delta t$	$\langle\eta_R^2\rangle = 2N_R\Delta t$ $\langle\eta_I^2\rangle = 2N_I\Delta t$ $N_R - N_I = 1$
	$\langle\eta\rangle = 0$	$\langle\eta_R\rangle = \langle\eta_I\rangle = 0$

Figure 3.1: The Langevin method with real-valued fields versus complex-valued fields.

With such an extension, the CL method proceeds very much in the same way as the real Langevin method (see Figure 3.1 for a side-by-side comparison), but now with a double system of coupled stochastic differential equations:

$$\Delta\phi_R = K_R\Delta t + \eta_R(t), \tag{3.43}$$

$$\Delta\phi_I = K_I\Delta t + \eta_I(t), \tag{3.44}$$

where the real and imaginary drift functions K_R and K_I are found by taking the real and imaginary parts of the functional derivative of the complex action:

$$K_R = -\mathrm{Re}\left[\frac{\delta S[\phi]}{\delta\phi}\right], \tag{3.45}$$

$$K_I = -\mathrm{Im}\left[\frac{\delta S[\phi]}{\delta\phi}\right]. \tag{3.46}$$

The real and imaginary noise obey the properties shown in Figure 3.1.

The extension to the complex manifold results in the set of coupled differential equations of Eq. (3.43), which treat the real and imaginary parts of the fields individually and generate results for both real and imaginary parts of the observables. While the amplitudes of the real and imaginary noise terms are related, the two Wiener processes are completely independent. In practice, the imaginary noise is usually set to zero, which satisfies the constraints shown in Figure 3.1 and it has been found to have the best numerical properties [60]. Finally, it should be pointed out that, beyond the complexification of each real degree of freedom, the above (coupled) Langevin processes are themselves real. After thermalization, the expectation values for the imaginary parts of the observables should average to zero.

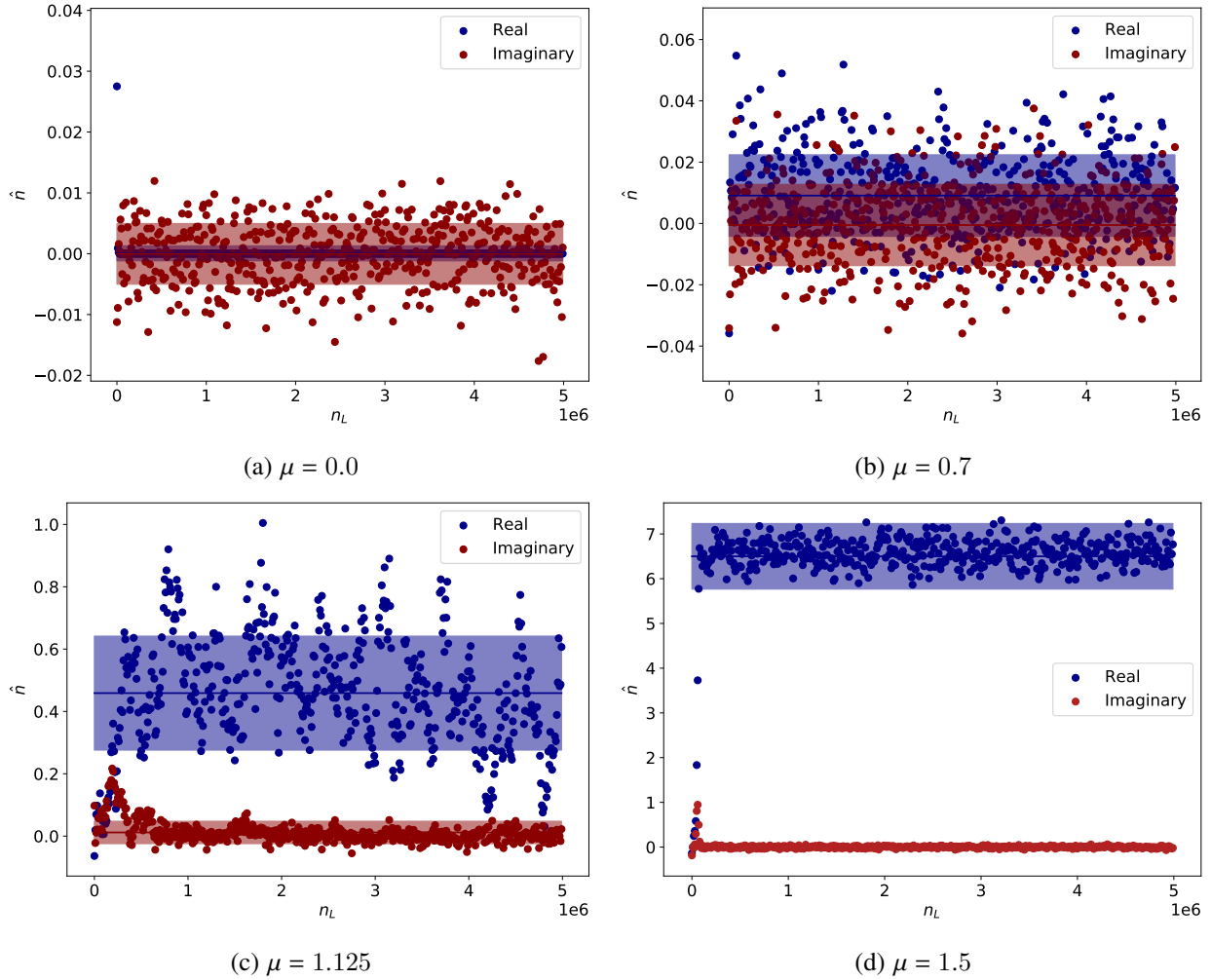

(a) $\mu = 0.0$

(b) $\mu = 0.7$

(c) $\mu = 1.125$

(d) $\mu = 1.5$

Figure 3.2: Real (blue) and imaginary (red) density generated by Complex Langevin for a relativistic Bose gas at finite chemical potential.

This can be seen clearly in Figure 3.2, which shows the real and imaginary parts of the density of a system of relativistic bosons at finite chemical potential in $3 + 1$ dimensions. As the chemical potential

increases, the real part of the density rises (as the system condenses), but the imaginary value stays at zero. This system is examined in more detail in Chapter 4.

Section 3.3: Formal justification and challenges for complex Langevin

Extension of the Langevin equation to complex variables is not perfect, so naturally some challenges arise in implementing this method. The challenges faced by the CL method can be roughly divided into two kinds: mathematical and practical. While these two areas share some overlap, they can be discussed individually, as we will do in this section.

3.3.1: Mathematical aspects: convergence, correctness, boundary terms, and ergodicity

As described above, the CL process defines a random walk in a complexified manifold, such that for a given configuration $\phi = \phi_R + i\phi_I$ there is a well-defined probability $\mathcal{P}[\phi_R, \phi_I, t]$ at time t. For a given observable O, there will be an expectation value

$$\langle O \rangle_{\mathcal{P}(t)} \equiv \int \mathcal{D}\phi_R \mathcal{D}\phi_I \, \mathcal{P}[\phi_R, \phi_I, t] O[\phi_R + i\phi_I]. \tag{3.47}$$

By virtue of the CL process, as discussed in the previous section, the real probability $\mathcal{P}[\phi_R, \phi_I, t]$ obeys the FP equation:

$$\frac{\partial \mathcal{P}}{\partial t} = L^T \mathcal{P}\,, \tag{3.48}$$

where

$$L^T = \int d\tau d^{\mathrm{d}}x \left\{ \frac{\delta}{\delta \phi_R} \left[N_R \frac{\delta}{\delta \phi_R} - K_R \right] + \frac{\delta}{\delta \phi_I} \left[N_I \frac{\delta}{\delta \phi_I} - K_I \right] \right\} . \tag{3.49}$$

It is not obvious *a priori* whether this process reproduces the desired expectation values of the physical observables, i.e. whether $\langle O \rangle_{\mathcal{P}(t)}$ actually corresponds to the physical expectation value of the theory. It is not even clear that the process will converge and if it does, whether it converges to the correct answer.

The fundamental question underlying the validity of the CL approach is the relation between the CL distribution $\mathcal{P}[\phi_R, \phi_I, t]$ and the desired complex distribution $\rho[\phi]$ in Eq. (3.40). The latter defines the physics

of interest and is a fixed point of its own FP equation

$$\frac{\partial \rho}{\partial t} = L_0^T \rho, \tag{3.50}$$

where

$$L_0^T = \int d\tau d^{\mathrm{d}}x \, \frac{\delta}{\delta \phi_R} \left[\frac{\delta}{\delta \phi_R} + \frac{\delta S}{\delta \phi_R} \right], \tag{3.51}$$

which is obtained by temporal differentiation of

$$\langle O \rangle_{\rho(t)} \equiv \int \mathcal{D}\phi_R \; \rho[\phi_R, t] O[\phi_R]. \tag{3.52}$$

Here, it is assumed (as in the above section) that the boundary terms vanish at infinity. More specifically, we want to know whether

$$\langle O \rangle_{\mathcal{P}(t)} = \langle O \rangle_{\rho(t)}, \tag{3.53}$$

holds.

In Refs. [60, 61] it was shown how the desired relationship Eq. (3.53) can be proven for holomorphic observables, as long as the action and the associated drift are both holomorphic functions of ϕ. The proof relies on analyzing the behavior of

$$F(t, \tau) = \int \mathcal{D}\phi_R \mathcal{D}\phi_I \; \mathcal{P}[\phi_R, \phi_I, t - \tau] O[\phi_R + i\phi_I, \tau], \tag{3.54}$$

where $0 \leq \tau \leq t$. The function $F(t, \tau)$ interpolates between the two expectation values of interest:

$$F(t, 0) = \langle O \rangle_{\mathcal{P}(t)}, \qquad F(t, t) = \langle O \rangle_{\rho(t)}. \tag{3.55}$$

where we have assumed that the initial conditions are chosen as

$$\mathcal{P}(\phi_R, \phi_I, 0) = \rho[\phi_R, 0] \delta(\phi_I - \phi_{I,0}). \tag{3.56}$$

We find that

$$F(t,0) = \int \mathcal{D}\phi_R \mathcal{D}\phi_I \mathcal{P}[\phi_R, \phi_I, t] O[\phi_R + i\phi_I, 0] = \langle O \rangle_{\mathcal{P}(t)}, \tag{3.57}$$

while, using the initial conditions of Eq. (3.56),

$$F(t,t) = \int \mathcal{D}\phi_R \mathcal{D}\phi_I \mathcal{P}[\phi_R, \phi_I, 0] O[\phi_R + i\phi_I, t] = \int \mathcal{D}\phi_R \; \rho[\phi_R, 0] O[\phi_R + i\phi_{I,0}, t] = \langle O \rangle_{\rho(t)}, \tag{3.58}$$

where we have used Eq. (3.50) and integration by parts to shift the Langevin evolution operator from O to ρ.

If $F(t,\tau)$ is independent of τ, then Eq. (3.53) holds, and the Langevin method is formally shown to be valid for complex-valued variables. This means that if it converges, it will converge to the correct physical answers. Naturally, this statement assumes that the expectation values in Eq. (3.53) agree at $t = 0$, which can be ensured by choosing the initial condition of the Langevin process as above. The τ derivative of $F(t,\tau)$ involves an integration by parts:

$$\frac{\partial}{\partial \tau} F(t,\tau) = \int \mathcal{D}\phi_R \mathcal{D}\phi_I \left\{ \mathcal{P}[\phi_R, \phi_I, t-\tau] L O[\phi_R + i\phi_I, \tau] - L^T \mathcal{P}[\phi_R, \phi_I, t-\tau] O[\phi_R + i\phi_I, \tau] \right\}, \tag{3.59}$$

where L is the Langevin operator and L^T its adjoint. If we integrate by parts and the boundary terms are zero, then $\frac{\partial}{\partial \tau} F(t,\tau) = 0$. If the decay of

$$\mathcal{P}[\phi_R, \phi_I, t-\tau] O[\phi_R + i\phi_I, \tau], \tag{3.60}$$

and its derivatives is not fast enough to ensure that the boundary terms will vanish, then it cannot be guaranteed that the expectation values of the quantities of interest obtained via a Langevin process will converge to the correct values [60, 61].

Two general issues for CL are raised by this examination: first, the behavior of the probability distribution at boundaries and second, the rate of decay of the drift function. We discuss these in more detail below:

Behavior of the probability distribution at boundaries

The behavior of boundaries at infinity is a relevant question for models in both relativistic and non-relativistic physics. In particular, for gauge theories the complexification of the link variables leads to

non-compact groups, e.g. SU(3) becomes SL(3,C). A similar effect is seen in nonrelativistic physics when using compact Hubbard-Stratonovich transformations. In either case, merely assuming that the derivative of $F(t, \tau)$ in Eq. (3.59) vanishes is a bad idea. For that to happen, the solutions to the FP equation must fall off sufficiently quickly along non-compact directions in the (complexified) space of field configurations[1]. That property is very difficult to determine *a priori*, but can be checked *a posteriori* following the arguments of Ref. [64]. Case studies show that in many cases, while the solutions fall off faster than exponentially in the real directions, the decay in the imaginary directions may be insufficient [60]. Such an insufficient decay at infinity can also lead to the so-called excursion problem, where the drift function grows uncontrollably in the imaginary direction, pulling the results away from the real line.

In addition to the boundaries at infinity in the imaginary space, under some conditions boundaries can arise in the complex space due to a singular drift function. This singular drift function can occur as a result of zeroes in the fermion determinant, and the probability distribution must also go to zero in the region of these poles. While this thesis is concerned with the application of CL to bosonic field theories, it is worth mentioning that there have been some techniques developed in order to address these issues in fermionic field theories.

For fermionic actions where poles appear naturally, the results for the holomorphic case can be used, provided that a region around the poles is cut out [65]. That procedure is justified as long as the probability measure vanishes around those poles sufficiently fast; in other words, the boundaries around the poles take on the same relevance as those at infinity. A detailed study of incorrect convergence due to poles in the drift function showed that the location of these poles, the decay of the probability distribution, and the behavior of the observables in the region near the poles all played a role in whether the method would return correct results [64, 65].

Distribution of the drift function

A re-examination of the conditions for correctness in Refs. [64, 66] revealed that failure of CL that in some cases has been attributed to the excursion and singular drift problems are actually due to the drift function falling off too slowly. It was argued in Ref. [67], using a semiclassical analysis, that when more than one saddle point in the complex plane contributes to the ensemble averages, the CL method can lead to

[1]See Refs. [62, 63] for an insightful discussion of an exactly solvable case)

incorrect answers due to the different complex phases associated with each saddle point.

While the condition of fast decay was recognized in [60, 61], the precise rate was not immediately clear. In Ref. [64], the above arguments were reviewed by considering a finite step-size in Langevin time. It was then found that the above integration by parts is valid if the probability distribution of the drift term falls off faster than any power at large drift magnitude. In practice, it is very difficult to establish the behavior of Eq. (3.59), but it is perfectly possible to study the probability distribution of the drift and establish whether the decay is exponential. If this condition is satisfied, then the drift function is unlikely to be singular and the system is a good candidate for complex Langevin without concern about the presence of poles.

3.3.2: Practical aspects: numerical instabilities, gauge cooling, dynamic stabilization, and regulators

On the practical side, several strategies have been identified to tackle specific issues that arise in a numerical treatment of complex Langevin. While some systems are not well-suited to CL because their probabilities don't decay fast enough at the boundaries, others are good candidates until numerical noise pulls the simulation off the acceptable trajectory. Numerical noise can incorrectly place something on the wrong trajectory, leading to excursions in the imaginary direction, and so most strategies to resolve issues with the CL algorithm are attempts to control the numerical instabilities without great sacrifice to computational resources.

One of the issues recognized early on is the appearance of instabilities in the form of runaway trajectories along the CL evolution [68, 69]. These can become frequent enough to completely spoil a calculation performed at fixed step size. In Ref. [45], the need for adaptive step size integration of the complex Langevin equations was identified. It was found that such an approach provides a solution to the problem of instabilities and has thus become the standard for CL calculations.

A separate issue for correctness, mentioned above, is that of insufficient decay at infinity. In practice, it can lead to uncontrolled excursions of the CL process into the complex plane, making calculations unstable. To that end, a few practical solutions have been explored.

Gauge cooling ([70–74]) is one example of such practical solutions which, though necessary, is often not sufficient. It remains, however, the best understood approach from a mathematical perspective [73]: gauge cooling is a mathematically exact procedure. The idea is that at each Langevin step, one can make a gauge transformation to keep the variables close to the compact subgroup. In gauge fields, this means transforming in SU(3,C) to maintain the link variables within an acceptable distance from SU(3).

Dynamic stabilization was developed to further aid with the excursion problem [75–78]. The essential idea of this approach is to add a term to the Langevin drift K in the schematic form

$$K \to -DS + i\alpha_{DS} M, \tag{3.61}$$

where $-DS$ is the standard CL drift, α_{DS} is a control parameter, and M acts only in the non-SU(3) directions and grows rapidly with the distance from the SU(3) manifold. The above modification to the Langevin evolution cannot be derived from the action but it vanishes in the continuum limit and prevents large excursions into the complex plane.

While gauge cooling and dynamic stabilization first appeared in relativistic calculations, regulators, or modified actions, first appeared in a nonrelativistic application, namely Ref. [79]. They were also discussed more recently in Ref. [63] and the idea is similar to dynamic stabilization, except that the resulting modifications on the Langevin equations are directly derived from the action. In both of those works, the modification consisted of adding a term of the form $\xi\phi^2$, which is decreased and the limit as $\xi \to 0$ examined in the final results. While the advantages of such a practical solution were clear, it is by no means a full solution and in many cases – especially at strong coupling or low temperatures – it is not possible to make ξ small and obtain a converging calculation.

CHAPTER 4: The relativistic Bose gas

Section 4.1: Motivation

As discussed in previous chapters, field theories with a complex action suffer from a sign problem when treated with conventional Monte Carlo approaches. This includes QCD at finite baryon density, but also bosonic field theories with a chemical potential and an action such that $S^*(\mu) = S(-\mu)$. The complex Langevin method was used to tackle the sign problem in the relativistic Bose gas at finite μ, and was one of the first successful examples of CL used in QFT on the lattice [1]. This chapter re-examines this application of CL to relativistic bosons as proof of concept and to establish the algorithm which will be later adapted to nonrelativistic bosons.

Section 4.2: Action and formalism: relativistic, interacting bosons at finite chemical potential

The system is a self-interacting complex scalar field in 4 spacetime dimensions, represented by the action:

$$S = \int \mathrm{d}^4x \left[|\partial_\nu \phi|^2 + (m^2 - \mu^2)|\phi|^2 + \mu(\phi^* \partial_4 \phi - \partial_4 \phi^2 \phi) + \lambda |\phi|^4 \right] \tag{4.1}$$

where $m^2 > 0$, μ is the chemical potential, and λ represents a contact interaction. It is expected that, at zero temperature, this system will undergo a phase transition to Bose-Einstein condensation at some critical chemical potential $\mu_c > 0$.

This action can be discretized, in order to treat the system with a lattice field theory, in the following way:

$$S = \sum_x \left[(2\mathrm{d} + m^2)\phi_x^* \phi_x + \lambda(\phi_x^* \phi_x)^2 - \sum_{\nu=1}^{\mathrm{d}} (\phi_x^* e^{-\mu \delta_{\nu,4}} \phi_{x+\hat{\nu}} + \phi_{x+\hat{\nu}}^* e^{\mu \delta_{\nu,4}} \phi_x) \right], \tag{4.2}$$

where here we have generalized the action to d spacetime dimensions. The lattice spacing in both space and time is given by $a = 1$, and the lattice volume is $V = N_t N_x^{\mathrm{d}-1}$, with periodic boundary conditions in all spacetime directions. The chemical potential, μ is an imaginary, constant vector potential function that points in the t direction. This results in an action such that $S^*(\mu) = S(-\mu)$, which suffers from the sign problem in ordinary Markov chain Monte Carlo (MCMC) approaches.

To circumvent the sign problem, we apply instead the complex Langevin method. As discussed in Chapter 3, the Langevin equations read:

$$\frac{\partial \phi_x(t_L)}{\partial t_L} = -\frac{\delta S[\phi]}{\delta \phi_x(t_L)} + \eta_x(t_L). \tag{4.3}$$

Here, t_L is the Langevin time and η is random noise (real and Gaussian-distributed, as discussed in Chapter 3). The fields $\phi_x(t_L)$ must then be expressed explicitly in terms of their components, in order to represent the complex action in terms of real fields. Thus, $\phi_x(t_L)$ is written as $\phi_x = \frac{1}{\sqrt{2}}(\phi_1 + i\phi_2)$. From this point, we drop the explicit dependence on t_L in the fields in our notation, for simplicity.

The complex action expressed in terms of real fields $\phi_{a=1,2}$ is:

$$S = \sum_x [(\mathrm{d} + \frac{m^2}{2})\phi_{a,x}^2 + \frac{\lambda}{4}(\phi_{a,x}^2)^2 - \sum_{i=1}^{\mathrm{d}-1} \phi_{a,x}\phi_{a,x+\hat{i}} - \cosh(\mu\phi_{a,x}\phi_{a,x+\hat{4}}) + i\sinh(\mu\epsilon_{ab}\phi_{a,x}\phi_{b,x+\hat{4}}) \tag{4.4}$$

with an implied summation over repeated indices and $a = 1, 2$, and d the Euclidean spacetime dimension. The real fields ϕ_a are then complexified:

$$\phi_a = \phi_a^R + i\phi_a^I \tag{4.5}$$

and the Langevin time, t_L, is discretized as $t_L = n\epsilon$. The resulting discretized and complexified Langevin equations then become:

$$\phi_{a,x}^R(n+1) = \phi_{a,x}^R(n) - \epsilon K_{a,x}^R(n) + \sqrt{\epsilon}\eta_{a,x} \tag{4.6}$$

$$\phi_{a,x}^I(n+1) = \phi_{a,x}^I(n) - \epsilon K_{a,x}^I(n) \tag{4.7}$$

With

$$K_{a,x}^R = -\mathrm{Re}\left[\left(\frac{\delta S[\phi]}{\delta \phi_{a,x}}\right)_{\phi_a \to \phi_a^R + i\phi_a^I}\right] \tag{4.8}$$

$$K_{a,x}^I = -\mathrm{Im}\left[\left(\frac{\delta S[\phi]}{\delta \phi_{a,x}}\right)_{\phi_a \to \phi_a^R + i\phi_a^I}\right] \tag{4.9}$$

These equations govern the evolution of our fields in the fictitious Langevin time, which will yield a set of configurations distributed according to the desired probability distribution $\mathcal{P}[\phi] = e^{-S[\phi]}$. The algorithm for

this process is given below:

1. Initialize the four fields ($\phi_1^R, \phi_1^I, \phi_2^R,$ and ϕ_2^I) at each site on an $N_t N_x^{\mathrm{d}-1}$ lattice using a uniform random number distribution centered around zero.

2. Evolve the whole lattice for n steps of size ϵ in complex Langevin time. At each Langevin step:

   - Generate real, Gaussian distributed noise.
   - Generate the action from the fields.
   - Update the four field components at each site using Eq. (4.6).
   - After some thermalization time, save decorrelated samples, to calculate averaged observables with good statistical properties

3. Repeat this over all the different sizes and values for the chemical potentials

We are interested in calculating the average particle density, $\langle \hat{n} \rangle$ and the square of the field modulus $\langle \phi^* \phi \rangle$, both quantities which are real-valued despite the complexity of the action. The density of the system is given by

$$\langle \hat{n} \rangle = \frac{1}{V} \sum_x \sum_{a,b=1}^{2} \left(\delta_{ab} \sinh \mu - i \epsilon_{ab} \cosh \mu \right) \phi_{a,x} \phi_{b+\hat{4}}. \tag{4.10}$$

The derivation of the density as a function of the four field components ($\phi_{1/2}^{R/I}$) is worked out in greater detail in Appendix B.1. The square of the field modulus is a simpler expression:

$$\langle \phi^* \phi \rangle = \frac{1}{V} \sum_x \sum_{a=1}^{2} \phi_{a,x} \phi_{a,x} \tag{4.11}$$

which can also be expressed in terms of our four field components by noting that $\phi_{a,x} = \phi_{a,x}^R + i \phi_{a,x}^I$.

At the critical chemical potential, $\mu = \mu_c$, there should be a 2nd order phase transition to a BEC, with

$$\langle n \rangle = \frac{1}{V} \frac{\partial \ln \mathcal{Z}}{\partial \mu} \neq 0 \tag{4.12}$$

The critical chemical potential μ_c is given in the non-interacting case by $|\mu_c^0| = 2 \operatorname{arcsinh}(m/2)$, while in the interacting case, it is expected that $|\mu_c| > |\mu_c^0|$.

Section 4.3: Results

4.3.1: Statistical and systematic effects

In order to calculate the quantities of interest, we must first determine the thermalization time of the system, as well as compute the autocorrelation of the observables.

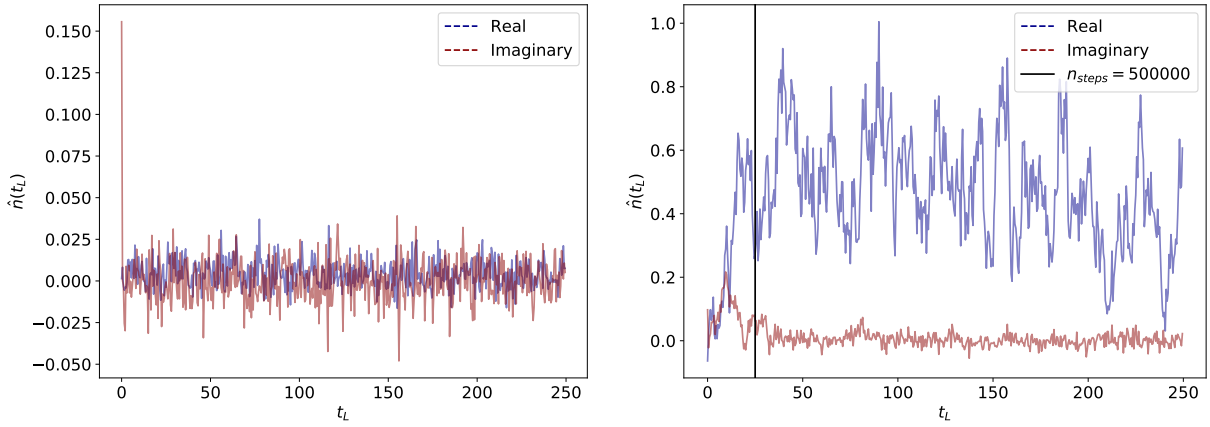

Figure 4.1: Thermalization of the Langevin simulation for chemical potentials below the critical point (left) and above it (right). After thermalization, the running average remains stable despite fluctuations in the individual samples.

We can see the thermalization point by looking at values of the observables as they evolve in Langevin time. They will begin at the point of initialization, and change rapidly under the influence of the Langevin drift function, until eventually they settle into a random walk around some stable, mean value. This is easy to see in the right panel of Figure 4.1, where our real and imaginary observables differ significantly from each other at the end of the Langevin evolution. While the samples fluctuate – and even appear to evolve – a running average shows that the average value remains stable after thermalization. In the left panel, we see the thermalization for an observable which averages to zero is harder to pick out, as the change from the initial values to the point of thermalization is not as pronounced. In this case, we can use the thermalization point for other observables to ensure we capture the correct behavior.

We also must compute the autocorrelation time, τ_A. This tells us how many steps we must take between samples in order to truly be using decorrelated samples, and we can also incorporate this into our error analysis. We use a bootstrap analysis to determine the autocorrelation time (in Langevin seconds), which we can then convert to autocorrelation steps by dividing the time by the Langevin spacing ($\epsilon = 5 \times 10^{-5}$). We

can update the error to include autocorrelation error into our standard statistical error in the following way

$$\Delta_A = \sqrt{\frac{\sigma^2}{N_{\text{samples}}}(1 + 2\tau_A)}, \tag{4.13}$$

where Δ_A includes both statistical error and autocorrelation error.

Now that we have established our basic practices for error analysis, we can discuss the results obtained via the CL method.

4.3.2: The noninteracting case

The noninteracting action can be expressed in the following way:

$$S = \sum_{x,x',a,a'} \phi^*_{x,a} M_{x,a;x'a'} \phi_{x',a'}. \tag{4.14}$$

This can be further simplified and then compared with results obtained using complex Langevin for $\lambda = 0$. When we write our lattice action of Eq. (4.2) in the form proposed in Eq. (4.14), we find that M is

$$M[m, \mathrm{d}, \mu] = (2\mathrm{d} + m^2)\delta_{x,x'} - \sum_{j=1}^{\mathrm{d}} (\delta_{x,x'-\hat{j}} + \delta_{x,x'+\hat{j}}) - (e^{-\mu}\delta_{x,x'-\hat{4}} + e^{\mu}\delta_{x,x'+\hat{4}}). \tag{4.15}$$

Since M only depends on the separation between x and x', it can be diagonalized by a Fourier transformation. The derivation of M and its subsequent Fourier transformation is shown in Appendix B, and the resulting diagonal matrix is:

$$D_{k,k'} = \left((2\mathrm{d} + m^2) - \sum_{j=1}^{\mathrm{d}} (e^{ik'_j} + e^{-ik'_j}) - (e^{-\mu - i\omega'} + e^{\mu + i\omega'}) \right) \delta_{k,k'}. \tag{4.16}$$

This diagonal representation of the lattice action is much simpler to work with than the position-space representation. We can use this matrix to determine analytical values for the density and the field modulus squared ($|\phi^2|$) and check the results of the CL method for this special case of $\lambda = 0$.

The partition function can be written the following way, for an action that can be expressed as Eq. (4.14)

$$\mathcal{Z} = \int \mathcal{D}\phi^* \mathcal{D}\phi e^{-S[\phi]} = \frac{1}{\det M}, \tag{4.17}$$

And we can produce analytical results for observables by taking derivatives of the partition function with

respect to various parameters, as in

$$\frac{-1}{V}\frac{\partial ln\mathcal{Z}}{\partial \alpha} = \frac{-1}{V\mathcal{Z}}\int \mathcal{D}\phi^*\mathcal{D}\phi e^{-S[\phi^*,\phi]}\frac{-\partial S}{\partial \alpha} = \left\langle \frac{\partial S}{\partial \alpha}\right\rangle. \tag{4.18}$$

The derivative of the action with respect to the mass squared (m^2) gives us $\phi^*\phi$:

$$\frac{-1}{V}\frac{\partial ln\mathcal{Z}}{\partial (m^2)} = \frac{1}{V\mathcal{Z}}\int \mathcal{D}\phi^*\mathcal{D}\phi e^{-S[\phi^*,\phi]}\,(\phi^*\phi) = \langle\phi^*\phi\rangle, \tag{4.19}$$

We can compare these analytical results against values produced by the CL algorithm. When we apply Eq. (4.17), we can find this in terms of our diagonal matrix D, and then compute the result exactly. When we do this, we find that

$$\langle\phi^*\phi\rangle = \sum_k \frac{D^*_{kk}}{|D_{kk}|^2}, \tag{4.20}$$

where the sum is restricted to values of k that correspond to the Fourier transformed lattice sites: $k^\alpha = 2\pi\frac{n}{N_x}$, with $n \in (0, N_x - 1)$.

Additionally, the density is found by taking a derivative with respect to the chemical potential, μ:

$$\frac{-1}{V}\frac{\partial ln\mathcal{Z}}{\partial \mu} = \langle\hat{n}\rangle\,. \tag{4.21}$$

In terms of D, this is

$$\langle\hat{n}\rangle = \sum_k \frac{D^*_{kk}(\cos k^4 \sinh\mu + i\sin k^4\cosh\mu)}{|D_{kk}|^2}, \tag{4.22}$$

with our k sum restricted to the same values as before.

The results are shown in Figure 4.2. We see that the CL algorithm correctly reproduces the exact values for this case.

4.3.3: Real initialization, no interaction, zero chemical potential

For the special case in which the imaginary fields are initialized to zero, the chemical potential is fixed to zero, and there are no interactions, the results should be entirely real. In this case, there is technically no need for complex Langevin, as there is no sign problem, but we should expect our code to return the

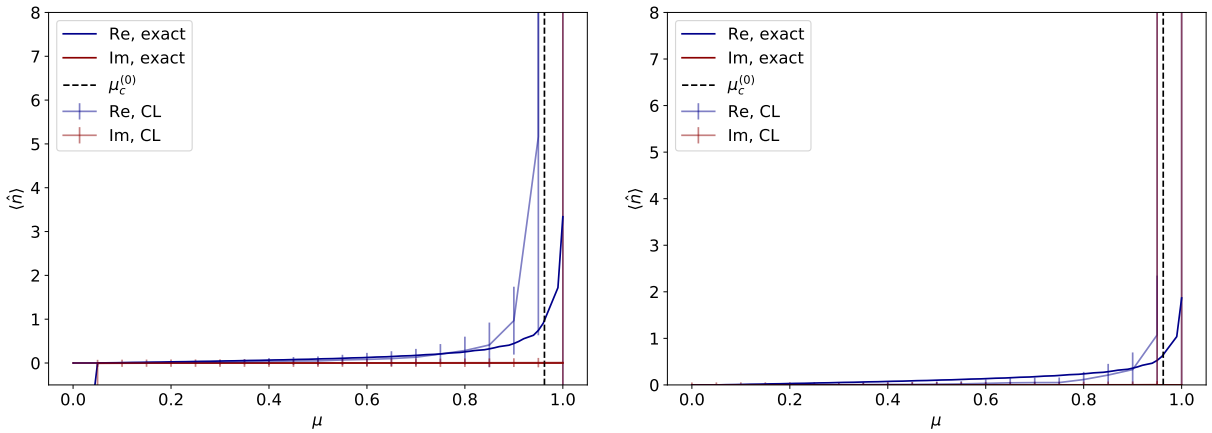

Figure 4.2: The real imaginary components of the density as a function of chemical potential, both exact and CL results, for $N_x = N_t = 4$ (left) and 6 (right).

appropriate results for an entirely real case.

We found that for $\phi^I_{1,2}(t_L = 0) = 0$, $\mu = 0$, and $\lambda = 0$, the code returned results with no imaginary parts. The imaginary fields and actions were identically zero, and the imaginary density averaged to zero (the imaginary density is a combination of real and imaginary fields, so we would not expect it to be identically zero, but we would expect it to be zero within its standard deviation).

4.3.4: Finite chemical potential and interaction: the full CL treatment

Values of the field modulus squared and density were computed with stepsize $\epsilon = 5 \times 10^{-5}$ for 5×10^6 steps in Langevin time. For thermalization, the first 5×10^4 steps were left out of analysis. These values were computed for lattices of size $N_x = N_t = 4, 6, 8,$ and 10 and chemical potential $0 \leq \mu \leq 1.7$. Our results were qualitatively consistent with Ref. [1], as seen in Figure 4.3 and Figure 4.4. Discrepancies between our computed values and the values from Ref. [1] are likely due to small differences that arise in digitizing the data from the original plots, as well as small differences in dealing with systematic effects. While the original work simply averages all the samples, our recreation takes into account the effects of autocorrelation, taking fewer, de-correlated samples to average for the final value.

Section 4.4: Summary and conclusions

We have shown in this chapter the ability of the complex Langevin method to treat a system with a sign problem. The method is able to handle a system whose action is complex, evolving a set of field values from which observables of interest can be computed. The resulting set of observables, after some thermalization, can then be averaged, much like with standard QMC methods. The statistical error is related to the number of

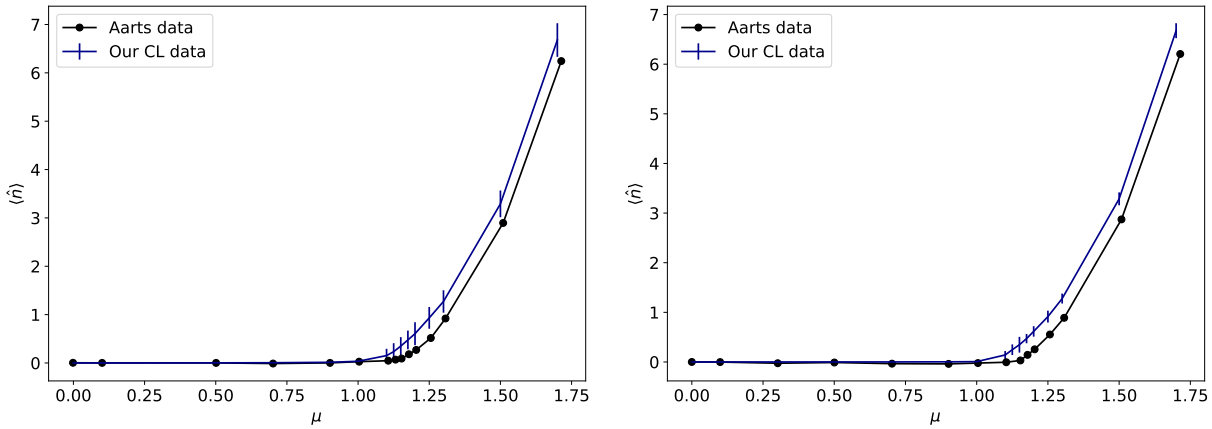

Figure 4.3: Comparison of our results for the density of the relativistic Bose gas at finite potential, against the results of Ref. [1] for $N_x = N_t = 4$ (left) and 6 (right).

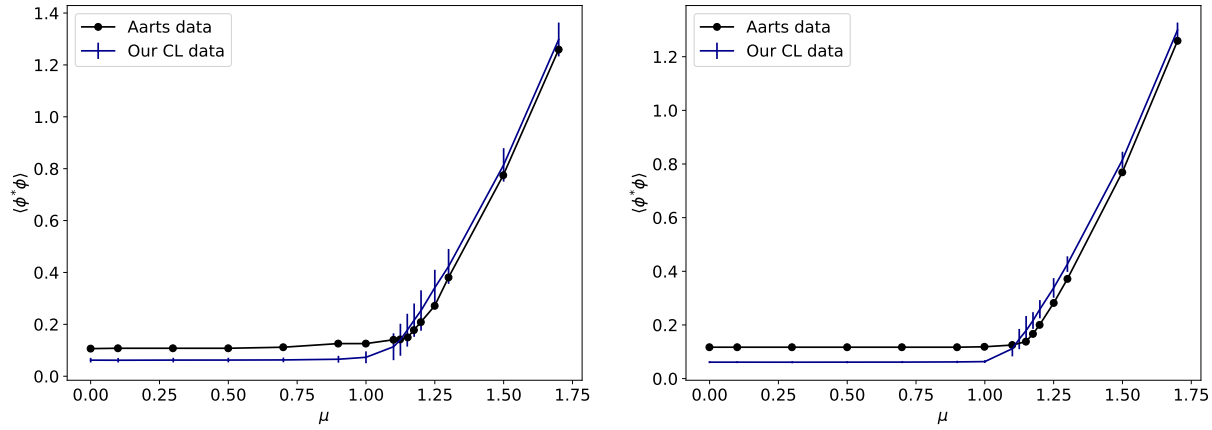

Figure 4.4: Comparison of our results for the field modulus squared of the relativistic Bose gas at finite potential, against the results of Ref. [1] for $N_x = N_t = 4$ (left) and 6 (right).

samples by the usual $1/\sqrt{N}$ factor, and therefore statistical error can be managed by increasing or decreasing the number of samples computed.

This method provides a useful tool for treating systems with a sign problem in relativistic physics. In the next chapter, we will apply it to a nonrelativistic bosonic system which also suffers from a sign problem: the rotating superfluid.

CHAPTER 5: Interacting Bose gas at finite chemical potential and angular momentum

Section 5.1: Motivation

In 1946, Fritz London first proposed that superconductivity and superfluidity were "quantum mechanisms on a macroscopic scale" [11]. Additionally, he linked superfluidity with the (then only theoretical and not observed) mechanism of Bose-Einstein condensation. Since London's early insights into superfluid behavior, the system has been studied extensively using super-cooled atoms [11].

In 1949, Lars Onsager predicted that vortices would form in rotating superfluids [12]. Richard Feynman expanded on Onsager's prediction a few years later, reiterating the expectation that quantized vortices would appear when superfluids were forced to rotate [13]. Another 30 years after these predictions, the first direct observation of quantum vortices was made in rotating superfluid helium [29].

Superfluid velocity has no curl, and therefore is irrotational. However, nonzero hydrodynamic circulation can exist, and must be quantized in units of $2\pi\hbar/m$ [11]. This disconnect between the finite circulation and the irrotational superfluid velocity forces the superfluid to form singular regions in the density, leading to the formation of vortices.

Experimentally, great progress has been made in studying rotating superfluids since the first direct observation of vortex formation. In 2000, vortex formation was observed in stirred, magnetically-trapped rubidium atoms [17]. The next year, the Ketterle Group at MIT observed triangular vortex lattices of up to 130 vortices in rotating ultracold sodium atoms [14]. Ultracold atoms provide a highly controlled, tuneable setting for studying vortex formation and other properties of rotating superfluids. Theoretically, treatment of these systems has stalled due to the presence of the sign problem. This chapter is an attempt to apply the complex Langevin method to circumvent the sign problem in a rotating superfluid.

Section 5.2: Action and formalism

We examine in this chapter a $2+1$ dimensional system of nonrelativistic bosons of mass m with a contact interaction λ in an external harmonic trap of frequency ω_{tr} and experiencing a rotation of frequency ω_z. Both the harmonic trap and the rotation are centered around the midpoint of the lattice, and we use hard-wall boundary conditions in the spatial extent of the lattice and periodic boundary conditions in Euclidean time.

The path integral for the system is

$$\mathcal{Z} = \int \mathcal{D}\phi e^{-S[\phi]} \tag{5.1}$$

with action

$$S = \int dxdyd\tau \left[\phi^* \left(\mathcal{H} - \mu - \frac{m}{2}\omega_{\rm tr}^2 r_\perp^2 - \omega_z L_z\right)\phi + \lambda(\phi^*\phi)^2\right] \tag{5.2}$$

where

$$r_\perp^2 = (x - x_c)^2 + (y - y_c)^2, \tag{5.3}$$

with x_c and y_c the center of the trap. The angular momentum is defined in terms of the quantum mechanical operator,

$$\omega_z L_z = i\omega_z(x\partial_y - y\partial_x). \tag{5.4}$$

The use of complex fields to represent the superfluid generates a sign problem even in the action of external trap, rotation, or interaction. This sign problem can be overcome with a straightforward rewriting of the problem in the simple cases – for example, the free gas – but the introduction of the angular momentum term prevents the use of this rewriting to overcome the sign problem. The imaginary term in the angular momentum forces the action to be complex, generating a sign problem that must be circumvented another way.

To take this action to a lattice representation, we must discretize the space. The origin becomes the center of the lattice, and therefore x and y are measured relative to the point $(x_c, y_c) = (\frac{N_x-1}{2}, \frac{N_x-1}{2})$ on the lattice. We use odd values of N_x in our simulations to ensure that the center of the lattice falls on a lattice site, rather than between sites.

Using a backward-difference derivative and denoting the position on the $2 + 1$ dimensional spacetime

lattice as r, we define:

$$\partial_j \phi = \frac{1}{a}(\phi_{r-\hat{j}} - \phi_r) \tag{5.5}$$

$$\partial_j^2 \phi = \frac{1}{a^2}(\phi_{r-\hat{j}} - 2\phi_r + \phi_{r-\hat{j}}). \tag{5.6}$$

We combine $\partial_\tau - \mu$ in the lattice representation and similarly represent the angular momentum, interaction, and external trap as external gauge fields in order to avoid divergences in the continuum limit (see Appendix C.1 for details and justification of these steps). Finally, using spatial lattice site separation $a = 1$ and temporal lattice spacing $d\tau$, our lattice action becomes

$$\begin{aligned} S_{\text{lat}} = \sum_r \Bigg[& \phi_r^* \phi_r - \phi_r^* e^{d\tau\mu} \phi_{r-\hat{\tau}} - \phi_r^* \frac{d\tau}{2m} \sum_{i=x,y} \left(\phi_r^* \phi_{r+\hat{i}} - 2\phi_r^* \phi_r + \phi_r^* \phi_{r-\hat{i}} \right) \\ & - id\tau\omega_z \left((\widetilde{x} - \widetilde{y}) \phi_r^* \phi_{r-\hat{\tau}} - \widetilde{x} \phi_r^* \phi_{r-\hat{y}-\hat{\tau}} + \widetilde{y} \phi_r^* \phi_{r-\hat{x}-\hat{\tau}} \right) \\ & - d\tau \frac{m}{2} \omega_{\text{tr}}^2 (\widetilde{x}^2 + \widetilde{y}^2) \phi_r^* \phi_{r-\hat{\tau}} + d\tau \lambda (\phi_r^* \phi_{r-\hat{\tau}})^2 \Bigg]. \end{aligned} \tag{5.7}$$

where $\widetilde{x}$ and $\widetilde{y}$ are our x and y coordinates shifted by the center of the trap:

$$\begin{aligned} \widetilde{x} &= x - \frac{N_x - 1}{2} \\ \widetilde{y} &= y - \frac{N_x - 1}{2}, \end{aligned}$$

where lattice sites are numbered from 0 to $N_x - 1$.

Section 5.3: The complex Langevin method for rotating bosons

In order to treat this action composed of complex-valued fields, we use the complex Langevin method described in detail in Chapter 3 and used in the study of the relativistic Bose gas in Chapter 4. This method uses a stochastic evolution of the complex fields in a fictitious time in order to produce sets of solutions distributed according to the weight $e^{-S[\phi]}$. While standard MCMC methods produce these sets by sampling from the distribution $e^{-S[\phi]}$, this method allows us to stochastically evaluate observables whose physical behavior is governed by our action, $S[\phi]$, without specifically sampling from the distribution as though it were a probability.

5.3.1: Evolving the fields

First, we must write our complex fields explicitly as a complex sum of two real fields (i.e. $\phi = \frac{1}{\sqrt{2}}(\phi_1 + i\phi_2)$. This is worked out in Appendix C.3 for all the contributions to our action. We then complexify the fields and evolve the real and imaginary part of each field according to the complex Langevin equations, a set of coupled stochastic differential equations shown here:

$$\phi^R_{a,r}(n+1) = \phi^R_{a,r}(n) + \epsilon K^R_{a,r}(n) + \sqrt{\epsilon}\eta_{a,r}(n) \tag{5.8}$$

$$\phi^I_{a,r}(n+1) = \phi^I_{a,r}(n) + \epsilon K^I_{a,r}(n), \tag{5.9}$$

where $a = 1, 2$ labels our two real fields, ϵ is the size of our discretized step in Langevin time, and η is Gaussian-distributed real noise with mean of 0 and standard deviation of $\sqrt{2}$ (this satisfies the requirements of Eq. (3.19)). The drift functions, K, are derived from the action:

$$K^R_{a,r} = -\mathrm{Re}\left[\frac{\delta S}{\delta \phi_{a,r}}|_{\phi_a \to \phi^R_a + i\phi^I_a}\right] \tag{5.10}$$

$$K^I_{a,r} = -\mathrm{Im}\left[\frac{\delta S}{\delta \phi_{a,r}}|_{\phi_a \to \phi^R_a + i\phi^I_a}\right] \tag{5.11}$$

The derivation of the Langevin drift functions is worked out in Appendix C.6, and the results are shown below. From this point, we scale our parameters by $d\tau$ for simplicity of notation

$$\bar{\mu} = d\tau\mu \tag{5.12}$$

$$\bar{m} = m/d\tau \tag{5.13}$$

$$\bar{\omega}_{\mathrm{tr}} = d\tau\omega_{\mathrm{tr}} \tag{5.14}$$

$$\bar{\omega}_z = d\tau\omega_z \tag{5.15}$$

$$\bar{\lambda} = d\tau\lambda. \tag{5.16}$$

The real drift function is then given by

$$
\begin{aligned}
-K^R_{a,r} \;=\;& \phi^R_{a,r} - \frac{e^{\bar{\mu}}}{2}\left(\phi^R_{a,r-\hat{\tau}} + \phi^R_{a,r+\hat{\tau}}\right) + \frac{2}{\bar{m}}\phi^R_{a,r} - \frac{1}{2\bar{m}}\sum_{i=\pm x,y}\phi^R_{a,r+\hat{i}} - \frac{\bar{\omega}_{\rm tr}^2 r_\perp^2}{4}(\phi^R_{a,r+\hat{\tau}} + \phi^R_{a,r-\hat{\tau}}) \\
& + \bar{\omega}_z(x-y)\phi^I_{a,r} - \frac{\bar{\omega}_z}{2}\left[x\left(\phi^I_{a,r-\hat{y}} + \phi^I_{a,r+\hat{y}}\right) - y\left(\phi^I_{a,r-\hat{x}} + \phi^I_{a,r+\hat{x}}\right)\right] \qquad (5.17) \\
& + \sum_{b=1}^{2}\left\{\epsilon_{ab}\left[\frac{e^{\bar{\mu}}}{2}\left(\phi^I_{b,r-\hat{\tau}} - \phi^I_{b,r+\hat{\tau}}\right) + \frac{\bar{\omega}_{\rm tr}^2 r_\perp^2}{4}\left(\phi^I_{b,r+\hat{\tau}} + \phi^I_{b,r-\hat{\tau}}\right) - \frac{\bar{\omega}_z}{2}x\left(\phi^R_{b,r-\hat{y}} - \phi^R_{b,r+\hat{y}}\right)\right.\right. \\
& \left.\left. + \frac{\bar{\omega}_z}{2}y\left(\phi^R_{b,r-\hat{x}} - \phi^R_{b,r+\hat{x}}\right)\right] + \bar{\lambda}\left(\phi^R_{a,r}\phi^R_{b,r}\phi^R_{b,r} - \phi^R_{a,r}\phi^I_{b,r}\phi^I_{b,r} - 2\phi^I_{a,r}\phi^R_{b,r}\phi^I_{b,r}\right)\right\},
\end{aligned}
$$

and the imaginary drift function is given by

$$
\begin{aligned}
-K^I_{a,r} \;=\;& \phi^I_{a,r} - \frac{e^{\bar{\mu}}}{2}\left(\phi^I_{a,r-\hat{\tau}} + \phi^I_{a,r+\hat{\tau}}\right) + \frac{2}{\bar{m}}\phi^I_{a,r} - \frac{1}{2\bar{m}}\sum_{i=\pm x,y}\phi^I_{a,r+\hat{i}} - \frac{\bar{\omega}_{\rm tr}^2 r_\perp^2}{4}(\phi^I_{a,r+\hat{\tau}} + \phi^I_{a,r-\hat{\tau}}) \\
& - \bar{\omega}_z(x-y)\phi^R_{a,r} - \frac{\bar{\omega}_z}{2}\left[y\left(\phi^R_{a,r-\hat{x}} + \phi^R_{a,r+\hat{x}}\right) - x\left(\phi^R_{a,r-\hat{y}} + \phi^R_{a,r+\hat{y}}\right)\right] \qquad (5.18) \\
& + \sum_{b=1}^{2}\left\{\epsilon_{ab}\left[-\frac{e^{\bar{\mu}}}{2}\left(\phi^R_{b,r-\hat{\tau}} - \phi^R_{b,r+\hat{\tau}}\right) - \frac{\bar{\omega}_{\rm tr}^2 r_\perp^2}{4}(\phi^R_{b,r+\hat{\tau}} + \phi^R_{b,r-\hat{\tau}}) - \frac{\bar{\omega}_z}{2}x(\phi^I_{b,r-\hat{y}} - \phi^I_{b,r+\hat{y}})\right.\right. \\
& \left.\left. + \frac{\bar{\omega}_z}{2}y(\phi^I_{b,r-\hat{x}} - \phi^I_{b,r+\hat{x}})\right] + \bar{\lambda}\left(\phi^I_{a,r}\phi^R_{b,r}\phi^R_{b,r} + 2\phi^R_{a,r}\phi^R_{b,r}\phi^I_{b,r} - \phi^I_{a,r}\phi^I_{b,r}\phi^I_{b,r}\right)\right\}.
\end{aligned}
$$

These equations are used to update the values of our complexified fields as in Eq. (5.10) at each step in the Langevin evolution. This evolution continues for a long period in Langevin time (determined by the observation of thermalization followed by enough steps to produce good statistical error). Observables of interest can be calculated as functions of the fields at each point in Langevin time and averaged to find the expectation value.

5.3.2: Calculating observables

The observables of interest in this simulation are the particle density $\langle\hat{n}\rangle$, the square of the field modulus $\langle\phi^*\phi\rangle$, and the angular momentum $\langle\hat{L}_z\rangle$.

Most of these observables can be computed by taking various derivatives of the action expressed as a function of the fields and the parameters. The details of these calculations are worked out in Appendix C.7.

The real and imaginary components as a function of the fields are shown here for the density

$$\mathrm{Re}\langle\hat{n}\rangle = \frac{1}{V}\sum_r \sum_{a,b=1}^{2} \frac{e^{\bar{\mu}}}{2}\left[\delta_{ab}\left(\phi^R_{a,r}\phi^R_{b,r-\hat{\tau}} - \phi^I_{a,r}\phi^I_{b,r-\hat{\tau}}\right) - \epsilon_{ab}\left(\phi^R_{a,r}\phi^I_{b,r-\hat{\tau}} + \phi^I_{a,r}\phi^R_{b,r-\hat{\tau}}\right)\right] \quad (5.19)$$

$$\mathrm{Im}\langle\hat{n}\rangle = \frac{1}{V}\sum_r \sum_{a,b=1}^{2} \frac{e^{\bar{\mu}}}{2}\left[\delta_{ab}\left(\phi^R_{a,r}\phi^I_{b,r-\hat{\tau}} + \phi^I_{a,r}\phi^R_{b,r-\hat{\tau}}\right) + \epsilon_{ab}\left(\phi^R_{a,r}\phi^R_{b,r-\hat{\tau}} - \phi^I_{a,r}\phi^I_{b,r-\hat{\tau}}\right)\right], \quad (5.20)$$

the square of the field modulus

$$\mathrm{Re}\langle\phi^*\phi\rangle = \frac{1}{V}\sum_r \sum_{a,b=1}^{2} \frac{1}{2}\left(\phi^R_{a,r}\phi^R_{a,r} - \phi^I_{a,r}\phi^I_{a,r}\right) \quad (5.21)$$

$$\mathrm{Im}\langle\phi^*\phi\rangle = \frac{1}{V}\sum_r \sum_{a,b=1}^{2} \phi^R_{a,r}\phi^I_{a,r}, \quad (5.22)$$

and the angular momentum

$$\mathrm{Re}\langle L_z\rangle = \frac{1}{V}\sum_r \sum_{a,b=1}^{2} \frac{L^R_{z,r}}{2} \quad (5.23)$$

$$\begin{aligned} L^R_{z,r} = {} & \widetilde{x}(\phi^R_{a,r}\phi^I_{a,r-\hat{y}} + \phi^I_{a,r}\phi^R_{a,r-\hat{y}}) - \widetilde{y}(\phi^R_{a,r}\phi^I_{a,r-\hat{x}} + \phi^I_{a,r}\phi^R_{a,r-\hat{x}}) + 2(\widetilde{y}-\widetilde{x})\phi^R_{a,r}\phi^I_{a,r} \\ & + \epsilon_{ab}\left(\widetilde{x}(\phi^R_{a,r}\phi^R_{b,r-\hat{y}} - \phi^I_{a,r}\phi^I_{b,r-\hat{y}}) - \widetilde{y}(\phi^R_{a,r}\phi^R_{b,r-\hat{x}} - \phi^I_{a,r}\phi^I_{b,r-\hat{x}})\right) \end{aligned}$$

$$\mathrm{Im}\langle L_z\rangle = \frac{1}{V}\sum_r \sum_{a,b=1}^{2} \frac{L^I_{z,r}}{2} \quad (5.24)$$

$$\begin{aligned} L^I_{z,r} = {} & \widetilde{y}(\phi^R_{a,r}\phi^R_{a,r-\hat{x}} - \phi^I_{a,r}\phi^I_{a,r-\hat{x}}) - \widetilde{x}(\phi^R_{a,r}\phi^R_{a,r-\hat{y}} - \phi^I_{a,r}\phi^I_{a,r-\hat{y}}) + (\widetilde{x}-\widetilde{y})\left((\phi^R_{a,r})^2 - (\phi^I_{a,r})^2\right) \\ & + \epsilon_{ab}\left(\widetilde{y}(\phi^R_{a,r}\phi^I_{b,r-\hat{x}} + \phi^I_{a,r}\phi^R_{b,r-\hat{x}}) - \widetilde{x}(\phi^R_{a,r}\phi^I_{b,r-\hat{y}} + \phi^I_{a,r}\phi^R_{b,r-\hat{y}})\right). \end{aligned}$$

In all of the above, $V = N_x^2 N_\tau$ is the spacetime lattice volume.

Section 5.4: Results

The simulation is allowed to run for $t_L = \epsilon n_L = 3000$ "Langevin seconds." For a Langevin stepsize ϵ of 0.001, this corresponds to $n_L = 3\times10^6$ steps in the simulation. Thermalization is determined by observing a leveling-off of the observables in Langevin time. This is shown in Figure 5.1 for the density of the superfluid.

5.4.1: The free Bose gas

Exact solutions exist for the free, nonrotating, noninteracting bosonic gas – the free Bose gas – in 1, 2, and 3 spatial dimensions. We can check that our code is producing reasonable results by comparing the results of our algorithm with $\bar{\omega}_{\mathrm{tr}} = \bar{\omega}_z = \bar{\lambda} = 0$ against those exact solutions. The details of these derivations

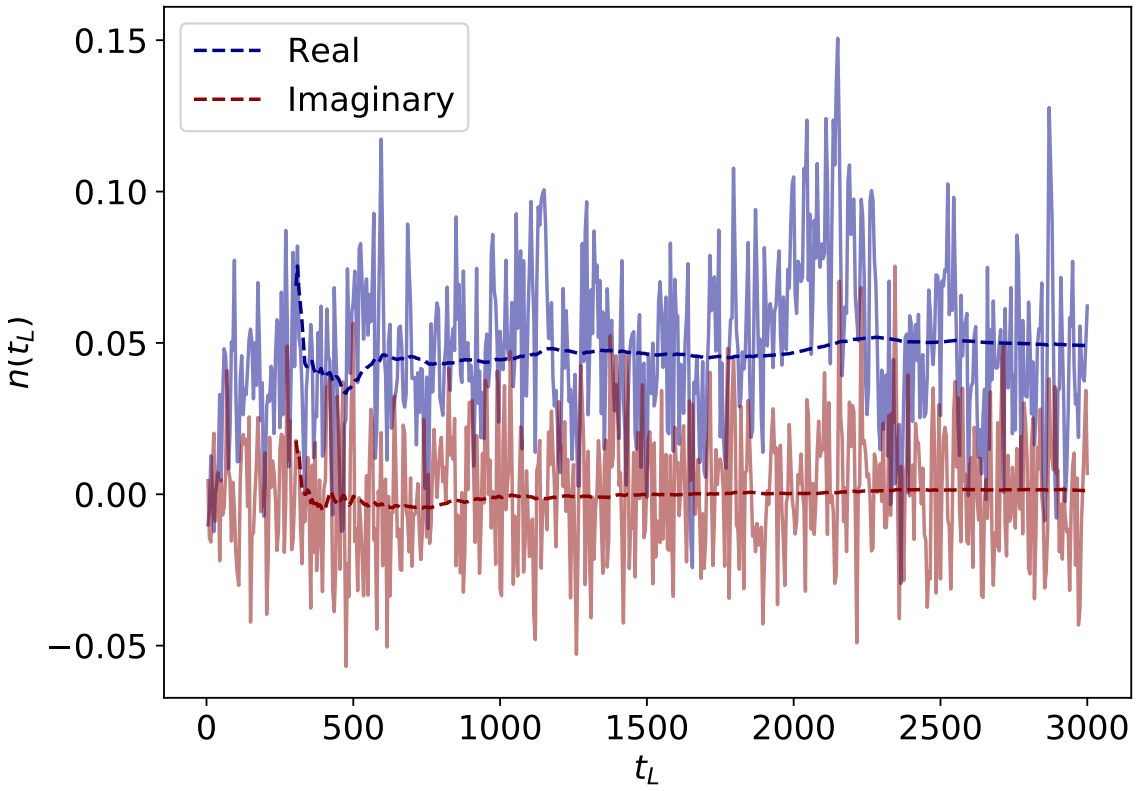

Figure 5.1: Averages of the observables are taken after discounting some fraction of the evolution, starting at $t_L = 0$. This gives the system time to thermalize and ensures that our observables samples are taken from a set which is independent of the simulation's initial conditions.

are shown in Appendix D.

In Figure 5.2, we can see the results of the CL calculation of the density and square of the field modulus compared with the exact solution. We see that the method accurately reproduces the known solutions, with some small disagreement in the region of the phase transition close to $\mu = 0$.

5.4.2: The trapped, rotating, interacting Bose gas

Now that we have shown that the CL method reproduces exactly-known values for a simplified system, we can proceed with computing the observables for a trapped, interacting, and rotating system. The real part of the density is shown in Figure 5.3 as a function of the chemical potential and as a function of the rotation frequency. The imaginary part of the density evaluated to zero within statistical error, and therefore is not shown in this figure.

We can see from the behavior of the density as a function of rotational frequency that we encounter a

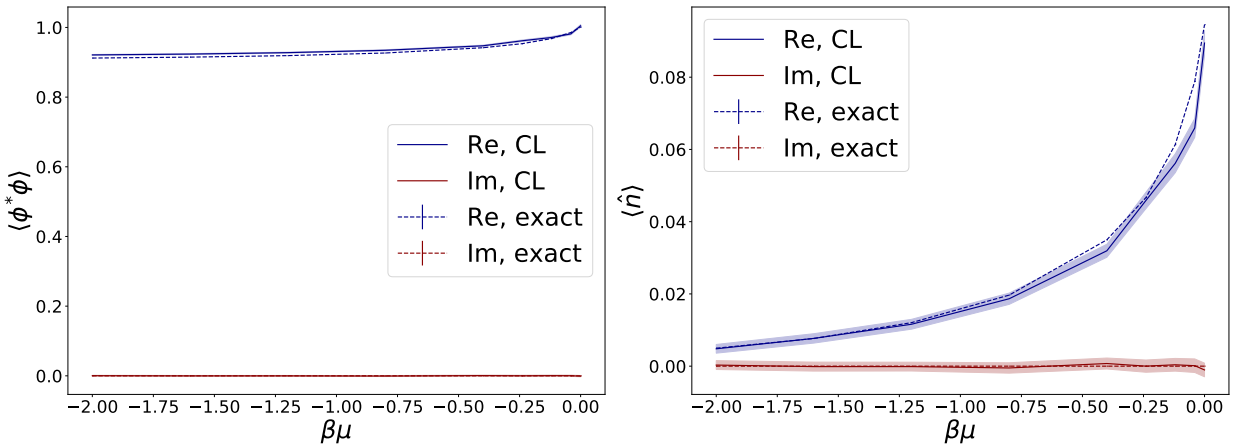

Figure 5.2: The field modulus squared (left) and density (right) of the free Bose gas in $2+1$ dimensions via CL, compared with the exact solutions.

similar issue to the phase transition discussed in Chapter 2, where the centrifugal force of the rotating fluid exceeds the force of the trapping potential which is containing the system. This results in negative values of the density, which is unphysical. We saw in Chapter 2 that when the rotation frequency exceeds the trapping potential, the angular momentum observable calculated via virial coefficients becomes negative. In addition, the particle number observable becomes negative at this critical point, which when scaled by the volume of the system corresponds to the density.

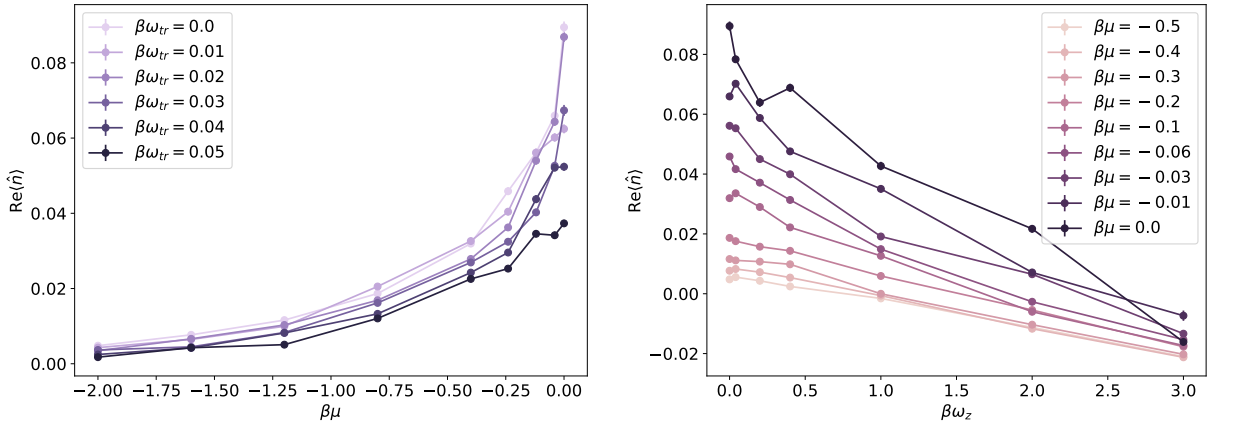

Figure 5.3: Density of the superfluid as a function of chemical potential without rotation or interaction and various trapping strengths (left) and as a function of the rotation with no trap or interactions and various chemical potentials (right).

In Figure 5.4, we see the angular momentum and moment of inertia as a function of the rotation frequency. The moment of inertia was determined from the angular momentum directly using a numerical derivative.

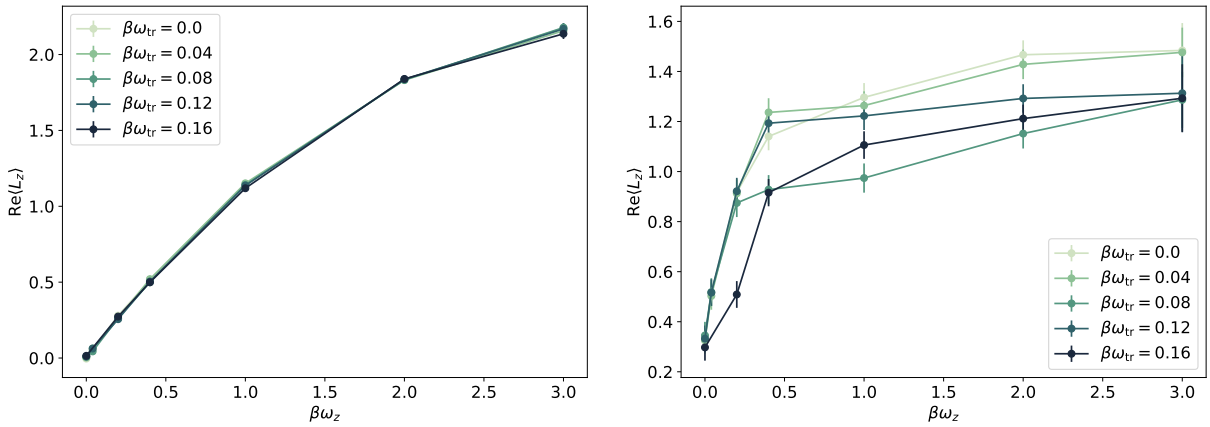

Figure 5.4: Angular momentum (left) and moment of inertia (right) as a function of the rotational frequency.

Section 5.5: Summary and conclusions

The results of the previous section have not been as illuminating as one might hope. This system has proven to be significantly more challenging than it appears from first glance.

The delicate balance of the various system parameters – in particular, the rotational frequency ω_z, the trap frequency ω_{tr}, and the interaction λ – requires extremely careful tuning, which is difficult to achieve in small systems. This meant that much of the data acquired from the CL simulation was very noisy, and it was easy to tip the system into an un-physical result (for example, the case of negative density we see in Figure 5.3) with very minor adjustments of the parameters.

In addition, we still see semi-classical behavior of the fluid, which suggests we are not in the superfluid regime yet. This is particularly visible in Figure 5.4, where the angular momentum exhibits approximately linear behavior instead of the quantized step-function behavior we would expect from a superfluid with forced rotation.

The challenge that arises here is one of computational resources. In order to see more quantum behavior, we must go to lower temperatures. However, lower temperatures in this non-relativistic treatment corresponds to longer lattices in the time direction, $T \propto 1/\beta = 1/(N_\tau d\tau)$. As the algorithm itself scales linearly both with the lattice volume and the length of the Langevin evolution, a significant increase in the time lattice results in a massive increase in the computational demand of the algorithm.

It is also possible that there is some information lost due to the finite time step of our Langevin evolution. However, this again raises the challenge of limited computational resources, as decreasing the Langevin stepsize ϵ requires a corresponding increase in the length of the Langevin evolution, which controls the

scaling of the algorithm in the same way that the volume increase does.

CHAPTER 6: Discussion and Conclusion

The sign problem remains a significant challenge in quantum many-body physics, and no one method has provided a general solution. A number of attempts in the field of quantum many-body computation have yielded results that are valid for specific systems or only in specific regimes. This thesis examined one system – that of non-relativistic, trapped, interacting, and rotating bosons – via two methods intended to circumvent the sign problem.

The first method, the virial expansion, is able to provide results for trapped, interacting, and rotating bosons, but only in a high-temperature, low-density regime. These results give us a glimpse into a system that has not been explored in depth before: that of high-temperature rotating Bose-Einstein condensates. It also provides benchmarks and insights into the behavior of this system at varying rotations and trapping potentials that can help us to interpret the results of other methods.

The second method, complex Langevin, does not restrict us to studying a high-temperature, low density regime. This means we can examine trapped, rotating, interacting bosons as they reach the superfluid regime and form vortices to sustain their angular momentum. This behavior has long been observed in experiment, but on the theoretical side has been limited to mean-field theory approaches, which do not capture the full behavior of this macroscopic quantum phenomenon.

Unfortunately, while the CL method is a well-established method for circumventing the sign problem in many similar systems, the particular sensitivity of the rotating superfluid to the various system parameters – rotation frequency, interaction strength, chemical potential, and trapping potential – means that the CL approach requires much greater computational intensity. The size of the spatial lattices must be increased in order to accommodate the delicate balance between thermal wavelength, harmonic oscillator scattering length, and rotational speed. Furthermore, early results from the system suggest that even the largest temporal lattice size used in this simulation is insufficient to capture the transition to the superfluid regime. The length of the temporal lattice is inversely proportional to the temperature of the system, meaning to reach the ultra-low temperatures needed to observe superfluidity in this system require very large lattices.

While the work here presents evidence of the CL method's effectiveness in treating this system, our current computational resources do not meet the needs of this particular problem. The CL algorithm has

shown that it can produce realistic results for a rotating bosonic gas, within the physical limits of the system, but in order to push this method to its limits and determine whether it successfully captures the quantum behavior of a rotating superfluid, much greater computational resources will be needed. This work is reserved for later study, as potential candidate for testing on the Exascale computing machines that will be arising in the near future through the Department of Energy.

APPENDIX A: DERIVATIONS FOR CALCULATING VIRIAL COEFFICIENTS

Section A.1: Single-particle basis in 2D

In this appendix we will show the solution of the Schrödinger equation for a harmonically trapped particle coupled to the z component of angular momentum in 2D. We begin with the Schrödinger equation in polar coordinates:

$$\left(-\frac{\partial^2}{\partial r^2}-\frac{1}{r}\frac{\partial}{\partial r}-\frac{1}{r^2}\frac{\partial^2}{\partial \phi^2}+m^2\omega_{\rm tr}^2 r^2-2mE\right)\Psi(r,\phi) \quad = \quad 0 \tag{A.1}$$

We then change variables such that $\rho = m\sqrt{\omega_{\rm tr}}r$, and $m, \hbar = 1$, which yields

$$r \quad \rightarrow \quad \frac{1}{\sqrt{\omega_{\rm tr}}}\rho, \tag{A.2}$$

$$\frac{\partial}{\partial r} \quad \rightarrow \quad \sqrt{\omega_{\rm tr}}\frac{\partial}{\partial \rho}, \tag{A.3}$$

$$\frac{\partial^2}{\partial r^2} \quad \rightarrow \quad \omega_{\rm tr}\frac{\partial^2}{\partial \rho^2}. \tag{A.4}$$

With those replacements, we write $\Psi(\rho,\phi)$ as a product of functions of two individual variables, $\Psi(\rho,\phi) = R(\rho)\Phi(\phi)$, such that

$$\left[-\left(\rho^2\frac{\partial^2}{\partial \rho^2}+\rho\frac{\partial}{\partial \rho}+\frac{\partial^2}{\partial \phi^2}\right)+\rho^4-2\rho^2\frac{E}{\omega_{\rm tr}}\right]R(\rho)\Phi(\phi)=0, \tag{A.5}$$

This decouples our partial differential equation into two ordinary equations, each of which must be equal to a constant $\widetilde{m}^2$:

$$-\frac{1}{\Phi(\phi)}\frac{\partial^2}{\partial \phi^2}\Phi(\phi)=\widetilde{m}^2, \tag{A.6}$$

$$-\frac{\rho^2}{R(\rho)}\frac{\partial^2 R(\rho)}{\partial \rho^2}-\frac{\rho}{R(\rho)}\frac{\partial R(\rho)}{\partial \rho}+\rho^4-2\rho^2\frac{E}{\omega_{\rm tr}}=-\widetilde{m}^2. \tag{A.7}$$

We can solve the equation for $\Phi(\phi)$ straightforwardly: $\Phi(\phi) \propto e^{i\widetilde{m}\phi}$, with the constraint that $\widetilde{m}$ must be an integer to ensure the solution is not multivalued [1].

[1] A thorough explanation of this derivation can be found in numerous mathematical methods texts, see e.g. Ref. [7]

The equation for ρ, setting $\frac{E}{\omega_{\text{tr}}} = \widetilde{E}$, is then

$$-\rho^2 \frac{\partial^2 R(\rho)}{\partial \rho^2} - \rho \frac{\partial R(\rho)}{\partial \rho} + \left(\widetilde{m}^2 + \rho^4 - 2\rho^2 \widetilde{E}\right) R(\rho) = 0. \tag{A.8}$$

At long distances ($\rho \to \infty$) we have a harmonic oscillator equation

$$-\frac{\partial^2 R(\rho)}{\partial \rho^2} + \rho^2 R(\rho) = 2\widetilde{E} R(\rho), \tag{A.9}$$

which indicates that at long distances the solution behaves as a Gaussian.

At short distances ($\rho \ll 1$), on the other hand, our equation reduces to

$$-\rho^2 \frac{\partial^2 R(\rho)}{\partial \rho^2} - \rho \frac{\partial R(\rho)}{\partial \rho} + \widetilde{m}^2 R(\rho) = 0. \tag{A.10}$$

We can approach this by proposing proposing $R(\rho) = R_0 \rho^c$, which leads to an equation for the power c in terms of our constant $\widetilde{m}$:

$$-c^2 = \widetilde{m}^2,\ c = \pm\widetilde{m}. \tag{A.11}$$

The case $\widetilde{m} = 0$ yields two solutions: a constant $R(\rho) = R_0$ and $R(\rho) = \ln \rho$. We can discard the second one since it diverges at the origin, which our wave function should not do. For the same reason we discard the case $\widetilde{m} < 0$. Therefore, the short-distance behavior is $R(\rho) \propto \rho^{|\widetilde{m}|}$.

Based on the above analysis, we propose for the full solution the form:

$$R(\rho) = e^{-\rho^2/2} \rho^{|\widetilde{m}|} F(\rho), \tag{A.12}$$

where $F(\rho)$ is a function to be determined. This captures the behavior of $R(\rho)$ in our limiting cases. With that form, the radial equation becomes

$$\rho^2 \frac{\partial^2 F(\rho)}{\partial \rho^2} + \frac{\partial F(\rho)}{\partial \rho}(b_{\widetilde{m}} \rho - 2\rho^3) - 2a_{\widetilde{m}} \rho^2 F(\rho) = 0, \tag{A.13}$$

where $a_{\widetilde{m}} \equiv 1 - \widetilde{E} + |\widetilde{m}|$ and $b_{\widetilde{m}} \equiv 2|\widetilde{m}| + 1$. We propose a power series form

$$F(\rho) = \sum_{n=0}^{\infty} \rho^n c_n \tag{A.14}$$

and obtain algebraic equations for c_n from Eq. (A.13). Analyzing the lowest powers we obtain the following conditions: From the lowest two powers of ρ, we find that c_0 is not fixed but that $c_1 = 0$. The remaining coefficients are related by the recursion

$$c_{n+2} = \frac{2(n + a_{\widetilde{m}})}{(n+2)(n+1+b_{\widetilde{m}})} c_n \tag{A.15}$$

Thus, if both c_0 and c_1 vanish, then the solution vanishes identically. On the other hand, setting $c_0 = 1$, only the odd coefficients vanish and we obtain the remaining coefficients recursively. The overall normalization can be set after the fact since the equation is linear. The series terminates if $n = -a_{\widetilde{m}}$ for some $n = 2k \geq 0$ (recall only the even n survive), which yields the quantization condition:

$$\frac{E}{\omega_{\rm tr}} = 2k + |\widetilde{m}| + 1. \tag{A.16}$$

Returning to Eq. (A.13) for $F(\rho)$, we perform another change of variables, such that $x = \rho^2$

$$x = \rho^2 \tag{A.17}$$

$$\frac{\partial}{\partial \rho} = 2\rho \frac{\partial}{\partial x} \tag{A.18}$$

$$\frac{\partial^2}{\partial \rho^2} = 2\frac{\partial}{\partial x} + 4\rho^2 \frac{\partial^2}{\partial x^2} \tag{A.19}$$

so that now we have our differential equation in terms of x instead of ρ:

$$0 = a_{\widetilde{m}} x F(x) + \left(2x^2 - (b_{\widetilde{m}} + 1)x\right) \frac{\partial}{\partial x} F(x) - 2x^2 \frac{\partial^2}{\partial x^2} F(x) \tag{A.20}$$

Divide through by x and recall that

$$b_{\widetilde{m}} = 2|m| + 1 \tag{A.21}$$

$$a_{\widetilde{m}} = 1 - \widetilde{E} + |\widetilde{m}| = 1 - (2k + |\widetilde{m}| + 1) + |\widetilde{m}| = -2k \tag{A.22}$$

With these substitutions, and slightly rearranging the equation, we see that this is the differential equation whose solution is the associated Laguerre functions:

$$x\frac{\partial^2}{\partial x^2}L(x) + (\alpha + 1 - x)\frac{\partial}{\partial x}L(x) + nL(x) = 0 \tag{A.23}$$

The final step is to normalize the full wavefunction, which leads us to the full solution for the single-particle wavefunctions in 2D:

$$\langle \mathbf{x}|\mathbf{k}\rangle = \frac{1}{\sqrt{2\pi}} N_{km}^{(2\mathrm{D})} \sqrt{\omega} e^{-\rho^2/2} \rho^{|m|} L_k^{|m|}(\rho^2) e^{im\phi}, \tag{A.24}$$

where $\rho = \sqrt{\omega} r$ and

$$N_{km}^{(2\mathrm{D})} = \sqrt{2}\sqrt{\frac{k!}{(k + |m|)!}}, \tag{A.25}$$

with $L_k^{|m|}$ the associated Laguerre functions.

APPENDIX B: DERIVATIONS FOR THE RELATIVISTIC BOSE GAS

Section B.1: The density as a function of the discretized fields

The lattice density is defined as follows:

$$\langle n \rangle = \frac{1}{V} \sum_x n_x \tag{B.1}$$

$$n_x = \sum_{a,b=1}^{2} \left(\delta_{ab} \sinh\mu - i\epsilon_{ab} \cosh\mu\right) \phi_{a,x} \phi_{b+\hat{4}} \tag{B.2}$$

$$= \sum_{a,b=1}^{2} \left(\delta_{ab} \sinh\mu - i\epsilon_{ab} \cosh\mu\right) \left(\phi^R_{a,x}\phi^R_{b,x+\hat{4}} - \phi^I_{a,x}\phi^I_{b,x+\hat{4}} + i\left(\phi^R_{a,x}\phi^I_{b,x+\hat{4}} + \phi^I_{a,x}\phi^R_{b,x+\hat{4}}\right)\right).$$

First, we explicitly compute the sum over a and b:

$$\begin{aligned} n_x = {} & \sinh\mu \left(\phi^R_{1,x}\phi^R_{1,x+\hat{4}} - \phi^I_{1,x}\phi^I_{1,x+\hat{4}} + i\left[\phi^R_{1,x}\phi^I_{1,x+\hat{4}} + \phi^I_{1,x}\phi^R_{1,x+\hat{4}}\right]\right) \\ & -i\cosh\mu \left(\phi^R_{1,x}\phi^R_{2,x+\hat{4}} - \phi^I_{1,x}\phi^I_{2,x+\hat{4}} + i\left[\phi^R_{1,x}\phi^I_{2,x+\hat{4}} + \phi^I_{1,x}\phi^R_{2,x+\hat{4}}\right]\right) \\ & +i\cosh\mu \left(\phi^R_{2,x}\phi^R_{1,x+\hat{4}} - \phi^I_{2,x}\phi^I_{1,x+\hat{4}} + i\left[\phi^R_{2,x}\phi^I_{1,x+\hat{4}} + \phi^I_{2,x}\phi^R_{1,x+\hat{4}}\right]\right) \\ & +\sinh\mu \left(\phi^R_{2,x}\phi^R_{2,x+\hat{4}} - \phi^I_{2,x}\phi^I_{2,x+\hat{4}} + i\left(\phi^R_{2,x}\phi^I_{2,x+\hat{4}} + \phi^I_{2,x}\phi^R_{2,x+\hat{4}}\right)\right). \end{aligned} \tag{B.3}$$

Now, separating this into real and imaginary parts:

$$\begin{aligned} \mathrm{Re}[n_x] = {} & \sinh\mu \left(\phi^R_{1,x}\phi^R_{1,x+\hat{4}} - \phi^I_{1,x}\phi^I_{1,x+\hat{4}} + \phi^R_{2,x}\phi^R_{2,x+\hat{4}} - \phi^I_{2,x}\phi^I_{2,x+\hat{4}}\right) \\ & + \cosh\mu \left(\phi^R_{1,x}\phi^I_{2,x+\hat{4}} + \phi^I_{1,x}\phi^R_{2,x+\hat{4}} - \phi^R_{2,x}\phi^I_{1,x+\hat{4}} - \phi^I_{2,x}\phi^R_{1,x+\hat{4}}\right) \end{aligned} \tag{B.4}$$

$$\begin{aligned} \mathrm{Im}[n_x] = {} & \sinh\mu \left(\phi^R_{1,x}\phi^I_{1,x+\hat{4}} + \phi^I_{1,x}\phi^R_{1,x+\hat{4}} + \phi^R_{2,x}\phi^I_{2,x+\hat{4}} + \phi^I_{2,x}\phi^R_{2,x+\hat{4}}\right) \\ & + \cosh\mu \left(\phi^R_{2,x}\phi^R_{1,x+\hat{4}} - \phi^I_{2,x}\phi^I_{1,x+\hat{4}} - \phi^R_{1,x}\phi^R_{2,x+\hat{4}} + \phi^I_{1,x}\phi^I_{2,x+\hat{4}}\right). \end{aligned} \tag{B.5}$$

This form can be plugged directly into the code to compute the density.

Section B.2: Analytic solutions for noninteracting Bose gas via diagonalization of the action

The lattice form of the noninteracting relativistic Bose gas at finite chemical potential can be computed exactly via Fourier transforms for $\mathrm{d} = 1, 2$, and 3 spatial dimensions plus time. It can be expressed in a matrix form, as

$$S = \sum_{x,x',a,a'} \phi^*_{x,a} M_{x,a;x'a'} \phi_{x',a'}, \tag{B.6}$$

where the matrix, M, is given by

$$M[m, \mathrm{d}, \mu] = (2\mathrm{d} + m^2)\delta_{x,x'} - \sum_{j=1}^{\mathrm{d}} (\delta_{x,x'-\hat{j}} + \delta_{x,x'+\hat{j}}) - (e^{-\mu}\delta_{x,x'-\hat{4}} + e^{\mu}\delta_{x,x'+\hat{4}}). \tag{B.7}$$

This matrix can be diagonalized using a Fourier transformation, which is a unitary transformation

$$D_{ij} = [U^{\dagger} M U]_{ij}$$

where (in three spatial dimensions)

$$\begin{aligned}
U_{xk} &= \frac{1}{\sqrt{N_x^{\mathrm{d}-1} N_t}} \exp(i\vec{k} \cdot \vec{x} - i\omega t) \\
\vec{x} &= a(x_1, x_2, x_3) \\
t &= a x_4 \\
\vec{k} &= \frac{2\pi}{a N_x}(k_1, k_2, k_3) \\
\omega &= \frac{2\pi}{a N_t} k_4 \\
\delta_{x,x'+\hat{4}} &= \delta_{t,t'+1}\delta_{x,x'}\delta_{y,y'}\delta_{z,z'}.
\end{aligned}$$

When these unitary matrices are applied and simplified, we obtain the following diagonal matrix:

$$\begin{aligned}
D &= \frac{1}{N_x^{\mathrm{d}-1} N_t} \sum_{x,x'} e^{-i\vec{k}\cdot\vec{x} + i\omega t} \left((2\mathrm{d} + m^2)\delta_{x,x'} - \sum_{j=1}^{\mathrm{d}} (\delta_{x,x'-\hat{j}} + \delta_{x,x'+\hat{j}}) - (e^{-\mu}\delta_{x,x'-\hat{4}} + e^{\mu}\delta_{x,x'+\hat{4}}) \right) e^{i\vec{k}'\cdot\vec{x}' - i\omega' t'} \\
&= \frac{1}{N_x^{\mathrm{d}-1} N_t} \sum_{x} e^{-i\vec{k}\cdot\vec{x} + i\omega t} \left((2\mathrm{d} + m^2) - \sum_{j=1}^{\mathrm{d}} (e^{ik'_j} + e^{-ik'_j}) - (e^{-\mu - i\omega'} + e^{\mu + i\omega'}) \right) e^{i\vec{k}'\cdot\vec{x} - i\omega' t} \\
&= \frac{1}{N_x^{\mathrm{d}-1} N_t} \sum_{x} \left((2\mathrm{d} + m^2) - \sum_{j=1}^{\mathrm{d}} (e^{ik'_j} + e^{-ik'_j}) - (e^{-\mu - i\omega'} + e^{\mu + i\omega'}) \right) e^{-i\vec{x}\cdot(\vec{k} - \vec{k}') + it(\omega - \omega')}.
\end{aligned} \tag{B.8}$$

Using the identity

$$\sum_{j=1}^{N} e^{i(a-a')j} = N\delta_{a,a'}, \tag{B.9}$$

our sum over x collapses and our factors of $N_x^{\mathrm{d}-1}N_t$ cancel, yielding

$$D_{k,k'} = \left((2\mathrm{d} + m^2) - \sum_{j=1}^{\mathrm{d}} (e^{ik'_j} + e^{-ik'_j}) - (e^{-\mu - i\omega'} + e^{\mu + i\omega'}) \right) \delta_{k,k'}, \tag{B.10}$$

which is diagonal in the momentum space basis.

Now that we have this diagonal matrix, we can determine the density and field modulus squared as a function of this density in the following way. First, the density:

$$\begin{aligned} \langle \hat{n} \rangle &= \frac{-1}{V} \frac{\partial \ln \mathcal{Z}}{\partial \mu} = \frac{-1}{V} \frac{\partial}{\partial \mu} (-\ln(\det(M))) \\ &= \frac{1}{V} \frac{\partial}{\partial \mu} \mathrm{Tr}(\ln M) = \frac{1}{V} \frac{\partial}{\partial \mu} \sum_k \ln D_{kk} = \frac{1}{V} \sum_k \frac{1}{D_{kk}} \frac{\partial D_{kk}}{\partial \mu} \\ &= \frac{1}{V} \sum_k \frac{1}{D_{kk}} (\cos k_4 \sinh \mu + i \sin k_4 \cosh \mu). \end{aligned} \tag{B.11}$$

And now, the field modulus squared:

$$\begin{aligned} \langle \hat{n} \rangle &= \frac{-1}{V} \frac{\partial \ln \mathcal{Z}}{\partial (m^2)} = \frac{-1}{V} \frac{\partial}{\partial (m^2)} (-\ln(\det(M))) \\ &= \frac{1}{V} \frac{\partial}{\partial (m^2)} \mathrm{Tr}(\ln M) = \frac{1}{V} \frac{\partial}{\partial (m^2)} \sum_k \ln D_{kk} = \frac{1}{V} \sum_k \frac{1}{D_{kk}} \frac{\partial D_{kk}}{\partial (m^2)} = \sum_k \frac{1}{D_{kk}}. \end{aligned} \tag{B.12}$$

APPENDIX C: DERIVATIONS FOR ROTATING SUPERFLUIDS VIA CL

Section C.1: Justification for the form of the non-relativistic lattice action

The continuum action for bosons in $2+1$ dimensions with a non-relativistic dispersion, a rotating external potential, a non-zero chemical potential, an external harmonic oscillator trapping potential, and an interaction term is as follows:

$$S = \int_V \mathrm{d}^2x\mathrm{d}\tau \left[\phi^* \left(\partial_\tau - \frac{1}{2m}\nabla^2 - \mu - i\omega_z(x\partial_y - y\partial_x) - \frac{m\omega_{\mathrm{tr}}^2}{2}(x^2+y^2)\right)\phi + \lambda(\phi^*\phi)^2\right]. \tag{C.1}$$

To convert this to a lattice action, we must first discretize the derivatives. We will use a backwards finite difference discretization for the single derivative and a central difference approximation for the double derivative, such that:

$$\partial_i\phi_r = \frac{1}{a}\left(\phi_r - \phi_{r-\hat{i}}\right) \tag{C.2}$$

$$\nabla^2\phi_r = \sum_i \frac{1}{a^2}\left(\phi_{r+\hat{i}} - 2\phi_r + \phi_{r-\hat{i}}\right), \tag{C.3}$$

where $r = (x, y, \tau)$ and the discretization length a (lattice spacing) is 1 for spatial derivatives and $\mathrm{d}\tau$ for temporal ones.

In order to treat the finite chemical potential, the external trapping potential, the rotation, and the interaction we must shift our indices on the field that is acted on by μ, ω_{tr}, ω_z, and λ by one step in the time direction. This is to make these potentials gauge invariant in the lattice formulation []. Since we have periodic boundary conditions in time, we don't have to worry about boundaries is. Therefore, our lattice action becomes, at each lattice site, r:

$$\begin{aligned} S_{\mathrm{lat},r} = {} & \phi_r^*\left[\phi_r - \phi_{r-\hat{\tau}} - \mathrm{d}\tau\mu\phi_{r-\hat{\tau}} - \frac{\mathrm{d}\tau}{2m}\sum_{i=x,y}\left(\phi_{r+\hat{i}} - 2\phi_r + \phi_{r-\hat{i}}\right) - \frac{\mathrm{d}\tau m\omega_{\mathrm{tr}}^2}{2}(x^2+y^2)\phi_{r-\hat{\tau}}\right] \\ & -\phi_r^*\left[i\mathrm{d}\tau\omega_z\left(x\phi_{r-\hat{\tau}} - x\phi_{r-\hat{y}-\hat{\tau}} - y\phi_{r-\hat{\tau}} + y\phi_{r-\hat{x}-\hat{\tau}}\right)\right] + \mathrm{d}\tau\lambda(\phi_r^*\phi_{r-\hat{\tau}})^2. \end{aligned} \tag{C.4}$$

The full action consists of summing over this value at each site on the spatiotemporal lattice as in

$$S_{\mathrm{lat}} = \sum_r S_{\mathrm{lat},r} \tag{C.5}$$

We can combine our time derivative and our chemical potential in the following way:

$$\begin{aligned} S_{\text{lat},r} &= \phi_r^* \left[\phi_r - (1 + \mathrm{d}\tau\mu)\phi_{r-\hat{\tau}} - \frac{\mathrm{d}\tau}{2m} \sum_{i=x,y} \left(\phi_{r+\hat{i}} - 2\phi_r + \phi_{r-\hat{i}} \right) - \mathrm{d}\tau \frac{m\omega_{\text{tr}}^2}{2} (x^2 + y^2)\phi_{r-\hat{\tau}} \right] \\ &\quad -\phi_r^* \left[i\mathrm{d}\tau\omega_z \left(x\phi_{r-\hat{\tau}} - x\phi_{r-\hat{y}-\hat{\tau}} - y\phi_{r-\hat{\tau}} + y\phi_{r-\hat{x}-\hat{\tau}} \right) \right] + \mathrm{d}\tau\lambda(\phi_r^*\phi_{r-\hat{\tau}})^2. \end{aligned} \tag{C.6}$$

Note that to second order in the lattice size, this is equivalent to:

$$\begin{aligned} S_{\text{lat},r} &= \phi_r^* \left[\phi_r - e^{\mathrm{d}\tau\mu}\phi_{r-\hat{\tau}} - \frac{\mathrm{d}\tau}{2m} \sum_{i=x,y} \left(\phi_{r+\hat{i}} - 2\phi_r + \phi_{r-\hat{i}} \right) - \mathrm{d}\tau \frac{m\omega_{\text{tr}}^2}{2} (x^2 + y^2)\phi_{r-\hat{\tau}} \right] \\ &\quad -i\mathrm{d}\tau\omega_z\phi_r^* \left[(x - y)\phi_{r-\hat{\tau}} - x\phi_{r-\hat{y}-\hat{\tau}} + y\phi_{r-\hat{x}-\hat{\tau}} \right] + \mathrm{d}\tau\lambda(\phi_r^*\phi_{r-\hat{\tau}})^2. \end{aligned} \tag{C.7}$$

This will be our lattice action, which we will complexify and use to evolve our system in Langevin time.

Section C.2: The non-relativistic lattice action

To simplify, let's divide the lattice action into smaller components:

$$S_{\text{lat}} = \sum_r \left(S_{\tau,r} + \mathrm{d}\tau S_{\nabla,r} - \mathrm{d}\tau S_{\text{tr},r} - \mathrm{d}\tau S_{\omega,r} + \mathrm{d}\tau S_{\text{int},r} \right) \tag{C.8}$$

with

$$S_{\tau,r} = \phi_r^*\phi_r - e^{\mathrm{d}\tau\mu}\phi_r^*\phi_{r-\hat{\tau}} \tag{C.9}$$

$$S_{\nabla,r} = \frac{2}{m}\phi_r^*\phi_r - \frac{1}{2m} \sum_{i=x,y} \left(\phi_r^*\phi_{r+\hat{i}} + \phi_r^*\phi_{r-\hat{i}} \right) \tag{C.10}$$

$$S_{\text{tr},r} = \frac{m\omega_{\text{tr}}^2}{2} (x^2 + y^2)\phi_r^*\phi_{r-\hat{\tau}} \tag{C.11}$$

$$S_{\omega,r} = i\omega_z \left[(x - y)\phi_r^*\phi_{r-\hat{\tau}} - x\phi_r^*\phi_{r-\hat{y}-\hat{\tau}} + y\phi_r^*\phi_{r-\hat{x}-\hat{\tau}} \right] \tag{C.12}$$

$$S_{\text{int},r} = \lambda(\phi_r^*\phi_{r-\hat{\tau}})^2. \tag{C.13}$$

Note that we are restricting ourselves to two spatial dimensions at this point in the work. The extension of this method to three-dimensional systems is saved for future work.

This action must next be rewritten with the complex fields expressed in terms of two real fields, $\phi = \frac{1}{\sqrt{2}} (\phi_1 + i\phi_2)$ and $\phi^* = \frac{1}{\sqrt{2}} (\phi_1 - i\phi_2)$. Each piece of the action is computed below:

First, the time derivative and chemical potential part of the action:

$$\begin{aligned} S_{\tau,r} &= \phi_r^* \phi_r - e^{\mathrm{d}\tau\mu} \phi_r^* \phi_{r-\hat{\tau}} \\ &= \frac{1}{2}\left[\phi_{1,r}^2 + \phi_{2,r}^2 - e^{\mathrm{d}\tau\mu}\left(\phi_{1,r}\phi_{1,r-\hat{\tau}} + i\phi_{1,r}\phi_{2,r-\hat{\tau}} - i\phi_{2,r}\phi_{1,r-\hat{\tau}} + \phi_{2,r}\phi_{2,r-\hat{\tau}}\right)\right] \\ &= \frac{1}{2}\sum_{a=1}^{2}\left[\phi_{a,r}^2 - e^{\mathrm{d}\tau\mu}\phi_{a,r}\phi_{a,r-\hat{\tau}} - ie^{\mathrm{d}\tau\mu}\sum_{b=1}^{2}\epsilon_{ab}\phi_{a,r}\phi_{b,r-\hat{\tau}}\right]. \end{aligned} \tag{C.14}$$

Next, the spatial derivative part (corresponding to the kinetic energy):

$$\begin{aligned} S_{\nabla,r} &= \frac{1}{2m}\left[4\phi_r^*\phi_r - \sum_{i=x,y}\left(\phi_r^*\phi_{r+\hat{i}} + \phi_r^*\phi_{r-\hat{i}}\right)\right] \\ &= \frac{1}{4m}\left[4\left(\phi_{1,r}^2 + \phi_{2,r}^2\right) - \sum_{i=\pm x,y}\left(\phi_{1,r}\phi_{1,r+\hat{i}} + i\phi_{1,r}\phi_{2,r+\hat{i}} - i\phi_{2,r}\phi_{1,r+\hat{i}} + \phi_{2,r}\phi_{2,r+\hat{i}}\right)\right] \\ &= \frac{1}{4m}\sum_{a=1}^{2}\left[4\phi_{a,r}^2 - \sum_{i=\pm x,y}\left(\phi_{a,r}\phi_{a,r+\hat{i}} + i\sum_{b=1}^{2}\epsilon_{ab}\phi_{a,r}\phi_{b,r+\hat{i}}\right)\right]. \end{aligned} \tag{C.15}$$

Then, for the part of the action due to the external trapping potential:

$$\begin{aligned} S_{\mathrm{tr},r} &= \frac{m\omega_{\mathrm{tr}}^2}{2}(x^2+y^2)\phi_r^*\phi_{r-\hat{\tau}} \\ &= \frac{m\omega_{\mathrm{tr}}^2(x^2+y^2)}{4}\left[\phi_{1,r}\phi_{1,r-\hat{\tau}} + i\phi_{1,r}\phi_{2,r-\hat{\tau}} - i\phi_{2,r}\phi_{1,r-\hat{\tau}} + \phi_{2,r}\phi_{2,r-\hat{\tau}}\right] \\ &= \frac{m\omega_{\mathrm{tr}}(x^2+y^2)}{4}\sum_{a=1}^{2}\left(\phi_{a,r}\phi_{a,r-\hat{\tau}} + i\sum_{b=1}^{2}\epsilon_{ab}\phi_{a,r}\phi_{b,r-\hat{\tau}}\right). \end{aligned} \tag{C.16}$$

Next, the rotational piece:

$$\begin{aligned} S_{\omega,r} &= i\omega_z\left[(x-y)\phi_r^*\phi_{r-\hat{\tau}} - x\phi_r^*\phi_{r-\hat{y}-\hat{\tau}} + y\phi_r^*\phi_{r-\hat{x}-\hat{\tau}}\right] \\ &= \frac{i\omega_z}{2}\left[(x-y)\left(\phi_{1,r}\phi_{1,r-\hat{\tau}} + \phi_{2,r}\phi_{2,r-\hat{\tau}}\right) + i(x-y)\left(\phi_{1,r}\phi_{2,r-\hat{\tau}} + \phi_{2,r}\phi_{1,r-\hat{\tau}}\right)\right] \\ &\quad -\frac{i\omega_z}{2}\left[x\left(\phi_{1,r}\phi_{1,r-\hat{y}-\hat{\tau}} + i\phi_{1,r}\phi_{2,r-\hat{y}-\hat{\tau}} - i\phi_{2,r}\phi_{1,r-\hat{y}-\hat{\tau}} + \phi_{2,r}\phi_{2,r-\hat{y}-\hat{\tau}}\right)\right] \\ &\quad +\frac{i\omega_z}{2}\left[y\left(\phi_{1,r}\phi_{1,r-\hat{x}-\hat{\tau}} + i\phi_{1,r}\phi_{2,r-\hat{x}-\hat{\tau}} - i\phi_{2,r}\phi_{1,r-\hat{x}-\hat{\tau}} + \phi_{2,r}\phi_{2,r-\hat{x}-\hat{\tau}}\right)\right] \\ &= \frac{\omega_z}{2}\sum_{a,b=1}^{2}\left[\epsilon_{ab}\left((x-y)\phi_{a,r}\phi_{b,r-\hat{\tau}} - x\phi_{a,r}\phi_{b,r-\hat{y}-\hat{\tau}} + y\phi_{a,r}\phi_{b,r-\hat{x}-\hat{\tau}}\right)\right. \\ &\quad \left. + i\left((y-x)\phi_{a,r}\phi_{a,r-\hat{\tau}} + x\phi_{a,r}\phi_{a,r-\hat{y}-\hat{\tau}} - y\phi_{a,r}\phi_{a,r-\hat{x}-\hat{\tau}}\right)\right]. \end{aligned} \tag{C.17}$$

And finally, the interaction term in the action:

$$\begin{aligned} S_{\mathrm{int},r} &= \lambda(\phi_r^*\phi_{r-\hat{\tau}})^2 \\ &= \frac{\lambda}{4}\left((\phi_{1,r}-i\phi_{2,r})(\phi_{1,r-\hat{\tau}}+i\phi_{2,r-\hat{\tau}})\right)^2 = \left(\phi_{1,r}\phi_{1,r-\hat{\tau}}+i\phi_{1,r}\phi_{2,r-\hat{\tau}}-i\phi_{2,r}\phi_{1,r-\hat{\tau}}+\phi_{2,r}\phi_{2,r-\hat{\tau}}\right)^2 \\ &= \frac{\lambda}{4}\sum_{a,b=1}^{2}\Big(2\phi_{a,r}\phi_{a,r-\hat{\tau}}\phi_{b,r}\phi_{b,r-\hat{\tau}}-\phi_{a,r}^2\phi_{b,r-\hat{\tau}}^2 \\ &\quad +2\,i\,\epsilon_{ab}(\phi_{a,r}^2\phi_{a,r-\hat{\tau}}\phi_{b,r-\hat{\tau}}-\phi_{a,r}\phi_{a,r-\hat{\tau}}^2\phi_{b,r})\Big) \end{aligned} \tag{C.18}$$

We will work with the lattice action in this form in order to derive the Langevin drift function.

Section C.3: Writing the complex action in terms of real fields

First, we take our complex field, ϕ, and represent it as the complex sum of two real fields: $\phi = \frac{1}{\sqrt{2}}(\phi_1+i\phi_2)$. For each of the action contributions, this gives us:

$$\mathrm{Re}[S_{\tau,r}] \rightarrow \frac{1}{2}\sum_{a=1}^{2}\left(\phi_{a,r}^2 - e^{\mathrm{d}\tau\mu}\,\phi_{a,r}\phi_{a,r-\hat{\tau}}\right) \tag{C.19}$$

$$\mathrm{Im}[S_{\tau,r}] \rightarrow \frac{-e^{\mathrm{d}\tau\mu}}{2}\sum_{a,b=1}^{2}\epsilon_{ab}\phi_{a,r}\phi_{b,r-\hat{\tau}} \tag{C.20}$$

$$\mathrm{Re}[S_{\nabla,r}] \rightarrow \sum_{a=1}^{2}\left(\frac{2}{m}\phi_{a,r}^2 - \frac{1}{4m}\sum_{i=\pm x,y}\phi_{a,r}\phi_{a,r+\hat{i}}\right) \tag{C.21}$$

$$\mathrm{Im}[S_{\nabla,r}] \rightarrow \frac{-1}{4m}\sum_{a,b=1}^{2}\sum_{i=\pm x,y}\epsilon_{ab}\phi_{a,r}\phi_{b,r+\hat{i}} \tag{C.22}$$

$$\mathrm{Re}[S_{\mathrm{tr},r}] \rightarrow \frac{m}{4}\omega_{\mathrm{tr}}^2\left(x^2+y^2\right)\sum_{a=1}^{2}\phi_{a,r}\phi_{a,r-\hat{\tau}} \tag{C.23}$$

$$\mathrm{Im}[S_{\mathrm{tr},r}] \rightarrow \frac{m}{4}\omega_{\mathrm{tr}}^2\left(x^2+y^2\right)\sum_{a,b=1}^{2}\epsilon_{ab}\phi_{a,r}\phi_{b,r-\hat{\tau}} \tag{C.24}$$

$$\mathrm{Re}[S_{\omega,r}] \rightarrow \frac{\omega_z}{2}\sum_{a,b=1}^{2}\epsilon_{ab}\left((\widetilde{y}-\widetilde{x})\phi_{a,r}\phi_{b,r-\hat{\tau}}+\widetilde{x}\phi_{a,r}\phi_{b,r-\hat{y}-\hat{\tau}}-\widetilde{y}\phi_{a,r}\phi_{b,r-\hat{x}-\hat{\tau}}\right) \tag{C.25}$$

$$\mathrm{Im}[S_{\omega,r}] \rightarrow \frac{\omega_z}{2}\sum_{a=1}^{2}\left((\widetilde{x}-\widetilde{y})\phi_{a,r}\phi_{a,r-\hat{\tau}}-\widetilde{x}\phi_{a,r}\phi_{a,r-\hat{y}-\hat{\tau}}+\widetilde{y}\phi_{a,r}\phi_{a,r-\hat{x}-\hat{\tau}}\right) \tag{C.26}$$

$$\mathrm{Re}[S_{\mathrm{int},r}] \rightarrow \frac{\lambda}{4}\sum_{a,b=1}^{2}\left(2\phi_{a,r}\phi_{b,r}\phi_{a,r-\hat{\tau}}\phi_{b,r-\hat{\tau}} - \phi_{a,r}^2\phi_{b,r-\hat{\tau}}^2\right) \tag{C.27}$$

$$\mathrm{Im}[S_{\mathrm{int},r}] \rightarrow \frac{\lambda}{2}\sum_{a,b=1}^{2}\epsilon_{ab}\left(\phi_{a,r}^2\phi_{a,r-\hat{\tau}}\phi_{b,r-\hat{\tau}} - \phi_{a,r}\phi_{b,r}\phi_{a,r-\hat{\tau}}^2\right), \tag{C.28}$$

where $\widetilde{x}$ and $\widetilde{y}$ are our x and y coordinates shifted by the center of the trap:

$$\begin{aligned}\widetilde{x} &= x - \frac{N_x - 1}{2}\\ \widetilde{y} &= y - \frac{N_x - 1}{2}\end{aligned}$$

and $S_{j,r} = \mathrm{Re}[S_{j,r}] + i\mathrm{Im}[S_{j,r}]$, and $\epsilon_{12} = 1$, $\epsilon_{21} = -1$, and $\epsilon_{11} = \epsilon_{22} = 0$. From here, we can compute the drift function we will need to evolve our fields in Langevin time.

Section C.4: Derivatives on the lattice

When taking derivatives of this lattice action with respect to the fields, we do the following:

$$\begin{aligned}\frac{\delta}{\delta\phi_{c,r}}\left(\sum_{q=1}^{N_r}\sum_{a=1}^{2}\phi_{a,q}\phi_{a,q+\hat{i}}\right) &= \sum_{a=1}^{2}\sum_{q=1}^{N_r}\left(\phi_{a,q}\frac{\delta}{\delta\phi_{c,r}}\phi_{a,q+\hat{i}} + \frac{\delta\phi_{a,q}}{\delta\phi_{c,r}}\phi_{a,q+\hat{i}}\right)\\ &= \sum_{a=1}^{2}\sum_{q=1}^{N_r}\left(\phi_{a,q}\delta_{c,a}\delta_{r,q+\hat{i}} + \delta_{c,a}\delta_{q,r}\phi_{a,q+\hat{i}}\right)\\ &= \phi_{c,r-\hat{i}} + \phi_{c,r+\hat{i}}.\end{aligned} \tag{C.29}$$

Similarly, when we have products of fields with different indices,

$$\frac{\delta}{\delta\phi_{c,r}}\left(\sum_{q=1}^{N_r}\sum_{a=1}^{2}\sum_{b=1}^{2}\epsilon_{ab}\phi_{a,q}\phi_{b,q+\hat{i}}\right) = \sum_{b=1}^{2}\epsilon_{cb}\left(\phi_{b,r-\hat{i}} + \phi_{b,r+\hat{i}}\right). \tag{C.30}$$

Section C.5: Computing the derivative of the action with respect to the real fields

The first step in computing the CL Equations is to find $\frac{\delta S_r}{\delta\phi_{a,r}}$.

$$\frac{\delta S_r}{\delta\phi_{a,r}} = \frac{\delta S_{\tau,r}}{\delta\phi_{a,r}} + \mathrm{d}\tau\frac{\delta S_{\nabla,r}}{\delta\phi_{a,r}} - \mathrm{d}\tau\frac{\delta S_{\mathrm{tr},r}}{\delta\phi_{a,r}} - \mathrm{d}\tau\frac{\delta S_{\omega,r}}{\delta\phi_{a,r}} + \mathrm{d}\tau\frac{\delta S_{\mathrm{int},r}}{\delta\phi_{a,r}} \tag{C.31}$$

Again, we proceed by modifying each of the parts of the action. First, the time and chemical potential term:

$$\begin{aligned}\frac{\delta}{\delta\phi_{a,r}}S_{\tau,r} &= \frac{1}{2}\frac{\delta}{\delta\phi_{a,r}}\sum_{a=1}^{2}\left[\phi_{a,r}^2 - e^{\mathrm{d}\tau\mu}\phi_{a,r}\phi_{a,r-\hat{\tau}} - ie^{\mathrm{d}\tau\mu}\sum_{b=1}^{2}\epsilon_{ab}\phi_{a,r}\phi_{b,r-\hat{\tau}}\right] \\ &= \phi_{a,r} - \frac{e^{\mathrm{d}\tau\mu}}{2}\left(\phi_{a,r-\hat{\tau}} + \phi_{a,r+\hat{\tau}}\right) - i\frac{e^{\mathrm{d}\tau\mu}}{2}\epsilon_{ab}\left(\phi_{b,r-\hat{\tau}} + \phi_{b,r+\hat{\tau}}\right) \qquad \text{(C.32)}\end{aligned}$$

Next, the spatial derivative part:

$$\begin{aligned}\frac{\delta}{\delta\phi_{a,r}}S_{\nabla,r} &= \frac{-1}{4m}\frac{\delta}{\delta\phi_{a,r}}\sum_{a=1}^{2}\left[\sum_{i=\pm x,y}\phi_{a,r}\phi_{a,r+\hat{i}} - 2\phi_{a,r}^2 + i\sum_{b=1}^{2}\sum_{i=\pm x,y}\epsilon_{ab}\phi_{a,r}\phi_{b,r+\hat{i}}\right] \\ &= \frac{-1}{4m}\sum_{i=\pm x,y}\left(\phi_{a,r+\hat{i}} + \phi_{a,r-\hat{i}}\right) + \frac{1}{m}\phi_{a,r} \\ &= \frac{-1}{2m}\sum_{i=\pm x,y}\phi_{a,r+\hat{i}} + \frac{1}{m}\phi_{a,r} \\ &= \frac{1}{m}\phi_{a,r} - \frac{1}{2m}\sum_{i=\pm x,y}\phi_{a,r+\hat{i}}. \qquad \text{(C.33)}\end{aligned}$$

Then the part of the action due to the external trapping potential:

$$\begin{aligned}\frac{\delta}{\delta\phi_{a,r}}S_{\mathrm{tr},r} &= \frac{m\omega_{\mathrm{tr}}^2 r_\perp^2}{4}\frac{\delta}{\delta\phi_{a,r}}\sum_{a=1}^{2}\left(\phi_{a,r}\phi_{a,r-\hat{\tau}} + i\sum_{b=1}^{2}\epsilon_{ab}\phi_{a,r}\phi_{b,r-\hat{\tau}}\right) \\ &= \frac{m\omega_{\mathrm{tr}}^2 r_\perp^2}{4}\left(\phi_{a,r+\hat{\tau}} + \phi_{a,r-\hat{\tau}} + i\sum_{b=1}^{2}\epsilon_{ab}\left(\phi_{b,r+\hat{\tau}} + \phi_{b,r-\hat{\tau}}\right)\right) \\ &= \frac{m\omega_{\mathrm{tr}}^2 r_\perp^2}{4}\left(\left(\phi_{a,r+\hat{\tau}} + \phi_{a,r-\hat{\tau}}\right) + i\sum_{b=1}^{2}\epsilon_{ab}\left(\phi_{b,r+\hat{\tau}} + \phi_{b,r-\hat{\tau}}\right)\right) \qquad \text{(C.34)}\end{aligned}$$

where $r_\perp^2 = x^2 + y^2$.

Next, the rotational piece:

$$\begin{aligned}
\frac{\delta}{\delta\phi_{a,r}}S_{\omega,r} &= \frac{\omega_z}{2}\frac{\delta}{\delta\phi_{a,r}}\sum_{a,b=1}^{2}\Big[\epsilon_{ab}\left(x\phi_{a,r}\phi_{b,r-\hat{y}} - y\phi_{a,r}\phi_{b,r-\hat{x}}\right) + \\
&\quad i\left((x-y)\phi_{a,r}^2 - x\phi_{a,r}\phi_{a,r-\hat{y}} + y\phi_{a,r}\phi_{a,r-\hat{x}}\right)\Big] \\
&= \frac{\omega_z}{2}\sum_{b=1}^{2}\epsilon_{ab}\left[x\left(\phi_{b,r-\hat{y}} + \phi_{b,r+\hat{y}}\right) - y\left(\phi_{b,r-\hat{x}} + \phi_{b,r+\hat{x}}\right)\right] \\
&\quad + i\,\frac{\omega_z}{2}\left[2(x-y)\phi_{a,r} - x\left(\phi_{a,r-\hat{y}} + \phi_{a,r+\hat{y}}\right) + y\left(\phi_{a,r-\hat{x}} + \phi_{a,r+\hat{x}}\right)\right] \\
&= \frac{\omega_z}{2}\sum_{b=1}^{2}\epsilon_{ab}\left[x\left(\phi_{b,r-\hat{y}} + \phi_{b,r+\hat{y}}\right) - y\left(\phi_{b,r-\hat{x}} + \phi_{b,r+\hat{x}}\right)\right] \\
&\quad + i\,\frac{\omega_z}{2}\left[2(x-y)\phi_{a,r} - x\left(\phi_{a,r-\hat{y}} + \phi_{a,r+\hat{y}}\right) + y\left(\phi_{a,r-\hat{x}} + \phi_{a,r+\hat{x}}\right)\right] \qquad \text{(C.35)}
\end{aligned}$$

And finally, the interaction term in the action:

$$\begin{aligned}
\frac{\delta}{\delta\phi_{a,r}}S_{\mathrm{int},r} &= \frac{\lambda}{4}\frac{\delta}{\delta\phi_{a,r}}\sum_{a,b=1}^{2}\Big(2\phi_{a,r}\phi_{a,r-\hat{\tau}}\phi_{b,r}\phi_{b,r-\hat{\tau}} - \phi_{a,r}^2\phi_{b,r-\hat{\tau}}^2 \\
&\qquad +2\,i\,\epsilon_{ab}(\phi_{a,r}^2\phi_{a,r-\hat{\tau}}\phi_{b,r-\hat{\tau}} - \phi_{a,r}\phi_{a,r-\hat{\tau}}^2\phi_{b,r})\Big) \\
&= \frac{\lambda}{2}\sum_{b=1}^{2}\left(2\phi_{b,r}(\phi_{a,r-\hat{\tau}}\phi_{b,r-\hat{\tau}} + \phi_{a,r+\hat{\tau}}\phi_{b,r+\hat{\tau}}) - \phi_{a,r}(\phi_{b,r-\hat{\tau}}^2 + \phi_{b,r+\hat{\tau}}^2)\right) \qquad \text{(C.36)} \\
&\quad + i\frac{\lambda}{2}\sum_{b=1}^{2}\epsilon_{ab}\left(2\phi_{a,r}(\phi_{a,r-\hat{\tau}}\phi_{b,r-\hat{\tau}} - \phi_{a,r+\hat{\tau}}\phi_{b,r+\hat{\tau}}) + (\phi_{b,r} - \phi_{a,r})(\phi_{a,r-\hat{\tau}}^2 - \phi_{a,r+\hat{\tau}}^2)\right)
\end{aligned}$$

Section C.6: Complexification of the drift function

The next step is to complexify our real fields, a and b, such that $\phi_a = \phi_a^R + i\phi_a^I$. We do this for each part of the drift function, $K_{a,r} = \frac{\delta S_r}{\delta\phi_{a,r}}$.

First, the time and chemical potential term:

$$\begin{aligned}
\frac{\delta}{\delta\phi_{a,r}}S_{\tau,r} &= \phi_{a,r} - \frac{e^{\mathrm{d}\tau\mu}}{2}\left(\phi_{a,r-\hat{\tau}} + \phi_{a,r+\hat{\tau}}\right) - i\frac{e^{d\tau\mu}}{2}\epsilon_{ab}\left(\phi_{b,r-\hat{\tau}} + \phi_{b,r+\hat{\tau}}\right) \\
&= \phi_{a,r}^R - \frac{e^{\mathrm{d}\tau\mu}}{2}\left(\phi_{a,r-\hat{\tau}}^R + \phi_{a,r+\hat{\tau}}^R\right) + \frac{e^{\mathrm{d}\tau\mu}}{2}\epsilon_{ab}\left(\phi_{b,r-\hat{\tau}}^I - \phi_{b,r+\hat{\tau}}^I\right) \\
&\quad + i\left[\phi_{a,r}^I - \frac{e^{\mathrm{d}\tau\mu}}{2}\left(\phi_{a,r-\hat{\tau}}^I + \phi_{a,r+\hat{\tau}}^I\right) - \frac{e^{\mathrm{d}\tau\mu}}{2}\epsilon_{ab}\left(\phi_{b,r-\hat{\tau}}^R - \phi_{b,r+\hat{\tau}}^R\right)\right]
\end{aligned}$$

So

$$\mathrm{Re}\left[\frac{\delta}{\delta\phi_{a,r}}S_{\tau,r}\right] = \phi^R_{a,r} - \frac{e^{d\tau\mu}}{2}\left(\phi^R_{a,r-\hat{\tau}} + \phi^R_{a,r+\hat{\tau}}\right) + \frac{e^{d\tau\mu}}{2}\epsilon_{ab}\left(\phi^I_{b,r-\hat{\tau}} - \phi^I_{b,r+\hat{\tau}}\right) \tag{C.37}$$

$$\mathrm{Im}\left[\frac{\delta}{\delta\phi_{a,r}}S_{\tau,r}\right] = \phi^I_{a,r} - \frac{e^{d\tau\mu}}{2}\left(\phi^I_{a,r-\hat{\tau}} + \phi^I_{a,r+\hat{\tau}}\right) - \frac{e^{d\tau\mu}}{2}\epsilon_{ab}\left(\phi^R_{b,r-\hat{\tau}} - \phi^R_{b,r+\hat{\tau}}\right) \tag{C.38}$$

Next, the spatial derivative part:

$$\begin{aligned}\frac{\delta}{\delta\phi_{a,r}}S_{\nabla,r} &= -\frac{1}{2m}\sum_{i=\pm1}^{d}\phi_{a,r+\hat{i}} + \frac{2}{m}\phi_{a,r} \\ &= -\frac{1}{2m}\sum_{i=\pm x,y}\phi^R_{a,r+\hat{i}} + \frac{2}{m}\phi^R_{a,r} - i\left(\sum_{i=\pm x,y}\phi^I_{a,r+\hat{i}} - \frac{2}{m}\phi^I_{a,r}\right)\end{aligned}$$

So

$$\mathrm{Re}\left[\frac{\delta}{\delta\phi_{a,r}}S_{\nabla,r}\right] = \frac{1}{2m}\left(4\phi^R_{a,r} - \sum_{i=\pm x,y}\phi^R_{a,r+\hat{i}}\right) \tag{C.39}$$

$$\mathrm{Im}\left[\frac{\delta}{\delta\phi_{a,r}}S_{\nabla,r}\right] = \frac{1}{2m}\left(4\phi^I_{a,r} - \sum_{i=\pm x,y}\phi^I_{a,r+\hat{i}}\right) \tag{C.40}$$

Then the part of the action due to the external trapping potential:

$$\begin{aligned}\frac{\delta}{\delta\phi_{a,r}}S_{\mathrm{tr},r} &= \frac{m\omega^2_{\mathrm{tr}}r^2_\perp}{4}\sum_{a=1}^{2}\left((\phi_{a,r+\hat{\tau}} + \phi_{a,r-\hat{\tau}}) + i\sum_{b=1}^{2}\epsilon_{ab}\left(\phi_{b,r+\hat{\tau}} + \phi_{b,r-\hat{\tau}}\right)\right) \\ &= \frac{m\omega^2_{\mathrm{tr}}r^2_\perp}{4}\sum_{a=1}^{2}\left((\phi^R_{a,r+\hat{\tau}} + \phi^R_{a,r-\hat{\tau}}) - \sum_{b=1}^{2}\epsilon_{ab}\left(\phi^I_{b,r+\hat{\tau}} + \phi^I_{b,r-\hat{\tau}}\right)\right) \\ &\quad + i\frac{m\omega^2_{\mathrm{tr}}r^2_\perp}{4}\sum_{a=1}^{2}\left((\phi^I_{a,r+\hat{\tau}} + \phi^I_{a,r-\hat{\tau}}) + \sum_{b=1}^{2}\epsilon_{ab}(\phi^R_{b,r+\hat{\tau}} + \phi^R_{b,r-\hat{\tau}})\right)\end{aligned}$$

So

$$\mathrm{Re}\left[\frac{\delta}{\delta\phi_{a,r}}S_{\mathrm{tr},r}\right] = \frac{m\omega^2_{\mathrm{tr}}r^2_\perp}{4}\sum_{a=1}^{2}\left((\phi^R_{a,r+\hat{\tau}} + \phi^R_{a,r-\hat{\tau}}) - \sum_{b=1}^{2}\epsilon_{ab}\left(\phi^I_{b,r+\hat{\tau}} + \phi^I_{b,r-\hat{\tau}}\right)\right) \tag{C.41}$$

$$\mathrm{Im}\left[\frac{\delta}{\delta\phi_{a,r}}S_{\mathrm{tr},r}\right] = \frac{m\omega^2_{\mathrm{tr}}r^2_\perp}{4}\sum_{a=1}^{2}\left((\phi^I_{a,r+\hat{\tau}} + \phi^I_{a,r-\hat{\tau}}) + \sum_{b=1}^{2}\epsilon_{ab}(\phi^R_{b,r+\hat{\tau}} + \phi^R_{b,r-\hat{\tau}})\right) \tag{C.42}$$

where $r^2_\perp = x^2 + y^2$.

Next, the rotational piece:

$$\begin{aligned}
\frac{\delta}{\delta\phi_{a,r}}S_{\omega,r} &= \frac{\omega_z}{2}\epsilon_{ab}\left[\widetilde{x}\left(\phi_{b,r-\hat{y}}+\phi_{b,r+\hat{y}}\right)-\widetilde{y}\left(\phi_{b,r-\hat{x}}+\phi_{b,r+\hat{x}}\right)\right] \\
&\quad +i\frac{\omega_z}{2}\left[2(\widetilde{x}-\widetilde{y})\phi_{a,r}-\widetilde{x}\left(\phi_{a,r-\hat{y}}+\phi_{a,r+\hat{y}}\right)+\widetilde{y}\left(\phi_{a,r-\hat{x}}+\phi_{a,r+\hat{x}}\right)\right] \\
&= -\omega_z(\widetilde{x}-\widetilde{y})\phi^I_{a,r}+\widetilde{x}\frac{\omega_z}{2}\left(\phi^I_{a,r-\hat{y}}+\phi^I_{a,r+\hat{y}}\right)-\widetilde{y}\frac{\omega_z}{2}\left(\phi^I_{a,r-\hat{x}}+\phi^I_{a,r+\hat{x}}\right) \\
&\quad +\epsilon_{ab}\frac{\omega_z}{2}\left[\widetilde{x}\left(\phi^R_{b,r-\hat{y}}+\phi^R_{b,r+\hat{y}}\right)-\widetilde{y}\left(\phi^R_{b,r-\hat{x}}+\phi^R_{b,r+\hat{x}}\right)\right] \\
&\quad +i\frac{\omega_z}{2}\left[2(\widetilde{x}-\widetilde{y})\phi^R_{a,r}-\widetilde{x}\left(\phi^R_{a,r-\hat{y}}+\phi^R_{a,r+\hat{y}}\right)+\widetilde{y}\left(\phi^R_{a,r-\hat{x}}+\phi^R_{a,r+\hat{x}}\right)\right] \\
&\quad +i\frac{\omega_z}{2}\epsilon_{ab}\left[\widetilde{x}\left(\phi^I_{b,r-\hat{y}}+\phi^I_{b,r+\hat{y}}\right)-\widetilde{y}\left(\phi^I_{b,r-\hat{x}}+\phi^I_{b,r+\hat{x}}\right)\right]
\end{aligned}$$

So

$$\begin{aligned}
\mathrm{Re}\left[\frac{\delta}{\delta\phi_{a,r}}S_{\omega_z,r}\right] &= \frac{\omega_z}{2}\left[\widetilde{x}\left(\phi^I_{a,r-\hat{y}}+\phi^I_{a,r+\hat{y}}\right)-\widetilde{y}\left(\phi^I_{a,r-\hat{x}}+\phi^I_{a,r+\hat{x}}\right)-2(\widetilde{x}-\widetilde{y})\phi^I_{a,r}\right] \\
&\quad +\frac{\omega_z}{2}\epsilon_{ab}\left[\widetilde{x}\left(\phi^R_{b,r-\hat{y}}+\phi^R_{b,r+\hat{y}}\right)-\widetilde{y}\left(\phi^R_{b,r-\hat{x}}+\phi^R_{b,r+\hat{x}}\right)\right] \qquad \text{(C.43)} \\
\mathrm{Im}\left[\frac{\delta}{\delta\phi_{a,r}}S_{\omega_z,r}\right] &= \frac{\omega_z}{2}\left[2(\widetilde{x}-\widetilde{y})\phi^R_{a,r}-\widetilde{x}\left(\phi^R_{a,r-\hat{y}}+\phi^R_{a,r+\hat{y}}\right)+\widetilde{y}\left(\phi^R_{a,r-\hat{x}}+\phi^R_{a,r+\hat{x}}\right)\right] \\
&\quad +\frac{\omega_z}{2}\epsilon_{ab}\left[\widetilde{x}\left(\phi^I_{b,r-\hat{y}}+\phi^I_{b,r+\hat{y}}\right)-\widetilde{y}\left(\phi^I_{b,r-\hat{x}}+\phi^I_{b,r+\hat{x}}\right)\right] \qquad \text{(C.44)}
\end{aligned}$$

And finally, the interaction term in the action, which requires quite a bit of algebra:

$$\begin{aligned}
\frac{\delta}{\delta\phi_{a,r}}S_{\mathrm{int},r} &= \frac{\lambda}{2}\sum_{b=1}^{2}\left(2\phi_{b,r}(\phi_{a,r-\hat{\tau}}\phi_{b,r-\hat{\tau}}+\phi_{a,r+\hat{\tau}}\phi_{b,r+\hat{\tau}})-\phi_{a,r}(\phi^2_{b,r-\hat{\tau}}+\phi^2_{b,r+\hat{\tau}})\right) \qquad \text{(C.45)} \\
&\quad +i\frac{\lambda}{2}\sum_{b=1}^{2}\epsilon_{ab}\left(2\phi_{a,r}(\phi_{a,r-\hat{\tau}}\phi_{b,r-\hat{\tau}}-\phi_{a,r+\hat{\tau}}\phi_{b,r+\hat{\tau}})+(\phi_{b,r}-\phi_{a,r})(\phi^2_{a,r-\hat{\tau}}-\phi^2_{a,r+\hat{\tau}})\right) \\
&\qquad \text{(C.46)}
\end{aligned}$$

$$
\begin{aligned}
= \quad & \frac{\lambda}{2}\sum_{b=1}^{2}\Big[2\phi^R_{b,r}\phi^R_{a,r-\hat\tau}\phi^R_{b,r-\hat\tau} - 2\phi^R_{b,r}\phi^I_{a,r-\hat\tau}\phi^I_{b,r-\hat\tau} + 2\phi^R_{b,r}\phi^R_{a,r+\hat\tau}\phi^R_{b,r+\hat\tau} - 2\phi^R_{b,r}\phi^I_{a,r+\hat\tau}\phi^I_{b,r+\hat\tau} \\
& -2\phi^I_{b,r}\phi^R_{a,r-\hat\tau}\phi^I_{b,r-\hat\tau} - 2\phi^I_{b,r}\phi^I_{a,r-\hat\tau}\phi^R_{b,r-\hat\tau} - 2\phi^I_{b,r}\phi^R_{a,r+\hat\tau}\phi^I_{b,r+\hat\tau} - 2\phi^I_{b,r}\phi^I_{a,r+\hat\tau}\phi^R_{b,r+\hat\tau} \\
& -\phi^R_{a,r}\phi^R_{b,r-\hat\tau}\phi^R_{b,r-\hat\tau} + 2\phi^I_{a,r}\phi^I_{b,r-\hat\tau}\phi^R_{b,r-\hat\tau} + \phi^R_{a,r}\phi^I_{b,r-\hat\tau}\phi^I_{b,r-\hat\tau} - \phi^R_{a,r}\phi^R_{b,r+\hat\tau}\phi^R_{b,r+\hat\tau} \\
& +2\phi^I_{a,r}\phi^R_{b,r+\hat\tau}\phi^I_{b,r+\hat\tau} + \phi^R_{a,r}\phi^I_{b,r+\hat\tau}\phi^I_{b,r+\hat\tau}\Big] \\
& +i\frac{\lambda}{2}\sum_{b=1}^{2}\Big[2\phi^R_{b,r}\phi^R_{a,r-\hat\tau}\phi^I_{b,r-\hat\tau} + 2\phi^R_{b,r}\phi^I_{a,r-\hat\tau}\phi^R_{b,r-\hat\tau} + 2\phi^R_{b,r}\phi^R_{a,r+\hat\tau}\phi^I_{b,r+\hat\tau} + 2\phi^R_{b,r}\phi^I_{a,r+\hat\tau}\phi^R_{b,r+\hat\tau}) \\
& +2\phi^I_{b,r}\phi^R_{a,r-\hat\tau}\phi^R_{b,r-\hat\tau} - 2\phi^I_{b,r}\phi^I_{a,r-\hat\tau}\phi^I_{b,r-\hat\tau} + 2\phi^I_{b,r}\phi^R_{a,r+\hat\tau}\phi^R_{b,r+\hat\tau} - 2\phi^I_{b,r}\phi^I_{a,r+\hat\tau}\phi^I_{b,r+\hat\tau} \\
& -\phi^I_{a,r}\phi^R_{b,r-\hat\tau}\phi^R_{b,r-\hat\tau} - 2\phi^R_{a,r}\phi^I_{b,r-\hat\tau}\phi^R_{b,r-\hat\tau} + \phi^I_{a,r}\phi^I_{b,r-\hat\tau}\phi^I_{b,r-\hat\tau} - \phi^I_{a,r}\phi^R_{b,r+\hat\tau}\phi^R_{b,r+\hat\tau} \\
& -2\phi^R_{a,r}\phi^R_{b,r+\hat\tau}\phi^I_{b,r+\hat\tau} + \phi^I_{a,r}\phi^I_{b,r+\hat\tau}\phi^I_{b,r+\hat\tau}\Big] \\
& -\frac{\lambda}{2}\sum_{b=1}^{2}\epsilon_{ab}\Big[2\phi^R_{a,r}\phi^I_{a,r-\hat\tau}\phi^R_{b,r-\hat\tau} - 2\phi^I_{a,r}\phi^I_{a,r-\hat\tau}\phi^I_{b,r-\hat\tau} + 2\phi^I_{a,r}\phi^R_{a,r-\hat\tau}\phi^R_{b,r-\hat\tau} + 2\phi^R_{a,r}\phi^R_{a,r-\hat\tau}\phi^I_{b,r-\hat\tau} \\
& +2\phi^R_{b,r}\phi^R_{a,r-\hat\tau}\phi^I_{a,r-\hat\tau} - 2\phi^R_{b,r}\phi^R_{a,r+\hat\tau}\phi^I_{a,r+\hat\tau} + \phi^I_{b,r}\phi^R_{a,r-\hat\tau}\phi^R_{a,r-\hat\tau} - \phi^I_{b,r}\phi^I_{a,r-\hat\tau}\phi^I_{a,r-\hat\tau} \\
& -2\phi^R_{a,r}\phi^R_{a,r+\hat\tau}\phi^I_{b,r+\hat\tau} - 2\phi^R_{a,r}\phi^I_{a,r+\hat\tau}\phi^R_{b,r+\hat\tau} - 2\phi^I_{a,r}\phi^R_{a,r+\hat\tau}\phi^R_{b,r+\hat\tau} + 2\phi^I_{a,r}\phi^I_{a,r+\hat\tau}\phi^I_{b,r+\hat\tau} \\
& +2\phi^R_{a,r}\phi^R_{a,r+\hat\tau}\phi^I_{a,r+\hat\tau} - \phi^I_{a,r}\phi^R_{a,r-\hat\tau}\phi^R_{a,r-\hat\tau} + \phi^I_{a,r}\phi^I_{a,r-\hat\tau}\phi^I_{a,r-\hat\tau} + \phi^I_{a,r}\phi^R_{a,r+\hat\tau}\phi^R_{a,r+\hat\tau} - \phi^I_{a,r}\phi^I_{a,r+\hat\tau}\phi^I_{a,r+\hat\tau} \\
& -\phi^I_{b,r}\phi^R_{a,r+\hat\tau}\phi^R_{a,r+\hat\tau} + \phi^I_{b,r}\phi^I_{a,r+\hat\tau}\phi^I_{a,r+\hat\tau} - 2\phi^R_{a,r}\phi^R_{a,r-\hat\tau}\phi^I_{a,r-\hat\tau}\Big] \\
& +i\frac{\lambda}{2}\sum_{b=1}^{2}\epsilon_{ab}\Big[2\phi^R_{a,r}\phi^R_{a,r-\hat\tau}\phi^R_{b,r-\hat\tau} - 2\phi^I_{a,r}\phi^R_{a,r-\hat\tau}\phi^I_{b,r-\hat\tau} - 2\phi^I_{a,r}\phi^I_{a,r-\hat\tau}\phi^R_{b,r-\hat\tau} - 2\phi^R_{a,r}\phi^I_{a,r-\hat\tau}\phi^I_{b,r-\hat\tau} \\
& -2\phi^R_{a,r}\phi^R_{a,r+\hat\tau}\phi^R_{b,r+\hat\tau} + 2\phi^R_{a,r}\phi^I_{a,r+\hat\tau}\phi^I_{b,r+\hat\tau} + 2\phi^I_{a,r}\phi^R_{a,r+\hat\tau}\phi^I_{b,r+\hat\tau} + 2\phi^I_{a,r}\phi^I_{a,r+\hat\tau}\phi^R_{b,r+\hat\tau} \\
& +\phi^R_{b,r}\phi^R_{a,r-\hat\tau}\phi^R_{a,r-\hat\tau} - \phi^R_{b,r}\phi^I_{a,r-\hat\tau}\phi^I_{a,r-\hat\tau} - \phi^R_{b,r}\phi^R_{a,r+\hat\tau}\phi^R_{a,r+\hat\tau} + \phi^R_{b,r}\phi^I_{a,r+\hat\tau}\phi^I_{a,r+\hat\tau} \\
& -2\phi^I_{b,r}\phi^R_{a,r-\hat\tau}\phi^I_{a,r-\hat\tau} + 2\phi^I_{b,r}\phi^R_{a,r+\hat\tau}\phi^I_{a,r+\hat\tau} - \phi^R_{a,r}\phi^R_{a,r-\hat\tau}\phi^R_{a,r-\hat\tau}\phi^R_{a,r}\phi^I_{a,r-\hat\tau}\phi^I_{a,r-\hat\tau} + \phi^R_{a,r}\phi^R_{a,r+\hat\tau}\phi^R_{a,r+\hat\tau} \\
& -\phi^R_{a,r}\phi^I_{a,r+\hat\tau}\phi^I_{a,r+\hat\tau} + 2\phi^I_{a,r}\phi^R_{a,r-\hat\tau}\phi^I_{a,r-\hat\tau} - 2\phi^I_{a,r}\phi^R_{a,r+\hat\tau}\phi^I_{a,r+\hat\tau})\Big]
\end{aligned}
$$

So when we rearrange this, we have

$$
\begin{aligned}
\mathrm{Re}\left[\frac{\delta}{\delta\phi_{a,r}}S_{\mathrm{int},r}\right] &= \frac{\lambda}{2}\sum_{b=1}^{2}\Big[2\phi^R_{b,r}\phi^R_{a,r-\hat\tau}\phi^R_{b,r-\hat\tau} - 2\phi^R_{b,r}\phi^I_{a,r-\hat\tau}\phi^I_{b,r-\hat\tau} + 2\phi^R_{b,r}\phi^R_{a,r+\hat\tau}\phi^R_{b,r+\hat\tau} \\
&\quad -2\phi^R_{b,r}\phi^I_{a,r+\hat\tau}\phi^I_{b,r+\hat\tau} - 2\phi^I_{b,r}\phi^R_{a,r-\hat\tau}\phi^I_{b,r-\hat\tau} - 2\phi^I_{b,r}\phi^I_{a,r-\hat\tau}\phi^R_{b,r-\hat\tau} - 2\phi^I_{b,r}\phi^R_{a,r+\hat\tau}\phi^I_{b,r+\hat\tau} \\
&\quad -2\phi^I_{b,r}\phi^I_{a,r+\hat\tau}\phi^R_{b,r+\hat\tau} - \phi^R_{a,r}\phi^R_{b,r-\hat\tau}\phi^R_{b,r-\hat\tau} + 2\phi^I_{a,r}\phi^I_{b,r-\hat\tau}\phi^R_{b,r-\hat\tau} + \phi^R_{a,r}\phi^I_{b,r-\hat\tau}\phi^I_{b,r-\hat\tau} \\
&\quad -\phi^R_{a,r}\phi^R_{b,r+\hat\tau}\phi^R_{b,r+\hat\tau} + 2\phi^I_{a,r}\phi^R_{b,r+\hat\tau}\phi^I_{b,r+\hat\tau} + \phi^R_{a,r}\phi^I_{b,r+\hat\tau}\phi^I_{b,r+\hat\tau}\Big] \\
&\quad -\frac{\lambda}{2}\sum_{b=1}^{2}\epsilon_{ab}\Big[2\phi^R_{a,r}\phi^I_{a,r-\hat\tau}\phi^R_{b,r-\hat\tau} - 2\phi^I_{a,r}\phi^I_{a,r-\hat\tau}\phi^I_{b,r-\hat\tau} + 2\phi^I_{a,r}\phi^R_{a,r-\hat\tau}\phi^R_{b,r-\hat\tau} \\
&\quad +2\phi^R_{a,r}\phi^R_{a,r-\hat\tau}\phi^I_{b,r-\hat\tau} + 2\phi^R_{b,r}\phi^R_{a,r-\hat\tau}\phi^I_{a,r-\hat\tau} - 2\phi^R_{b,r}\phi^R_{a,r+\hat\tau}\phi^I_{a,r+\hat\tau} + \phi^I_{b,r}\phi^R_{a,r-\hat\tau}\phi^R_{a,r-\hat\tau} \\
&\quad -\phi^I_{b,r}\phi^I_{a,r-\hat\tau}\phi^I_{a,r-\hat\tau} - 2\phi^R_{a,r}\phi^R_{a,r+\hat\tau}\phi^I_{b,r+\hat\tau} - 2\phi^R_{a,r}\phi^I_{a,r+\hat\tau}\phi^R_{b,r+\hat\tau} - 2\phi^I_{a,r}\phi^R_{a,r+\hat\tau}\phi^R_{b,r+\hat\tau} \\
&\quad +2\phi^I_{a,r}\phi^I_{a,r+\hat\tau}\phi^I_{b,r+\hat\tau} + 2\phi^R_{a,r}\phi^R_{a,r+\hat\tau}\phi^I_{a,r+\hat\tau} - \phi^I_{a,r}\phi^R_{a,r-\hat\tau}\phi^R_{a,r-\hat\tau} \\
&\quad +\phi^I_{a,r}\phi^I_{a,r-\hat\tau}\phi^I_{a,r-\hat\tau} + \phi^I_{a,r}\phi^R_{a,r+\hat\tau}\phi^R_{a,r+\hat\tau} - \phi^I_{a,r}\phi^I_{a,r+\hat\tau}\phi^I_{a,r+\hat\tau} \\
&\quad -\phi^I_{b,r}\phi^R_{a,r+\hat\tau}\phi^R_{a,r+\hat\tau} + \phi^I_{b,r}\phi^I_{a,r+\hat\tau}\phi^I_{a,r+\hat\tau} - 2\phi^R_{a,r}\phi^R_{a,r-\hat\tau}\phi^I_{a,r-\hat\tau}\Big]
\end{aligned}
$$

$$
\begin{aligned}
\mathrm{Im}\left[\frac{\delta}{\delta\phi_{a,r}}S_{\mathrm{int},r}\right] &= \frac{\lambda}{2}\sum_{b=1}^{2}\Big[2\phi^R_{b,r}\phi^R_{a,r-\hat\tau}\phi^I_{b,r-\hat\tau} + 2\phi^R_{b,r}\phi^I_{a,r-\hat\tau}\phi^R_{b,r-\hat\tau} + 2\phi^R_{b,r}\phi^R_{a,r+\hat\tau}\phi^I_{b,r+\hat\tau} \\
&\quad +2\phi^R_{b,r}\phi^I_{a,r+\hat\tau}\phi^R_{b,r+\hat\tau}) + 2\phi^I_{b,r}\phi^R_{a,r-\hat\tau}\phi^R_{b,r-\hat\tau} - 2\phi^I_{b,r}\phi^I_{a,r-\hat\tau}\phi^I_{b,r-\hat\tau} + 2\phi^I_{b,r}\phi^R_{a,r+\hat\tau}\phi^R_{b,r+\hat\tau} \\
&\quad -2\phi^I_{b,r}\phi^I_{a,r+\hat\tau}\phi^I_{b,r+\hat\tau} - \phi^I_{a,r}\phi^R_{b,r-\hat\tau}\phi^R_{b,r-\hat\tau} - 2\phi^R_{a,r}\phi^I_{b,r-\hat\tau}\phi^R_{b,r-\hat\tau} + \phi^I_{a,r}\phi^I_{b,r-\hat\tau}\phi^I_{b,r-\hat\tau} \\
&\quad -\phi^I_{a,r}\phi^R_{b,r+\hat\tau}\phi^R_{b,r+\hat\tau} - 2\phi^R_{a,r}\phi^R_{b,r+\hat\tau}\phi^I_{b,r+\hat\tau} + \phi^I_{a,r}\phi^I_{b,r+\hat\tau}\phi^I_{b,r+\hat\tau}\Big] \\
&\quad +\frac{\lambda}{2}\sum_{b=1}^{2}\epsilon_{ab}\Big[2\phi^R_{a,r}\phi^R_{a,r-\hat\tau}\phi^R_{b,r-\hat\tau} - 2\phi^I_{a,r}\phi^R_{a,r-\hat\tau}\phi^I_{b,r-\hat\tau} - 2\phi^I_{a,r}\phi^I_{a,r-\hat\tau}\phi^R_{b,r-\hat\tau} \\
&\quad -2\phi^R_{a,r}\phi^I_{a,r-\hat\tau}\phi^I_{b,r-\hat\tau} - 2\phi^R_{a,r}\phi^R_{a,r+\hat\tau}\phi^R_{b,r+\hat\tau} + 2\phi^R_{a,r}\phi^I_{a,r+\hat\tau}\phi^I_{b,r+\hat\tau} + 2\phi^I_{a,r}\phi^R_{a,r+\hat\tau}\phi^I_{b,r+\hat\tau} \\
&\quad +2\phi^I_{a,r}\phi^I_{a,r+\hat\tau}\phi^R_{b,r+\hat\tau} + \phi^R_{b,r}\phi^R_{a,r-\hat\tau}\phi^R_{a,r-\hat\tau} - \phi^R_{b,r}\phi^I_{a,r-\hat\tau}\phi^I_{a,r-\hat\tau} \\
&\quad -\phi^R_{b,r}\phi^R_{a,r+\hat\tau}\phi^R_{a,r+\hat\tau} + \phi^R_{b,r}\phi^I_{a,r+\hat\tau}\phi^I_{a,r+\hat\tau} - 2\phi^I_{b,r}\phi^R_{a,r-\hat\tau}\phi^I_{a,r-\hat\tau} \\
&\quad +2\phi^I_{b,r}\phi^R_{a,r+\hat\tau}\phi^I_{a,r+\hat\tau} - \phi^R_{a,r}\phi^R_{a,r-\hat\tau}\phi^R_{a,r-\hat\tau}\phi^R_{a,r}\phi^I_{a,r-\hat\tau}\phi^I_{a,r-\hat\tau} + \phi^R_{a,r}\phi^R_{a,r+\hat\tau}\phi^R_{a,r+\hat\tau} \\
&\quad -\phi^R_{a,r}\phi^I_{a,r+\hat\tau}\phi^I_{a,r+\hat\tau} + 2\phi^I_{a,r}\phi^R_{a,r-\hat\tau}\phi^I_{a,r-\hat\tau} - 2\phi^I_{a,r}\phi^R_{a,r+\hat\tau}\phi^I_{a,r+\hat\tau})\Big]
\end{aligned}
$$

Section C.7: Lattice observables

The average density is the sum over the local density at each spatial site, normalized by the spatial lattice volume:

$$\langle \hat{n} \rangle = \frac{1}{N_x^d} \sum_r n_r \tag{C.47}$$

where n_r can be found by taking the derivative of the lattice action with respect to the chemical potential, and then complexifying the fields as we have done before. We start by noting that $\mathrm{d}\tau\mu = \beta\mu/N_\tau$ and take a derivative with respect to $\beta\mu$:

$$\begin{aligned} n_r &= -\frac{\partial}{\partial(\beta\mu)} S_{\tau,r} = -\frac{\partial}{\partial(\beta\mu)} \left(\phi_r^* \phi_r - \phi_r^* e^{\beta\mu/N_\tau} \phi_{r-\hat{\tau}} \right) \\ &= \frac{1}{N_\tau} e^{\beta\mu/N_\tau} \left(\phi_r^* \phi_{r-\hat{\tau}} \right) \\ &= \frac{1}{2N_\tau} e^{\beta\mu/N_\tau} \sum_{a=1}^{2} \left[\phi^R_{a,r} \phi^R_{a,r-\hat{\tau}} - \phi^I_{a,r} \phi^I_{a,r-\hat{\tau}} - \sum_{b=1}^{2} \epsilon_{ab} (\phi^I_{a,r} \phi^R_{b,r-\hat{\tau}} + \phi^R_{a,r} \phi^I_{b,r-\hat{\tau}}) \right] \\ &+ \frac{i}{2N_\tau} e^{\beta\mu/N_\tau} \sum_{a=1}^{2} \left[\phi^I_{a,r-\hat{\tau}} \phi^R_{a,r-\hat{\tau}} + \phi^R_{a,r-\hat{\tau}} \phi^I_{a,r-\hat{\tau}} + \sum_{b=1}^{2} \epsilon_{ab} (\phi^R_{a,r} \phi^R_{b,r-\hat{\tau}} - \phi^I_{a,r} \phi^I_{b,r-\hat{\tau}}) \right] \end{aligned} \tag{C.48}$$

The angular momentum operator, L_z can be written

$$L_z = ((x - x_0) p_y - (y - y_0) p_x) = -i\hbar((x - x_0)\partial_y - (y - y_0)\partial_x). \tag{C.49}$$

We are interested in the expectation value of this operator: $\langle L_z \rangle$, which is found by summing over the lattice:

$$\langle L_z \rangle = -i \sum_r \phi_r^* ((x - \frac{N_x - 1}{2})\partial_y - (y - \frac{N_x - 1}{2})\partial_x)\phi_r, \tag{C.50}$$

where $\hbar \to 1$. First, let us implement our lattice derivative: $\partial_j \phi_r = \frac{1}{a^2}(\phi_{r-\hat{j}} - \phi_r)$ (recall that our lattice spacing is $a = 1$):

$$\begin{aligned} \langle L_z \rangle &= -i \sum_r \phi_r^* ((x - r_c)\phi_{r-\hat{y}} - x\phi_r - (y - r_c)\phi_{r-\hat{x}} + y\phi_r) \\ &= i \sum_r \left((y - r_c)\phi_r^* \phi_{r-\hat{x}} - (x - r_c)\phi_r^* \phi_{r-\hat{y}} - (y - x)\phi_r^* \phi_r \right) \end{aligned} \tag{C.51}$$

Here we have also written $\frac{N_x - 1}{2}$ as r_c for simplicity. Let us write ϕ as $\frac{1}{\sqrt{2}}(\phi_1 + i\phi_2)$; then, our angular

momentum operator becomes a sum over the lattice sites and the real fields ϕ_1 and ϕ_2:

$$\begin{aligned}
\langle L_z \rangle &= \frac{i}{2}\sum_r (y-r_c)\left(\phi_{1,r}\phi_{1,r-\hat{x}} + i\phi_{1,r}\phi_{2,r-\hat{x}} - i\phi_{2,r}\phi_{1,r-\hat{x}} + \phi_{2,r}\phi_{2,r-\hat{x}}\right) \\
&\quad -\frac{i}{2}\sum_r (x-r_c)\left(\phi_{1,r}\phi_{1,r-\hat{y}} + i\phi_{1,r}\phi_{2,r-\hat{y}} - i\phi_{2,r}\phi_{1,r-\hat{y}} + \phi_{2,r}\phi_{2,r-\hat{y}}\right) \qquad \text{(C.52)} \\
&\quad -\frac{i}{2}\sum_r (y-x)(\phi_{1,r}^2 + \phi_{2,r}^2) \\
&= \frac{1}{2}\sum_r \sum_{a=1}^{2}\left((y-r_c)\phi_{a,r}\phi_{a,r-\hat{x}} - (x-r_c)\phi_{a,r}\phi_{a,r-\hat{y}} - (y-x)\phi_{a,r}^2\right) \qquad \text{(C.53)} \\
&\quad -\frac{i}{2}\sum_r \sum_{a,b=1}^{2}\epsilon_{ab}\left((x-r_c)\phi_{a,r}\phi_{b,r-\hat{y}} - (y-r_c)\phi_{a,r}\phi_{b,r-\hat{x}}\right)
\end{aligned}$$

Next, we must complexify our real fields: $\phi_a = \phi_a^R + i\phi_a^I$, leading us to the following equation for the angular momentum in terms of our four lattice fields:

$$\begin{aligned}
\langle L_z \rangle &= -\frac{i}{2}\sum_r \sum_{a=1}^{2}\left((x-r_c)(\phi_{a,r}^R\phi_{a,r-\hat{y}}^R - \phi_{a,r}^I\phi_{a,r-\hat{y}}^I) - (y-r_c)(\phi_{a,r}^R\phi_{a,r-\hat{x}}^R - \phi_{a,r}^I\phi_{a,r-\hat{x}}^I)\right) \\
&\quad -\frac{i}{2}\sum_r \sum_{a=1}^{2}(y-x)\left((\phi_{a,r}^R)^2 - (\phi_{a,r}^I)^2\right) \\
&\quad -\frac{i}{2}\sum_r \sum_{a,b=1}^{2}\epsilon_{ab}\left((x-r_c)(\phi_{a,r}^R\phi_{b,r-\hat{y}}^I + \phi_{a,r}^I\phi_{b,r-\hat{y}}^R) - (y-r_c)(\phi_{a,r}^R\phi_{b,r-\hat{x}}^I + \phi_{a,r}^I\phi_{b,r-\hat{x}}^R)\right) \\
&\quad +\frac{1}{2}\sum_r \sum_{a=1}^{2}\left((x-r_c)(\phi_{a,r}^R\phi_{a,r-\hat{y}}^I + \phi_{a,r}^I\phi_{a,r-\hat{y}}^R) - (y-r_c)(\phi_{a,r}^R\phi_{a,r-\hat{x}}^I + \phi_{a,r}^I\phi_{a,r-\hat{x}}^R)\right) \\
&\quad +\sum_r \sum_{a,b=1}^{2}(y-x)\phi_{a,r}^R\phi_{a,r}^I \\
&\quad +\frac{1}{2}\sum_r \sum_{a,b=1}^{2}\epsilon_{ab}\left((x-r_c)(\phi_{a,r}^R\phi_{b,r-\hat{y}}^R - \phi_{a,r}^I\phi_{b,r-\hat{y}}^I) - (y-r_c)(\phi_{a,r}^R\phi_{b,r-\hat{x}}^R - \phi_{a,r}^I\phi_{b,r-\hat{x}}^I)\right).
\end{aligned}$$

When this is divided into the real and imaginary parts of the observable, we get:

$$\begin{aligned}
\mathrm{Re}\langle L_z\rangle &= \frac{1}{2}\sum_r\sum_{a=1}^{2}\left((x-r_c)(\phi^R_{a,r}\phi^I_{a,r-\hat{y}}+\phi^I_{a,r}\phi^R_{a,r-\hat{y}})-(y-r_c)(\phi^R_{a,r}\phi^I_{a,r-\hat{x}}+\phi^I_{a,r}\phi^R_{a,r-\hat{x}})\right)\\
&\quad+\sum_r\sum_{a=1}^{2}(y-x)\phi^R_{a,r}\phi^I_{a,r} \qquad\qquad (C.54)\\
&\quad+\frac{1}{2}\sum_r\sum_{a,b=1}^{2}\epsilon_{ab}\left((x-r_c)(\phi^R_{a,r}\phi^R_{b,r-\hat{y}}-\phi^I_{a,r}\phi^I_{b,r-\hat{y}})-(y-r_c)(\phi^R_{a,r}\phi^R_{b,r-\hat{x}}-\phi^I_{a,r}\phi^I_{b,r-\hat{x}})\right).\\
\mathrm{Im}\langle L_z\rangle &= -\frac{1}{2}\sum_r\sum_{a=1}^{2}\left((x-r_c)(\phi^R_{a,r}\phi^R_{a,r-\hat{y}}-\phi^I_{a,r}\phi^I_{a,r-\hat{y}})-(y-r_c)(\phi^R_{a,r}\phi^R_{a,r-\hat{x}}-\phi^I_{a,r}\phi^I_{a,r-\hat{x}})\right)\\
&\quad-\frac{1}{2}\sum_r\sum_{a=1}^{2}(y-x)\left((\phi^R_{a,r})^2-(\phi^I_{a,r})^2\right) \qquad\qquad (C.55)\\
&\quad-\frac{1}{2}\sum_r\sum_{a,b=1}^{2}\epsilon_{ab}\left((x-r_c)(\phi^R_{a,r}\phi^I_{b,r-\hat{y}}+\phi^I_{a,r}\phi^R_{b,r-\hat{y}})-(y-r_c)(\phi^R_{a,r}\phi^I_{b,r-\hat{x}}+\phi^I_{a,r}\phi^R_{b,r-\hat{x}})\right)
\end{aligned}$$

Section C.8: Some exact solution for the nonrelativistic system

C.8.1: Nonrotating, noninteracting, nonrelativistic, finite chemical potential in 1, 2, and 3 dimensions

The lattice action for a nonrotating, noninteracting, and nonrelativistic system is the following:

$$S_{\mathrm{lat},r}=\phi^*_r\left[\phi_r-e^{d\tau\mu}\phi_{r-\hat{\tau}}-\frac{d\tau}{2m}\sum_{i=1}^{d}\left(\phi_{r+\hat{i}}-2\phi_r+\phi_{r-\hat{i}}\right)\right]. \qquad (C.56)$$

This can be written as fields multiplying a matrix:

$$S_{\mathrm{lat},r}=\sum_r\sum_{r'}\phi^*_r M\phi_{r'}=\sum_r\sum_{r'}\phi^*_r\left[(1+\frac{d\tau d}{m})\delta_{r,r'}-e^{d\tau\mu}\delta_{r-\hat{\tau},r'}-\frac{d\tau}{2m}\sum_{i=1}^{d}\left(\delta_{r+\hat{i},r'}+\delta_{r-\hat{i},r'}\right)\right]\phi_{r'}, \qquad (C.57)$$

which we can use to determine analytically the density and field modulus squared of this system in order to check against our code's results. Recall that

$$\begin{aligned}
\langle\hat{n}\rangle &= \frac{-1}{V}\frac{\partial ln\mathcal{Z}}{\partial(\beta\mu)}=\frac{-1}{V}\frac{\partial}{\partial(\beta\mu)}(-ln(det(M))) \qquad\qquad (C.58)\\
&= \frac{1}{V}\frac{\partial}{\partial(\beta\mu)}Tr(lnM)=\frac{1}{V}\frac{\partial}{\partial(\beta\mu)}\sum_k lnD_{kk}=\frac{1}{V}\sum_k\frac{1}{D_{kk}}\frac{\partial D_{kk}}{\partial(\beta\mu)}
\end{aligned}$$

with $\beta\mu = N_\tau d\tau\mu$, and note that for a nonrelativistic system,

$$\begin{aligned}\langle\phi^*\phi\rangle &= \frac{-1}{V}\frac{\partial ln\mathcal{Z}}{\partial(d/m)} = \frac{-1}{V}\frac{\partial}{\partial(d/m)}(-ln(det(M))) \\ &= \frac{1}{V}\frac{\partial}{\partial(d/m)}Tr(lnM) = \frac{1}{V}\frac{\partial}{\partial(d/m)}\sum_k lnD_{kk} \\ &= \frac{1}{V}\sum_k \frac{1}{D_{kk}}\frac{\partial D_{kk}}{\partial(d/m)} = \sum_k \frac{1}{D_{kk}}.\end{aligned} \tag{C.59}$$

Diagonalizing our matrix, M

We can represent the nonrotating, noninteracting action as

$$S[\lambda = \omega = 0] = \sum_{r,r'} \phi^*_r M_{r,r'}[d, m, \mu]\phi_{r'} \tag{C.60}$$

where

$$M_{r,r'}[d, m, \mu] = \left[(1 + \frac{d\tau d}{m})\delta_{r,r'} - e^{d\tau\mu}\delta_{r-\hat{t},r'} - \frac{d\tau}{2m}\sum_{i=x,y}^{d}(\delta_{r+\hat{i},r'} + \delta_{r-\hat{i},r'})\right]. \tag{C.61}$$

We want to diagonalize M by applying a transformation matrix, such that $D_{kk'} = U^\dagger MU$, where

$$U_{r,k} = \frac{\sqrt{2^d}}{\sqrt{N_x^d N_\tau}} e^{ik_0 t}\prod_{i=1}^{d}\sin(k_i x_i) \tag{C.62}$$

$$U^\dagger_{r,k} = \frac{\sqrt{2^d}}{\sqrt{N_x^d N_\tau}} e^{-ik_0 t}\prod_{i=1}^{d}\sin(k_i x_i) \tag{C.63}$$

$$k_0 = \frac{2\pi n_0}{N_\tau},\ n_0 \in [1, 2, ..., N_\tau] \tag{C.64}$$

$$k_i = \frac{\pi n_i}{(N_x + 1)},\ n_i \in [1, 2, ..., N_x]. \tag{C.65}$$

Applying the transformation matrix, we get

$$\begin{aligned}
D_{k,k'} &= \frac{2^d}{N_x^d N_t}\sum_{r,r'} e^{-ik_0 t}\prod_{i=1}^{d}\sin(k_i x_i)\left[(1+\frac{d\tau d}{m})\delta_{r,r'}\right]e^{ik_0' t'}\prod_{i=1}^{d}\sin(k_i' x_i') \\
&-\frac{2^d}{N_x^d N_t}\sum_{r,r'} e^{-ik_0 t}\prod_{i=1}^{d}\sin(k_i x_i)\left[e^{d\tau\mu}\delta_{r-\hat{i},r'}\right]e^{ik_0' t'}\prod_{i=1}^{d}\sin(k_i' x_i') \\
&-\frac{2^d}{N_x^d N_t}\sum_{r,r'} e^{-ik_0 t}\prod_{i=1}^{d}\sin(k_i x_i)\left[\frac{d\tau}{2m}\sum_{i=1}^{d}\delta_{r+\hat{i},r'}\right]e^{ik_0' t'}\prod_{i=1}^{d}\sin(k_i' x_i') \\
&-\frac{2^d}{N_x^d N_t}\sum_{r,r'} e^{-ik_0 t}\prod_{i=1}^{d}\sin(k_i x_i)\left[\frac{d\tau}{2m}\sum_{i=1}^{d}\delta_{r-\hat{i},r'}\right]e^{ik_0' t'}\prod_{i=1}^{d}\sin(k_i' x_i').
\end{aligned} \tag{C.66}$$

Resolving the delta functions, performing the sum over r', and pulling everything that does not depend on $r = (t, \vec{x})$ outside the sum, this reduces to

$$\begin{aligned}
D_{k,k'} &= \frac{2^d}{N_x^d N_t}(1+\frac{d\tau d}{m})\sum_{r} e^{-it(k_0-k_0')}\prod_{i=1}^{d}\sin(k_i x_i)\sin(k_i' x_i) \\
&-\frac{2^d}{N_x^d N_t}e^{d\tau\mu}e^{-ik_0'}\sum_{r} e^{-it(k_0-k_0')}\prod_{i=1}^{d}\sin(k_i x_i)\sin(k_i' x_i) \\
&-\frac{2^d}{N_x^d N_t}\frac{d\tau}{2m}\sum_{r} e^{-it(k_0-k_0')}\prod_{i=1}^{d}\sin(k_i x_i)\sum_{i=1}^{d}\sin(k_i' x_i + k_i') \\
&-\frac{2^d}{N_x^d N_t}\frac{d\tau}{2m}\sum_{r} e^{-it(k_0-k_0')}\prod_{i=1}^{d}\sin(k_i x_i)\sum_{i=1}^{d}\sin(k_i' x_i - k_i').
\end{aligned} \tag{C.67}$$

To further expand the last two lines, we use the following trig identity: $\sin(a \pm b) = \sin(a)\cos(b) \pm \sin(b)\cos(a)$, which gives us:

$$\begin{aligned}
D_{k,k'} &= \frac{2^d}{N_x^d N_t}(1+\frac{d\tau d}{m}-e^{d\tau\mu}e^{-ik_0'})\sum_{r} e^{-it(k_0-k_0')}\prod_{i=1}^{d}\sin(k_i x_i)\sin(k_i' x_i) \\
&-\frac{2^d}{N_x^d N_t}\frac{d\tau}{2m}\sum_{i=1}^{d}\cos(k_i')\sum_{r} e^{-it(k_0-k_0')}\prod_{i=1}^{d}\sin(k_i x_i)\sin(k_i' x_i) \\
&-\frac{2^d}{N_x^d N_t}\frac{d\tau}{2m}\sum_{i=1}^{d}\sin(k_i')\sum_{r} e^{-it(k_0-k_0')}\prod_{i=1}^{d}\sin(k_i x_i)\cos(k_i' x_i) \\
&-\frac{2^d}{N_x^d N_t}\frac{d\tau}{2m}\sum_{i=1}^{d}\cos(k_i')\sum_{r} e^{-it(k_0-k_0')}\prod_{i=1}^{d}\sin(k_i x_i)\sin(k_i' x_i) \\
&+\frac{2^d}{N_x^d N_t}\frac{d\tau}{2m}\sum_{i=1}^{d}\sin(k_i')\sum_{r} e^{-it(k_0-k_0')}\prod_{i=1}^{d}\sin(k_i x_i)\cos(k_i' x_i).
\end{aligned} \tag{C.68}$$

Using the following Fourier identities

$$\begin{aligned}\sum_x \sin(kx)\sin(k'x) &= \frac{N_x}{2}\delta_{k,k'} \\ \sum_x \sin(kx)\cos(k'x) &= 0 \qquad (C.69)\\ \sum_x e^{-ix(k-k')} &= N_x\delta_{k,k'} \qquad (C.70)\end{aligned}$$

we find that

$$\begin{aligned}D_{k,k'} &= \frac{2^d}{N_x^d N_t}\left(1+\frac{d\tau d}{m}-e^{d\tau\mu}e^{-ik_0'}-\frac{d\tau}{m}\sum_{i=1}^{d}\cos(k_i')\right)N_t\delta_{k_0,k_0'}\prod_{i=1}^{d}\frac{N_{x_i}}{2}\delta_{k_i,k_i'} \\ &= \frac{2^d}{N_x^d N_t}\left(1+\frac{d\tau d}{m}-e^{d\tau\mu}e^{-ik_0'}-\frac{d\tau}{m}\sum_{i=1}^{d}\cos(k_i')\right)N_t\left(\frac{N_x}{2}\right)^d\delta_{k,k'} \\ D_{k,k'} &= \left(1+\frac{d\tau d}{m}-e^{d\tau\mu}e^{-ik_0'}-\frac{d\tau}{m}\sum_{i=1}^{d}\cos(k_i')\right)\delta_{k,k'},\end{aligned}$$

or, slightly rearranged:

$$D_{k,k'} = \left(1-e^{d\tau\mu}e^{-ik_0'}+\frac{d\tau}{m}\sum_{i=1}^{d}(1-\cos(k_i'))\right)\delta_{k,k'}. \qquad (C.71)$$

Note that this is a complex matrix, with real and imaginary parts:

$$\begin{aligned}\mathrm{Re}\left[D_{k,k'}\right] &= \left(1-e^{d\tau\mu}\cos(k_0')+\frac{d\tau}{m}\sum_{i=1}^{d}(1-\cos(k_i'))\right)\delta_{k,k'} \qquad (C.72)\\ \mathrm{Im}\left[D_{k,k'}\right] &= e^{d\tau\mu}\sin(k_0')\delta_{k,k'}. \qquad (C.73)\end{aligned}$$

C.8.2: Analytical solution for the nonrotating, noninteracting density

We can now use our diagonal matrix $D_{k,k'} = D_{k,k}$ to solve for the density of this system. Recall that

$$\langle\hat{n}\rangle = \frac{1}{VN_\tau}\sum_k \frac{1}{D_{kk}}\frac{\partial D_{kk}}{\partial(d\tau\mu)}. \qquad (C.74)$$

We first need to solve for $\frac{\partial D_{kk}}{\partial(d\tau\mu)}$:

$$\begin{aligned}\frac{\partial D_{kk}}{\partial \mu} &= \frac{\partial}{\partial(d\tau\mu)}\left[\left(1 - e^{d\tau\mu}e^{-ik'_0} + \frac{d\tau}{m}\sum_{i=1}^{d}(1-\cos(k'_i))\right)\delta_{k,k'}\right] \\ &= -e^{d\tau\mu}e^{-ik'_0}\delta_{k,k'}.\end{aligned} \tag{C.75}$$

Plugging this in to our equation for the density gives us:

$$\langle\hat{n}\rangle = \frac{1}{N_x^d N_t}\sum_k \frac{D^*_{kk}}{|D_{kk}|^2}\left(-e^{d\tau\mu}e^{-ik'_0}\delta_{k,k'}\right). \tag{C.76}$$

C.8.3: Analytical solution for the nonrotating, noninteracting field modulus squared

$$\langle\phi^*\phi\rangle = \sum_k \frac{1}{D_{kk}} = \sum_k \frac{D^*_{kk}}{|D_{kk}|^2}. \tag{C.77}$$

APPENDIX D: THE FREE (NONRELATIVISTIC) BOSE GAS

The lattice action for a nonrotating, noninteracting, and nonrelativistic system in $d+1$ dimensions is the following:

$$S_{\mathrm{lat},r} = \phi_r^* \left[\phi_r - e^{\mathrm{d}\tau\mu}\phi_{r-\hat{\tau}} - \frac{\mathrm{d}\tau}{2m}\sum_{i=1}^{d}\left(\phi_{r+\hat{i}} - 2\phi_r + \phi_{r-\hat{i}}\right)\right]. \tag{D.1}$$

This can be written as fields multiplying a matrix, just as we saw in Chapter **??**, which we can use to determine analytically the density and field modulus squared of this system in order to check against our code's results. Recall that

$$\begin{aligned}\langle\hat{n}\rangle &= \frac{-1}{V}\frac{\partial \ln\mathcal{Z}}{\partial(\beta\mu)} = \frac{-1}{V}\frac{\partial}{\partial(\beta\mu)}(-\ln(\det(M))) \\ &= \frac{1}{V}\frac{\partial}{\partial(\beta\mu)}\mathrm{Tr}(\ln M) = \frac{1}{V}\frac{\partial}{\partial(\beta\mu)}\sum_k \ln D_{kk} = \frac{1}{V}\sum_k \frac{1}{D_{kk}}\frac{\partial D_{kk}}{\partial(\beta\mu)}\end{aligned} \tag{D.2}$$

with $\beta\mu = N_\tau \mathrm{d}\tau\mu$, and note that for a nonrelativistic system,

$$\begin{aligned}\langle\phi^*\phi\rangle &= \frac{-1}{V}\frac{\partial \ln\mathcal{Z}}{\partial(d/m)} = \frac{-1}{V}\frac{\partial}{\partial(d/m)}(-\ln(\det(M))) \\ &= \frac{1}{V}\frac{\partial}{\partial(d/m)}\mathrm{Tr}(\ln M) = \frac{1}{V}\frac{\partial}{\partial(d/m)}\sum_k \ln D_{kk} \\ &= \frac{1}{V}\sum_k \frac{1}{D_{kk}}\frac{\partial D_{kk}}{\partial(d/m)} = \sum_k \frac{1}{D_{kk}}.\end{aligned} \tag{D.3}$$

Section D.1: Diagonalizing our matrix

We can represent the nonrotating, noninteracting action as

$$S_{\mathrm{FBG}} = \sum_{r,r'} \phi_r^* M_{r,r'}[d,m,\mu]\phi_{r'} \tag{D.4}$$

where

$$M_{r,r'}[d,m,\mu] = \left[(1+\frac{\mathrm{d}\tau d}{m})\delta_{r,r'} - e^{\mathrm{d}\tau\mu}\delta_{r-\hat{i},r'} - \frac{\mathrm{d}\tau}{2m}\sum_{i=1}^{d}(\delta_{r+\hat{i},r'} + \delta_{r-\hat{i},r'})\right]. \tag{D.5}$$

We want to diagonalize M again by applying a transformation matrix, such that $D_{kk'} = U^\dagger M U$, where

$$\begin{aligned}
U_{r,k} &= \sqrt{\frac{2^d}{N_x^d N_\tau}} e^{ik_0 t} \prod_{i=1}^{d} \sin(k_i x_i) \\
U^\dagger_{r,k} &= \sqrt{\frac{2^d}{N_x^d N_\tau}} e^{-ik_0 t} \prod_{i=1}^{d} \sin(k_i x_i) \\
k_0 &= \frac{2\pi n_0}{N_\tau},\ n_0 \in [1, 2, ..., N_\tau] \\
k_i &= \frac{\pi n_i}{(N_x + 1)},\ n_i \in [1, 2, ..., N_x].
\end{aligned}$$

Applying the transformation matrix, we get

$$\begin{aligned}
D_{k,k'} &= \frac{2^d}{N_x^d N_t} \sum_{r,r'} e^{-ik_0 t} \prod_{i=1}^{d} \sin(k_i x_i) \left[(1 + \frac{\mathrm{d}\tau d}{m}) \delta_{r,r'} \right] e^{ik'_0 t'} \prod_{i=1}^{d} \sin(k'_i x'_i) \\
&\quad - \frac{2^d}{N_x^d N_t} \sum_{r,r'} e^{-ik_0 t} \prod_{i=1}^{d} \sin(k_i x_i) \left[e^{\mathrm{d}\tau\mu} \delta_{r-\hat{t},r'} \right] e^{ik'_0 t'} \prod_{i=1}^{d} \sin(k'_i x'_i) \\
&\quad - \frac{2^d}{N_x^d N_t} \sum_{r,r'} e^{-ik_0 t} \prod_{i=1}^{d} \sin(k_i x_i) \left[\frac{\mathrm{d}\tau}{2m} \sum_{i=1}^{d} \delta_{r+\hat{i},r'} \right] e^{ik'_0 t'} \prod_{i=1}^{d} \sin(k'_i x'_i) \\
&\quad - \frac{2^d}{N_x^d N_t} \sum_{r,r'} e^{-ik_0 t} \prod_{i=1}^{d} \sin(k_i x_i) \left[\frac{\mathrm{d}\tau}{2m} \sum_{i=1}^{d} \delta_{r-\hat{i},r'} \right] e^{ik'_0 t'} \prod_{i=1}^{d} \sin(k'_i x'_i).
\end{aligned} \tag{D.6}$$

Resolving the delta functions, performing the sum over r', and pulling everything that does not depend on $r = (t, \vec{x})$ outside the sum, this reduces to

$$\begin{aligned}
D_{k,k'} &= \frac{2^d}{N_x^d N_t} (1 + \frac{\mathrm{d}\tau d}{m}) \sum_{r} e^{-it(k_0 - k'_0)} \prod_{i=1}^{d} \sin(k_i x_i) \sin(k'_i x_i) \\
&\quad - \frac{2^d}{N_x^d N_t} e^{\mathrm{d}\tau\mu} e^{-ik'_0} \sum_{r} e^{-it(k_0 - k'_0)} \prod_{i=1}^{d} \sin(k_i x_i) \sin(k'_i x_i) \\
&\quad - \frac{2^d}{N_x^d N_t} \frac{\mathrm{d}\tau}{2m} \sum_{r} e^{-it(k_0 - k'_0)} \prod_{i=1}^{d} \sin(k_i x_i) \sum_{i=1}^{d} \sin(k'_i x_i + k'_i) \\
&\quad - \frac{2^d}{N_x^d N_t} \frac{\mathrm{d}\tau}{2m} \sum_{r} e^{-it(k_0 - k'_0)} \prod_{i=1}^{d} \sin(k_i x_i) \sum_{i=1}^{d} \sin(k'_i x_i - k'_i).
\end{aligned} \tag{D.7}$$

To further expand the last two lines, we use the trig identity $\sin(a \pm b) = \sin(a)\cos(b) \pm \sin(b)\cos(a)$, which gives us:

$$\begin{aligned}
D_{k,k'} &= \frac{2^d}{N_x^d N_t}(1 + \frac{\mathrm{d}\tau d}{m} - e^{\mathrm{d}\tau\mu}e^{-ik'_0}) \sum_r e^{-it(k_0-k'_0)} \prod_{i=1}^{d} \sin(k_i x_i)\sin(k'_i x_i) \\
&\quad -\frac{2^d}{N_x^d N_t}\frac{\mathrm{d}\tau}{2m} \sum_{i=1}^{d} \cos(k'_i) \sum_r e^{-it(k_0-k'_0)} \prod_{i=1}^{d} \sin(k_i x_i)\sin(k'_i x_i) \\
&\quad -\frac{2^d}{N_x^d N_t}\frac{\mathrm{d}\tau}{2m} \sum_{i=1}^{d} \sin(k'_i) \sum_r e^{-it(k_0-k'_0)} \prod_{i=1}^{d} \sin(k_i x_i)\cos(k'_i x_i) \\
&\quad -\frac{2^d}{N_x^d N_t}\frac{\mathrm{d}\tau}{2m} \sum_{i=1}^{d} \cos(k'_i) \sum_r e^{-it(k_0-k'_0)} \prod_{i=1}^{d} \sin(k_i x_i)\sin(k'_i x_i) \\
&\quad +\frac{2^d}{N_x^d N_t}\frac{\mathrm{d}\tau}{2m} \sum_{i=1}^{d} \sin(k'_i) \sum_r e^{-it(k_0-k'_0)} \prod_{i=1}^{d} \sin(k_i x_i)\cos(k'_i x_i).
\end{aligned} \tag{D.8}$$

Using the following Fourier identities

$$\begin{aligned}
\sum_x \sin(kx)\sin(k'x) &= \frac{N_x}{2}\delta_{k,k'} \\
\sum_x \sin(kx)\cos(k'x) &= 0 \\
\sum_x e^{-ix(k-k')} &= N_x\delta_{k,k'}
\end{aligned} \tag{D.9}$$

we find that

$$\begin{aligned}
D_{k,k'} &= \frac{2^d}{N_x^d N_t}\left(1 + \frac{\mathrm{d}\tau d}{m} - e^{\mathrm{d}\tau\mu}e^{-ik'_0} - \frac{\mathrm{d}\tau}{m}\sum_{i=1}^{d}\cos(k'_i)\right) N_t\delta_{k_0,k'_0} \prod_{i=1}^{d} \frac{N_{x_i}}{2}\delta_{k_i,k'_i} \\
&= \frac{2^d}{N_x^d N_t}\left(1 + \frac{\mathrm{d}\tau d}{m} - e^{\mathrm{d}\tau\mu}e^{-ik'_0} - \frac{\mathrm{d}\tau}{m}\sum_{i=1}^{d}\cos(k'_i)\right) N_t \left(\frac{N_x}{2}\right)^d \delta_{k,k'} \\
D_{k,k'} &= \left(1 + \frac{\mathrm{d}\tau d}{m} - e^{\mathrm{d}\tau\mu}e^{-ik'_0} - \frac{\mathrm{d}\tau}{m}\sum_{i=1}^{d}\cos(k'_i)\right)\delta_{k,k'},
\end{aligned}$$

or, slightly rearranged:

$$D_{k,k'} = \left(1 - e^{\mathrm{d}\tau\mu}e^{-ik'_0} + \frac{\mathrm{d}\tau}{m}\sum_{i=1}^{d}(1-\cos(k'_i))\right)\delta_{k,k'}. \tag{D.10}$$

Note that this is a complex matrix, with real and imaginary parts:

$$\mathrm{Re}\left[D_{k,k'}\right] = \left(1 - e^{\mathrm{d}\tau\mu}\cos(k_0') + \frac{\mathrm{d}\tau}{m}\sum_{i=1}^{d}(1-\cos(k_i'))\right)\delta_{k,k'} \tag{D.11}$$

$$\mathrm{Im}\left[D_{k,k'}\right] = e^{\mathrm{d}\tau\mu}\sin(k_0')\delta_{k,k'}. \tag{D.12}$$

We can now use our diagonal matrix $D_{k,k'} = D_{k,k}$ to solve for the density of this system. Recall that

$$\langle\hat{n}\rangle = \frac{1}{VN_\tau}\sum_k \frac{1}{D_{kk}}\frac{\partial D_{kk}}{\partial(\mathrm{d}\tau\mu)}. \tag{D.13}$$

We first need to solve for $\frac{\partial D_{kk}}{\partial(\mathrm{d}\tau\mu)}$:

$$\begin{aligned}\frac{\partial D_{kk}}{\partial\mu} &= \frac{\partial}{\partial(\mathrm{d}\tau\mu)}\left[\left(1 - e^{\mathrm{d}\tau\mu}e^{-ik_0'} + \frac{\mathrm{d}\tau}{m}\sum_{i=1}^{d}(1-\cos(k_i'))\right)\delta_{k,k'}\right] \\ &= -e^{\mathrm{d}\tau\mu}e^{-ik_0'}\delta_{k,k'}.\end{aligned} \tag{D.14}$$

Plugging this in to our equation for the density gives us:

$$\langle\hat{n}\rangle = \frac{1}{N_x^d N_t}\sum_k \frac{D_{kk}^*}{|D_{kk}|^2}\left(-e^{\mathrm{d}\tau\mu}e^{-ik_0'}\delta_{k,k'}\right). \tag{D.15}$$

and doing the same for the field modulus gives us:

$$\langle\phi^*\phi\rangle = \sum_k \frac{1}{D_{kk}} = \sum_k \frac{D_{kk}^*}{|D_{kk}|^2}. \tag{D.16}$$

REFERENCES

[1] G. Aarts, *Can Stochastic Quantization Evade the Sign Problem? The Relativistic Bose Gas at Finite Chemical Potential*, Phys. Rev. Lett. **102**, 13, 131601 (2009).

[2] J. Taylor, *Classical Mechanics*, (University Science Books, 2005).

[3] D. Morin, *Introduction to Classical Mechanics: With Problems and Solutions*, (Cambridge University Press, 2008).

[4] N. Zettili, *Quantum Mechanics: Concepts and Applications*, (Wiley, 2009).

[5] D. McIntyre, C. Manogue, and J. Tate, *Quantum Mechanics*, (Pearson Education, 2012).

[6] J. Sakurai and J. Napolitano, *Modern Quantum Mechanics*, (Addison-Wesley, 2011).

[7] G. Arfken, H. Weber, and F. Harris, *Mathematical Methods for Physicists: A Comprehensive Guide*, (Elsevier Science, 2011).

[8] P. Navrátil, S. Quaglioni, G. Hupin, C. Romero-Redondo, and A. Calci, *Unified ab initio approaches to nuclear structure and reactions*, Physica Scripta **91**, 5, 053002 (2016).

[9] A. Schmitt, *Introduction to Superfluidity: Field-theoretical Approach and Applications*, vol. 4 of *888*, (Springer, Lecture Notes in Physics, 2015).

[10] J. F and J. Annett, *Superconductivity, Superfluids and Condensates*, Oxford Master Series in Physics, (OUP Oxford, 2004).

[11] W. Vinen, *The physics of superfluid helium* (2004).

[12] L. Onsager, *Statistical hydrodynamics*, Il Nuovo Cimento (1943-1954) **6**, 2, 279 (1949).

[13] R. Feynman, *Chapter II Application of Quantum Mechanics to Liquid Helium*, in C. Gorter, ed., *Progress in Low Temperature Physics*, vol. 1, 17 – 53, (Elsevier, 1955).

[14] J. R. Abo-Shaeer, C. Raman, J. M. Vogels, and W. Ketterle, *Observation of Vortex Lattices in Bose-Einstein Condensates*, Science **292**, 5516, 476 (2001).

[15] A. L. Fetter, *Rotating trapped Bose-Einstein condensates*, Rev. Mod. Phys. **81**, 647 (2009).

[16] A. Kato, Y. Nakano, K. Kasamatsu, and T. Matsui, *Vortex formation of a Bose-Einstein condensate in a rotating deep optical lattice*, Phys. Rev. A **84**, 053623 (2011).

[17] K. W. Madison, F. Chevy, W. Wohlleben, and J. Dalibard, *Vortex Formation in a Stirred Bose-Einstein Condensate*, Phys. Rev. Lett. **84**, 806 (2000).

[18] M. Zwierlein, J. Abo-Shaeer, A. Schirotzek, C. Schunck, and W. Ketterle, *Vortices and Superfluidity in a Strongly Interacting Fermi Gas*, Nature **435**, 1047 (2005).

[19] F. X. Sun, Z. X. Niu, Q. H. Gong, Q. Y. He, and W. Zhang, *Emergence and stability of spontaneous vortex lattices in exciton-polariton condensates*, arXiv e-prints arXiv:1901.03172 (2019).

[20] L. Madeira, S. Gandolfi, K. E. Schmidt, and V. S. Bagnato, *Vortices in low-density neutron matter and cold Fermi gases*, arXiv e-prints arXiv:1903.06724 (2019).

[21] S. K. Adhikari, *Vortex lattice in a uniform Bose-Einstein condensate in a box trap*, arXiv e-prints arXiv:1903.08672 (2019).

[22] G. Eriksson, J. Bengtsson, G. M. Kavoulakis, and S. M. Reimann, *A two-state model for vortex nucleation in a rotating Bose-Einstein condensate*, arXiv e-prints arXiv:1910.11461 (2019).

[23] B. Jeevanesan and S. Moroz, *Thermodynamics of two-dimensional bosons in the lowest Landau level*, arXiv e-prints arXiv:1910.07808 (2019).

[24] S. Forstner, Y. Sachkou, M. Woolley, G. I. Harris, X. He, W. P. Bowen, and C. G. Baker, *Modelling of vorticity, sound and their interaction in two-dimensional superfluids*, arXiv e-prints arXiv:1901.05167 (2019).

[25] T. Ozawa and G. Baym, *Striped states in weakly trapped ultracold Bose gases with Rashba spin-orbit coupling*, Phys. Rev. A **85**, 063623 (2012).

[26] X.-L. Chen, S.-G. Peng, P. Zou, X.-J. Liu, and H. Hu, *Angular Stripe Phase in Spin-Orbital-Angular-Momentum Coupled Bose Condensates*, arXiv e-prints arXiv:1901.02595 (2019).

[27] H. Zhai, *Degenerate quantum gases with spin-orbit coupling: a review*, Reports on Progress in Physics **78**, 026001 (2015).

[28] E. Kawasaki and M. Holzmann, *Finite-temperature phases of two-dimensional spin-orbit-coupled bosons*, Physical Review A **95**, 051601 (2017).

[29] E. J. Yarmchuk, M. J. V. Gordon, and R. E. Packard, *Observation of Stationary Vortex Arrays in Rotating Superfluid Helium*, Phys. Rev. Lett. **43**, 214 (1979).

[30] C. R. Shill and J. E. Drut, *Virial coefficients of one-dimensional and two-dimensional Fermi gases by stochastic methods and a semiclassical lattice approximation*, Phys. Rev. A **98**, 053615 (2018).

[31] Y. Hou, A. J. Czejdo, J. DeChant, C. R. Shill, and J. E. Drut, *Leading- and next-to-leading-order semiclassical approximation to the first seven virial coefficients of spin-1/2 fermions across spatial dimensions*, Phys. Rev. A **100**, 063627 (2019).

[32] K. J. Morrell, C. E. Berger, and J. E. Drut, *Third- and fourth-order virial coefficients of harmonically trapped fermions in a semiclassical approximation*, Phys. Rev. A **100**, 063626 (2019).

[33] R. Shankar, *Principles of Quantum Mechanics*, (Springer US, 1995).

[34] C. E. Berger, E. R. Anderson, and J. E. Drut, *Energy, contact, and density profiles of one-dimensional fermions in a harmonic trap via nonuniform-lattice Monte Carlo calculations*, Phys. Rev. A **91**, 053618 (2015).

[35] Z. Luo, C. E. Berger, and J. E. Drut, *Harmonically trapped fermions in two dimensions: Ground-state energy and contact of SU(2) and SU(4) systems via a nonuniform lattice Monte Carlo method*, Phys. Rev. A **93**, 033604 (2016).

[36] C. E. Berger, J. E. Drut, and W. J. Porter, *Hard-wall and non-uniform lattice Monte Carlo approaches to one-dimensional Fermi gases in a harmonic trap*, Computer Physics Communications **208**, 103 (2016).

[37] C. E. Berger, K. J. Morrell, and J. E. Drut, *Thermodynamics of rotating quantum matter in the virial expansion* (2020).

[38] J. R. Klauder, *Coherent-state Langevin equations for canonical quantum systems with applications to the quantized Hall effect*, Phys. Rev. A **29**, 2036 (1984).

[39] J. Berges and I.-O. Stamatescu, *Simulating Nonequilibrium Quantum Fields with Stochastic Quantization Techniques*, Phys. Rev. Lett. **95**, 202003 (2005).

[40] J. Berges, S. Borsányi, D. Sexty, and I.-O. Stamatescu, *Lattice simulations of real-time quantum fields*, Phys. Rev. D **75**, 045007 (2007).

[41] C. E. Berger, L. Rammelmüller, A. C. Loheac, F. Ehmann, J. Braun, and J. E. Drut, *Complex Langevin and other approaches to the sign problem in quantum many-body physics* (2019).

[42] G. Aarts and I.-O. Stamatescu, *Stochastic quantization at finite chemical potential*, JHEP **09**, 018 (2008).

[43] G. Aarts, *Complex Langevin dynamics at finite chemical potential: mean field analysis in the relativistic Bose gas*, JHEP **2009**, 05, 052 (2009).

[44] Jürgen Berges and Dénes Sexty, *Real-time gauge theory simulations from stochastic quantization with optimized updating*, Nucl. Phys. B **799**, 3, 306 (2008).

[45] G. Aarts, F. A. James, E. Seiler, and I.-O. Stamatescu, *Adaptive stepsize and instabilities in complex Langevin dynamics*, Phys. Lett. B **687**, 2, 154 (2010).

[46] G. Aarts and F. A. James, *On the convergence of complex Langevin dynamics: the three-dimensional XY model at finite chemical potential*, JHEP **8**, 20 (2010).

[47] L. Rammelmüller, W. J. Porter, J. E. Drut, and J. Braun, *Surmounting the sign problem in nonrelativistic calculations: A case study with mass-imbalanced fermions*, Phys. Rev. D **96**, 094506 (2017).

[48] A. C. Loheac and J. E. Drut, *Third-order perturbative lattice and complex Langevin analyses of the finite-temperature equation of state of nonrelativistic fermions in one dimension*, Phys. Rev. D **95**, 094502 (2017).

[49] L. Rammelmüller, A. C. Loheac, J. E. Drut, and J. Braun, *Finite-Temperature Equation of State of Polarized Fermions at Unitarity*, Phys. Rev. Lett. **121**, 173001 (2018).

[50] L. RammelmÃijller, J. E. Drut, and J. Braun, *A complex Langevin approach to ultracold fermions*, J. Phys. Conf. Ser. **1041**, 012006 (2018).

[51] A. C. Loheac, J. Braun, and J. E. Drut, *Polarized fermions in one dimension: Density and polarization from complex Langevin calculations, perturbation theory, and the virial expansion*, Phys. Rev. D **98**, 054507 (2018).

[52] L. Rammelmüller, J. E. Drut, and J. Braun, *Pairing patterns in one-dimensional spin- and mass-imbalanced Fermi gases* (2020).

[53] F. Attanasio and J. E. Drut, *Thermodynamics of spin-orbit coupled bosons in two dimensions from complex Langevin* (2019).

[54] G. Parisi and Y.-s. Wu, *Perturbation Theory Without Gauge Fixing*, Sci. Sin. **24**, 483 (1981).

[55] P. H. Damgaard and H. Hüffel, *Stochastic quantization*, Phys. Rept. **152**, 5, 227 (1987).

[56] K. Okano, L. Schulke, and B. Zheng, *Complex Langevin simulation*, Prog. Theor. Phys. Suppl. **111**, 313 (1993).

[57] G. Parisi, *On complex probabilities*, Phys. Lett. B **131**, 4, 393 (1983).

[58] J. R. Klauder, *Stochastic Quantization*, Acta Phys. Austriaca Suppl. **25**, 251 (1983).

[59] J. R. Klauder, *A Langevin approach to fermion and quantum spin correlation functions*, Journal of Physics A: Mathematical and General **16**, 10, L317 (1983).

[60] G. Aarts, E. Seiler, and I.-O. Stamatescu, *Complex Langevin method: When can it be trusted?*, Phys. Rev. D **81**, 054508 (2010).

[61] G. Aarts, F. A. James, E. Seiler, and I.-O. Stamatescu, *Complex Langevin: Etiology and Diagnostics of its Main Problem*, Eur. Phys. J. C **71**, 1756 (2011).

[62] L. L. Salcedo, *Does the complex Langevin method give unbiased results?*, Phys. Rev. D **94**, 114505 (2016).

[63] M. Scherzer, E. Seiler, D. Sexty, and I.-O. Stamatescu, *Complex Langevin and boundary terms*, Phys. Rev. D **99**, 014512 (2019).

[64] K. Nagata, J. Nishimura, and S. Shimasaki, *Argument for justification of the complex Langevin method and the condition for correct convergence*, Phys. Rev. D **94**, 114515 (2016).

[65] G. Aarts, E. Seiler, D. Sexty, and I.-O. Stamatescu, *Complex Langevin dynamics and zeroes of the fermion determinant*, JHEP **2017**, 5, 44 (2017).

[66] J. Nishimura and S. Shimasaki, *New insights into the problem with a singular drift term in the complex Langevin method*, Phys. Rev. D **92**, 011501 (2015).

[67] T. Hayata, Y. Hidaka, and Y. Tanizaki, *Complex saddle points and the sign problem in complex Langevin simulation*, Nucl. Phys. B **911**, 94 (2016).

[68] J. Ambjorn, M. Flensburg, and C. Peterson, *Langevin Simulations of Configurations With Static Charges*, Phys. Lett. **159B**, 335 (1985).

[69] J. Ambjorn and S. K. Yang, *Numerical Problems in Applying the Langevin Equation to Complex Effective Actions*, Phys. Lett. **165B**, 140 (1985).

[70] E. Seiler, D. Sexty, and I.-O. Stamatescu, *Gauge cooling in complex Langevin for QCD with heavy quarks*, Phys. Lett. B **723**, 213 (2013).

[71] L. Bongiovanni, G. Aarts, E. Seiler, D. Sexty, and I.-O. Stamatescu, *Adaptive gauge cooling for complex Langevin dynamics*, PoS **LATTICE2013**, 449 (2014).

[72] H. Makino, H. Suzuki, and D. Takeda, *Complex Langevin method applied to the 2D $SU(2)$ Yang-Mills theory*, Phys. Rev. D **92**, 085020 (2015).

[73] K. Nagata, J. Nishimura, and S. Shimasaki, *Justification of the complex Langevin method with the gauge cooling procedure*, PTEP **2016**, 1, 013B01 (2016).

[74] K. Nagata, J. Nishimura, and S. Shimasaki, *Gauge cooling for the singular-drift problem in the complex Langevin method - a test in Random Matrix Theory for finite density QCD*, JHEP **07**, 073 (2016).

[75] G. Aarts, F. Attanasio, B. Jäger, and D. Sexty, *Complex Langevin in Lattice QCD: dynamic stabilisation and the phase diagram*, Acta Phys. Polon. Supp. **9**, 621 (2016).

[76] F. Attanasio and B. Jäger, *Testing dynamic stabilisation in complex Langevin simulations*, PoS **LATTICE2016**, 053 (2016).

[77] Attanasio, Felipe and Jäger, Benjamin, *Improved convergence of Complex Langevin simulations*, EPJ Web Conf. **175**, 07039 (2018).

[78] F. Attanasio and B. Jäger, *Dynamical stabilisation of complex Langevin simulations of QCD*, Eur. Phys. J. C **79**, 1, 16 (2019).

[79] A. C. Loheac and J. E. Drut, *Third-order perturbative lattice and complex Langevin analyses of the finite-temperature equation of state of nonrelativistic fermions in one dimension*, Phys. Rev. D **95**, 094502 (2017).